TOWARDS THE UNDERSTANDING OF *BRUCELLA*-INDUCED ARTHRITIS FOR VACCINE DEVELOPMENT

A Dissertation

by

OMAR H. KHALAF

Submitted to the Office of Graduate and Professional Studies of
Texas A&M University
in partial fulfillment of the requirements for the degree of

DOCTOR OF PHILOSOPHY

Chair of Committee,	Angela M. Arenas-Gamboa
Committee Members,	Thomas A. Ficht
	Robert C. Burghardt
	Larry J. Suva
Head of Department,	Ramesh Vemulapalli

December 2019

Major Subject: Biomedical Sciences

ABSTRACT

Osteoarticular brucellosis is the most common complication in *Brucella*-infected humans. The mechanism of bone destruction caused by *Brucella* remains partially unknown due to the lack of a suitable animal model. Of greater concern is the fact that development of vaccines to protect humans against brucellosis is hampered by safety concerns and no effective models exist to assess the safety of candidate vaccines in the context of osteoarticular disease. To address this issue, we explored the suitability of the NOD-*scid IL2rγ*^{null} (NSG) mouse and examined the potential use of this strain to evaluate the safety of live attenuated vaccine candidates. Mice were inoculated intraperitoneally with *B. abortus* S19 or the vaccine candidate *B. abortus* S19*ΔvjbR*. Hypothermia, weight loss, splenomegaly, and tail deformation were observed in mice inoculated with *B. abortus* S19 but not with S19*ΔvjbR*. Histologically, all S19 but not S19*ΔvjbR* inoculated mice exhibited severe dose-dependent osteomyelitis in the tail characterized by large numbers of neutrophils, macrophages, and osteoclasts with marked bone destruction. Interestingly, myriad bacteria were observed within osteoclasts of S19-infected mice. To further investigate the role of osteoclasts during *Brucella* infection, murine bone marrow-derived macrophages were derived into mature osteoclasts and infected with *B. abortus* 2308, S19, and attenuated mutants S19*ΔvjbR* and *B. abortus*2308*ΔvirB2*. While *B. abortus* 2308 and S19 replicated inside mature osteoclasts, the attenuated mutants were progressively killed. Interestingly, *B. abortus* 2308 impaired the growth of osteoclasts without reducing resorptive activity while

osteoclasts infected with *B. abortus* S19 and S19*ΔvjbR* were significantly larger and exhibited enhanced resorption. None of the *Brucella* strains induced apoptosis or stimulated nitric oxide or lactose dehydrogenase production in osteoclasts. Finally, infection of macrophages or osteoclast precursors with *B. abortus* 2308 resulted in generation of smaller osteoclasts with decreased resorptive activity. Overall, *Brucella* exhibits similar growth characteristics in mature osteoclasts compared to the primary target cell, the macrophage, but is able to impair the maturation and alter the resorptive capacity of these cells. These results suggest that osteoclasts play an important role in osteoarticular brucellosis and could serve as a useful *in vitro* model for both analyzing host-pathogen interactions and assessing vaccine safety.

DEDICATION

I dedicate my dissertation work to my country Iraq and to the souls of my father, Hussein, and my, sister Athra. A special feeling of gratitude to my loving mother Sikna, my beautiful wife Shaymaa, and my wonderful children Al-Hussein, Yousif, and Lara for their encouragement and support throughout this long journey. I also dedicate my work to my oldest brother Ali and many friends who were always there for me throughout this process.

ACKNOWLEDGEMENTS

I would like to thank my committee chair, Dr. Angela Arenas, and my committee members, Dr. Thomas Ficht, Dr. Robert Burghardt, and Dr. Larry Suva for their guidance and support throughout the course of this research.

I am extremely thankful to Dr. Sankar P. Chaki for his supervision and technical advice throughout my research project. I am thankful to Daniel Garcia for his encouragement and support. Thanks also go to my close friends, Ana-Lucia Cabello, Slim Zriba, Lauren Stranahan, Shakirat Adetunji, Martha Hensel, and Jamie Benn.

I would like to thank the department faculty Dr. Linda Logan, Dr. Joanne Mansell, Dr. Aline Rodrigues-Hoffman, Dr. Raquel Rech, Dr. Brian Porter, and Dr. Andy Ambrus, for their considerable assistance. My special thanks and gratitude extend to Dr. Dana Gaddy, Dr. Rola Barhoumi, Dr. Diarra Williams, Alyssa Falck, and Shannon Huggins for sharing ideas, times, and reagents.

Special acknowledgements and thank go to the Department Head of Veterinary Pathobiology, Dr. Ramesh Vemulapalli, and the graduate academic advisors Dr. David Kessler, Kathi Smith, Demetria Cooper, Eleni Vonda, and Katharina Ojala for their time and support during my studies.

A special thanks and love go to my beautiful wife, Shaymaa, and my beautiful children, for their encouragement and their patience and love.

Lastly, I am extremely thankful to the College of Veterinary Medicine & Biomedical Science, Texas A&M University and to the College of Veterinary Medicine, University of Baghdad, Iraq for giving me this fantastic opportunity to accomplish my Ph.D. study.

CONTRIBUTORS AND FUNDING SOURCES

Contributors

This work was supervised by a dissertation committee consisting of Professor Angela M. Arenas-Gamboa and Professor Thomas A. Ficht of the Department of Veterinary Pathobiology (VTPB), Professor Robert C. Burghardt of the Department of Veterinary Integrative Bioscience (VIBS), and Professor Larry J. Suva or the Department of Veterinary Physiology and Pharmacology (VTPP).

All other work conducted for the dissertation was completed by the student independently.

Funding Sources

Graduate study was supported by a Research Scholarship by the College of Veterinary Medicine, University of Baghdad, Iraqi and a graduate research trainee grant from the College of Veterinary Medicine & Biomedical Sciences, Texas A&M University. This work was also made possible in part by the faculty startup grant from Texas A&M University (TAMU), a grant from NIH to A.M.A.G under Grant Number KO1TW009981, and a grant from NIH to T.A.F. under Grant Number -RO1HD084339.

NOMENCLATURE

BMDMs	Bone marrow-derived macrophages
M-CSF	Macrophage Colony-Stimulating Factor
mOCs	Multinucleated mature osteoclasts
NF-kB	Receptor activator of nuclear factor-kB
OAB	Osteoarticular brucellosis
pOCs	Osteoclasts precursors
RANKL	Receptor Activator of Nuclear Factor-κB ligand
TRAP stain	Tartrate-resistant acid phosphatase stain
TUNEL	Terminal deoxynucleotidyl transferase (TdT) dUTP nick-end labeling of fragmented DNA

TABLE OF CONTENTS

Page

LIST OF FIGURES

Page

LIST OF TABLES

Page

1. INTRODUCTION

1.1. Brucellosis

Brucella is a gram-negative intracellular microbe that causes brucellosis, a neglected zoonotic disease of worldwide significance. Brucellosis remains endemic in several countries throughout Asia, the Middle East, Africa, and South America (1-3). Among the 12 recognized *Brucella* species (4), *B. abortus* (cattle), *B. melitensis* (goats and sheep), and *B. suis* (pigs) are considered the most pathogenic for both the natural livestock hosts and humans (5-9). Although the available epidemiological data regarding infected patients is incomplete, and for some countries unavailable, more than 500,000 new human brucellosis cases are reported annually (10). Brucellosis in animals is primarily a reproductive disease characterized by placentitis and abortion in pregnant females and epididymitis and orchitis in males (11, 12). *B. melitensis*, one of the most highly pathogenic among *Brucella* species, infects small ruminants and causes orchitis in infected males as well as abortion in pregnant dams with the capability of being shed in the milk (13). *Brucella* infection in cattle is primarily caused by *B. abortus*, which is also capable of infecting camels, buffaloes, deer, horses, dogs, and small ruminants. Abortion, stillbirth, necrotizing placentitis, and mastitis are the most common clinical signs associated with *B. abortus* infection, as well as orchitis and epididymitis in the infected bull. Brucellosis in swine is caused by *B. suis,* which infects domestic, wild pigs, and occasionally other livestock species. Infertility, abortion, and orchitis, frequently accompanied by osteoarticular manifestations have been observed in swine

brucellosis (14-16). The placenta and aborted fetus, which contain high levels of shed *Brucella* organisms, are considered the major source of infection to natural and incidental animal hosts for all three of the most pathogenic *Brucella* spp (17-19).

In humans, transmission occurs as a result of direct exposure to the excretions and products of infected animals, including genital secretions, aborted fetuses and fetal membranes, unpasteurized dairy products, or accidental injection during vaccine handling (5, 20, 21). The clinical manifestations of acute human brucellosis include undulant fever accompanied by non-specific symptoms such as malaise, sweating, arthralgia, splenomegaly, and hepatomegaly (6, 9, 22). Of greater concern, *Brucella* is able to survive and persist in several organs, leading to the development of lifelong, chronic complications including osteoarticular disease, hepatic or splenic abscessation, neurological disorders, and endocarditis (23-26). Although the infection is seldom spread from one infected human to another, rare cases of transmission between infected individuals have been reported (27, 28).

For decades, vaccination policy has been a critical component of control and/or eradication campaigns against *Brucella* infection in animals. Live attenuated vaccines such as S19, RB51, and Rev1 (29, 30) have played a crucial role throughout the world in prevention of brucellosis in livestock species; however, several drawbacks with these vaccines exist, most importantly the induction of abortion in pregnant animals and the ability to cause disease in humans (31, 32). These pitfalls have been the impetus for ongoing research into the development of new vaccines that are safer yet retain an equivalent or superior level of protection as those currently in use.

1.2. Osteoarticular brucellosis

Brucella-induced osteoarticular disease is the most common clinical manifestation associated with *Brucella* infection in humans (33-36). Osteoarticular brucellosis (OAB) is considered a major public health challenge in several countries, especially in the Mediterranean, Middle East, and Central and South America. Alarmingly, an estimated 40-80% of *Brucella*-infected patients develop OAB (10, 37, 38). Regardless of age or gender, OAB can occur at any point during infection and can produce a variety of lesions, including peripheral arthritis, sacroiliitis, and spondylitis (36). In peripheral arthritis, one or multiple articular sites may be involved, and large joints such as the hips and knees are the most frequently affected (39, 40). Sacroiliitis involves unilateral or bilateral inflammation of the sacroiliac joints and may manifest with non-specific clinical signs such as fever, chills, and severe lower back pain (41-44). The last form of osteoarticular brucellosis is spondylitis, inflammation of the vertebrae at the level of the disco-vertebral junction. In severe cases, multiple consecutive vertebrae may be involved, resulting in severe and disabling complications (45-47). Untreated OAB may result in marked bone and cartilage destruction, synovial rupture, or osteopenia causing permanent damage and disability (48-51). Therefore, early diagnosis and rigorous antibiotic treatment are essential to prevent relapses and manifestations of OAB (38, 52, 53). OAB in animals has also been reported, with reports of arthritis in goats and sheep, carpal hygromas in dairy cattle, and diskospondylitis in dogs (54-56).

1.3. Animals models of osteoarticular brucellosis

Although several studies regarding *Brucella*-induced arthritis have been published, the pathobiology underlying osteoarticular brucellosis remains unclear due to the lack of suitable animal models which replicate the clinical symptoms seen in humans (36, 57, 58). A single study utilizing a natural host demonstrated that young cattle developed arthritis following direct intra-articular administration of *B. abortus* S19 vaccine strain (55). However, several challenges concerning the use of natural hosts in such experiments, including financial costs, animal husbandry issues, limited housing space in Biosafety level three (BL3) laboratories, and ethical issues are significant limitations.

To address these issues, mice have been utilized as a surrogate to understand the pathogenesis of osteoarticular brucellosis (59). Wild type mice have been widely used as a valuable model to study the pathogenesis of *Brucella* infection, evaluate the safety and efficacy of vaccine candidates, and investigate new therapeutics (60, 61). However, wild type mice are naturally resistant to *Brucella* infection and systemic inoculation of up to 10^6 colony-forming units (CFU) fails to induce osteoarticular lesions (57, 58). Other laboratory animals such as monkeys, rats, and guinea pigs have also been evaluated as models, but none of these models have demonstrated bone damage (62). In contrast, knockout mice, such as IFN-$\gamma^{-/-}$, CXCR$^{-/-}$, and IL-1R$^{-/-}$ immunocompromised mice, consistently develop acute bone lesions and at a much earlier time point than wild type mice when infected with wild type *Brucella* spp (57, 58). Such findings highlight the

potential of immunocompromised mice to be used as a model to study the pathogenesis of osteoarticular brucellosis.

1.4. Cells involved in osteoarticular brucellosis

Bone is a dynamic and highly regulated connective tissue that is continuously remodeled under the influence of three different cell types: osteoblasts, osteocytes, and osteoclasts. These cells work together to develop and maintain healthy bone structure. Osteoblasts are bone-forming cells involved in bone matrix mineralization that provides rigidity and strength to the bone (63). Osteocytes are differentiated osteoblasts located within the mineralized bone matrix and comprise approximately 95% of bone cells. The location of these cells gives them the ability to sense mechanical stress and regulate bone remodeling processes through the secretion of various cytokines and chemokines (64, 65). Lastly, osteoclasts are highly specialized multinucleated bone-resorbing cells derived from the monocyte/macrophage lineage under the regulation of two cytokines: Macrophage Colony-Stimulating Factor (M-CSF) and Receptor Activator of Nuclear Factor-κB ligand (RANKL) (66, 67). Bone resorption is a complex and multi-step process that includes osteoclast polarization onto the bone, reorganization of the cytoskeleton, and ruffled border formation (68), followed by the release of protons and proteolytic enzymes into resorption lacuna and bone matrix degradation (69, 70). Modifications of the functional activity of any of these cells are associated with the development of various bone diseases such as osteoporosis, osteopetrosis, and chronic osteoarthritis (71).

Several *in vitro* studies have highlighted the direct interaction between resident bone cells and *Brucella* in an effort to elucidate the pathogenesis of osteoarticular brucellosis. For instance, *in vitro* studies have demonstrated that *B. abortus* is able to invade and replicate within osteoblasts and osteocytes, modify the metabolic activity of these cells, and upregulate the expression of metalloproteinases (MMPs) as well as RANKL, the main cytokine involved in osteoclast differentiation (72-74). These results suggest that these cells are directly and indirectly involved in the bone destruction observed during osteoarticular brucellosis (36). However, the role of osteoclasts is the pathogenesis of this disease process remains to be explored.

1.5. Goals and Experimental Approach

Due to the numerous pitfalls involving the use of natural hosts or wild type mice to study the mechanism of osteoarticular brucellosis as mentioned earlier, immunocompromised mice have been developed as a promising animal model to study bone disease following *Brucella* infection. However, only wild type *Brucella* strains have been shown to cause osteoarticular lesions in these mice while attenuated vaccine strains do not. This distinction is important, as the currently available *B. abortus* S19 vaccine strain is able to induce osteoarticular lesions in cattle, yet no laboratory animal model exists to investigate this mechanism. It is also important to consider that new vaccine candidates may have the potential to induce osteoarticular lesions in humans or natural hosts, changes which would likely be missed using the established wild type mouse model. Therefore, developing an improved mouse model able to detect pathologic

bone changes induced by attenuated *Brucella* strains is a priority. This new model would have the potential not only to improve safety evaluation of vaccine candidates but also to understand the mechanism behind *Brucella*-induced arthritis. Moreover, investigation of the interaction between *Brucella* spp and osteoclasts is needed to understand the pathogenesis of osteoarticular brucellosis.

2. THE NOD-*SCID IL2RGAMMA* ^{NULL} MOUSE MODEL IS SUITABLE TO STUDY OSTEOARTICULAR BRUCELLOSIS AND VACCINE SAFETY*

2.1. Summary

Osteoarticular brucellosis is the most common complication in *Brucella*-infected humans regardless of age, sex, or immune status. The mechanism of bone destruction caused by *Brucella* species remained partially unknown due to the lack of a suitable animal model. Here, to study this complication, we explored the suitability of the use of theNOD-*scid IL2rγ*^{null} mouse to study osteoarticular brucellosis and examined the potential use of this strain to evaluate the safety of live attenuated vaccine candidates. Mice were inoculated intraperitoneally with a single dose of either $1x10^4$, $1x10^5$, or $1x10^6$ CFU of *B. abortus* S19 or the vaccine candidate *B. abortus* S19*ΔvjbR* and monitored for the development of side effects, including osteoarticular disease, for 13 weeks. Decreased in body temperature, weight loss, splenomegaly, and deformation of the tails was observed in mice inoculated with *B. abortus* S19 but not with S19*ΔvjbR*. Histologically, all S19 inoculated mice had a severe dose-dependent inflammatory response in multiple organs. The inflammatory response at the tail was characterized by the recruitment of large numbers of neutrophils, macrophages and osteoclasts with

---

*Reprinted with permission from "The NOD-SCID IL2rγ ^{null} Mouse Model Is Suitable For the Study of Osteoarticular Brucellosis and Vaccine Safety" By Khalaf OH, Chaki SP, Garcia-Gonzalez DG, Ficht TA, Arenas-Gamboa AM, 2019, Infection and Immunity, 87(6). pii: e00901-18, Copyright (2019) by American Society for Microbiology

marked bone destruction. These lesions histologically resembled what is typically observed in *Brucella*-infected patients. In contrast, mice inoculated with *B. abortus* S19*ΔvjbR* did not show significant bone changes. Immunofluorescence, *in situ* hybridization, and confocal imaging demonstrated the presence of *Brucella* at the sites of inflammation, both intra- and extracellularly, and large numbers were observed within mature osteoclasts. These results demonstrate the potential use of the NOD-*scid IL2rγ*^{null} mouse model to evaluate vaccine safety and further study osteoarticular brucellosis.

2.2. Introduction

Brucellosis is a zoonotic disease caused by gram-negative facultative intracellular bacteria of the genus *Brucella* (75). Among the 12 species currently recognized, *B. abortus* (cattle), *B. melitensis* (goats and sheep), *and B. suis* (swine) are the most pathogenic to humans, with more than half a million new cases of human brucellosis reported annually (6). In animals, brucellosis is usually manifested as infertility and abortions in females and epididymitis in males (19, 62). In humans, acute brucellosis is frequently associated with non-specific clinical signs including undulant fever, headache, sweating, and joint pain requiring long-term antibiotic treatment (24). Clinical signs of chronic infection include endocarditis, orchitis, neurological disorders, and hepatitis (76, 77). Infection in humans occurs through contact with infected animals and animal products (17) with a very low number (10-100 CFU) of microorganisms required to induce infection (78). It is well accepted that vaccination is one of the most effective approaches to control brucellosis in animals (79). However, currently available

vaccines are not suitable for human use and can induce undesirable side effects in livestock including residual virulence in pregnant animals leading to abortion and shedding of the organism in milk (80). Osteoarticular brucellosis in humans has been reported in 40-80% of infected patients and is the most common complication of *Brucella* infection (37, 38, 81). Peripheral arthritis, sacroiliitis, and spondylitis are the three most commonly reported predilection sites (38, 48) and people of all ages are susceptible in both acute and chronic cases (82). The mechanism driving osteoarticular tropism by *Brucella* species remains unknown, due in part to the lack for many years of an animal model to study *Brucella*-induced osteoarticular disease. Immunocompetent mice have proven to be a valuable tool for understanding basic host-agent interactions during *Brucella* infection (59, 83). However, arthritis is not typically manifested in this host species, and in the few cases observed, osteoarticular damage can take up to 6 months to develop, making it very challenging to use these mice to study this process (59). Recently, immunocompromised mice including IFN-$\gamma^{-/-}$, CXCR2$^{-/-}$, IL-1R$^{-/-}$ have been used to study osteoarticular brucellosis (57, 58). However, only wild type *B. melitensis* 16M and *B. abortus* 2308 were able to induce pathological changes. Although, RB51 is known to cause infection in humans (80), development of osteoarticular disease was not evident using these models (57). Therefore, an animal model that is highly sensitive to develop osteoarticular disease would be invaluable to screen potential side-effects associated with live attenuated vaccines.

The aim of this study was to investigate the suitability of the NOD.Cg-*Prkdc*^{scid}*Il2r*γ^{tm1Wjl}*/SzJ* (NOD-*scid IL2r*γ^{null}, NSG) mouse as an improved method to

further evaluate the safety of potential vaccine candidates. NSG mice are characterized by the lack of functional mature T and B lymphocytes, natural killer cells, and dendritic cells; undetectable hemolytic complement activity; and severe impairment in cytokine signaling due to a defect in the IL-2 receptor gamma chain (84), which makes them highly susceptible to infection by *Brucella* spp. Further, NSG mice can also be used as a humanized mouse model (84-86) to study host-pathogen interactions and mechanism of diseases following human cell transplantation. For this study, we utilized the vaccine candidate *B. abortus* S19*ΔvjbR* that was designed in our laboratories by deletion of the LuxR-like transcriptional regulator *vjbR* gene, which is essential for intracellular survival and virulence in mice (61, 87, 88). Prior *in vitro* and *in vivo* studies have noted that *B. abortus* S19*ΔvjbR* is highly attenuated and confers a significant level of immune protection (61, 87). In the current study, we have investigated NSG mice as a model to determine if there are any potential side effects associated with vaccination when using live attenuated vaccine candidates in immunocompromised individuals like in pregnancy, chronic infections, childhood and aging.

2.3. Results

2.3.1. Clinical manifestation and survival of NSG mice infected with *B. abortus* S19 and *B. abortus* S19*ΔvjbR*

NSG mice were inoculated intraperitoneally (i.p.) with different doses ranging from $1x10^4$ to $1x10^6$ CFU/mouse of either 1) *B. abortus* S19, 2) *B. abortus* S19*ΔvjbR*, or 3) PBS alone. All animals were monitored daily for the development of any adverse

effects associated with vaccination (Table 2.1). Interestingly, only mice infected with S19 developed clinical signs that started approximately 7 weeks post-inoculation and consisted of hunched posture, ruffled coat, malaise, hypothermia, and weight loss. By 10 weeks (73 days) post-inoculation, 40% of the mice infected with $1x10^4$ and $1x10^6$ CFU/mouse *B. abortus* S19 were euthanized due to the severity of clinical signs (Fig. 1), with remaining 60% mice euthanized at week 13 (90 days) and week 12 (86 days) post-inoculation, respectively. All mice receiving $1x10^5$ CFU/mouse of *B. abortus* S19 required euthanasia at week 12 (87 days) post-inoculation. Interestingly, none of the mice inoculated with *B. abortus* S19*ΔvjbR* developed clinical signs ($P < 0.001$) and exhibited a 100% survival rate (Fig. 2.1). These results confirm that *B. abortus* S19*ΔvjbR* is safer in NSG immunocompromised mice compared to *B. abortus* S19.

2.3.2. NSG mice inoculated with *B. abortus* S19 but not with *B. abortus* S19*ΔvjbR* developed hypothermia

To determine whether inoculation with *B. abortus* S19 and *B. abortus* S19*ΔvjbR* induced body temperature fluctuations in NSG mice as a correlate of the severity of infection, mice were monitored daily for the duration of the experiment. Basal pre-inoculation body temperatures ranged from 36.3°C to 37.8°C. Mice inoculated with *B. abortus* S19 developed significant hypothermia from week 7 onwards ($P<0.001$) when compared to the basal level, and was used as an indicator for early euthanasia (Fig. 2.2 panels A-C). Mice inoculated with *B. abortus* S19*ΔvjbR* (Fig. 2.2 panels D-F) or PBS (Fig. 2.2 panel G) did not show any significant changes in body temperature throughout

the study. Similar results have been previously observed in IRF-1-/- mice inoculated with *B. abortus* S19*ΔvjbR* (89).

2.3.3. NSG mice inoculated with *B. abortus* S19 but not with *B. abortus* S19*ΔvjbR* demonstrated weight loss

Body weight was monitored daily for the duration of the experiment. Except one animal from 10^4 dose group, all mice inoculated with *B. abortus* S19 at $1x10^5$ and $1x10^6$ CFU/mouse exhibited a substantial decrease in body weight (Fig. 2.3 panels A-C) in a dose-dependent manner and was associated with high bacterial colonization ($*P < 0.05$). No significant differences in body weight were noted for mice inoculated with *B. abortus* S19 at $1x10^4$ CFU/mouse, *B. abortus* S19*ΔvjbR*, or the control group (Fig. 2.3 panels D-G).

2.3.4. *B. abortus* S19 inoculated NSG mice depicted high bacterial colonization and inflammatory response

The extent of bacterial colonization of different organs was evaluated to determine if the degree of colonization was correlated with the manifestation of clinical signs as well as the induction of an inflammatory response. Spleens, livers, and lungs were collected at different time points, weighed, and homogenized in 1 ml PBS, and bacterial colony-forming units (CFU) determined by plating onto TSA media. Mice inoculated with *B. abortus* S19, regardless of the dose, exhibited an overwhelming bacterial burden in the spleen, liver, and lung. In contrast, mice inoculated with

S19*ΔvjbR* exhibited significantly less bacterial growth ($P < 0.05$) in the spleen (except 10^4 dose), liver, and lung (Fig. 2.4 panels C-E). Mice inoculated with *B. abortus* S19 also developed splenomegaly with a significant increase in spleen weight ($P < 0.05$), whereas mice inoculated either with *B. abortus* S19*ΔvjbR* or PBS had no changes in splenic weight (Fig. 2.4 panel A). None of the groups showed a significant difference in liver weight (Fig. 2.4 panel B).

2.3.5. Evaluation of pathological changes in NSG mice following *Brucella* inoculation

To determine the extent of any gross and histologic changes, a full post-mortem examination was performed in all *Brucella* inoculated mice. Gross changes were most prominent in the tail, spleen, and liver of mice inoculated with *B. abortus* S19. *B. abortus* S19 inoculated mice developed swelling and deviation of the tail vertebrae (Fig 2.5 panel A). The spleens were markedly pale and enlarged, and the livers were pale. Interestingly, NSG mice inoculated with S19*ΔvjbR* or PBS did not show any apparent gross changes. Histologically, all mice inoculated with *B. abortus* S19 demonstrated severe inflammation of the tail in a dose-dependent manner characterized by the presence of large numbers of macrophages and neutrophils and massive bone resorption, and intervertebral disk erosion with fibrosis (Fig. 2.5 B bottom panel 40X magnification). As expected, due to their immune compromised status of NSG mice, the spleen of PBS group did not exhibit normal architecture or well-defined white and red pulp with lack of lymphoid follicle formation (Fig. 2.6 panel A 40X magnification).

Interestingly, the spleen from *B. abortus* S19 group had a marked histiocytic and granulomatous splenitis (Fig. 2.6 A bottom panel 40X magnification) associated with bacterial colonization (Fig. 2.6 B bottom right panel). Livers exhibited a multifocal, random histiocytic hepatitis with the presence of microgranulomas (Fig. 2.7 A bottom panel 60X magnification) associated with bacterial colonization (Fig. 2. 7 B bottom panel). In contrast, mice inoculated with *B. abortus* S19*ΔvjbR* did not show any significant changes in bone pathology, except with the presence of scattered neutrophils observed in the medullary cavity (Fig. 2.5 B middle panel 40X magnification). The spleens of S19*ΔvjbR* group exhibited mild neutrophilic infiltration (Fig. 2.6 panel A 40X magnification) associated with the presence of bacterial colonies (Fig. 2.6 panel B) but in lesser numbers compared to *B. abortus* S19. No histologic changes were observed in the liver of S19*ΔvjbR* (Fig. 2.7 A middle 40X magnification).

2.3.6. Identification of *Brucella* in NSG mouse tissues via immunohistochemistry (IHC), immunofluorescence (IF), and fluorescent *in situ* hybridization (FISH) techniques

In order to identify the distribution of *Brucella* antigen in different tissues, immunohistochemical analysis was performed using brightfield (Fig. 2.8 panel A) and fluorescence microscopy (Fig. 2.8 panel B). Formalin-fixed paraffin-embedded tissue sections (FFPE) were immunolabeled with polyclonal rabbit anti-*Brucella abortus* primary antibody. The tail vertebrae from mice inoculated with *B. abortus* S19 demonstrated positive, strong immunostaining scattered throughout the section.

Distribution of *Brucella* antigen in the medullary cavity, subchondral bone, and within necrotic areas was evident (Fig. 2.8 A bottom panel). In contrast, only one of five mice inoculated with $1x10^6$ CFU/mouse of *B. abortus* S19*ΔvjbR* demonstrated a weak positive signal of *Brucella* antigen in the tail vertebrae, while the remaining mice had no detectable immunoreactive signal (Fig. 2.8 A middle panel). As an alternative with increased sensitivity and specificity of IHC, we performed immunofluorescence staining (90) of *Brucella* antigen that further supported *Brucella* distribution of antigens in the tail of S19 or S19*ΔvjbR* inoculated mice (Fig. 2.8 B middle and bottom panel). In addition, fluorescent *in situ* hybridization using a Bru-996 Alexa-flour 555 labeled DNA probe, that specifically hybridizes *Brucella* 16S rRNA, confirmed *B. abortus* S19 distribution within the lesions (Fig. 2.8 panel C).

2.3.7. *B. abortus* S19 colonizes osteoclasts in NSG mice

IHC and IF staining demonstrated the abundance of *Brucella* antigen in multinucleated osteoclasts (arrow) and to a lesser degree in other cell types as well as in extracellular space surrounding the affected area in *B. abortus* S19 inoculated mice (Fig. 2.8 A and B bottom panel). To further confirm the association of *Brucella* with osteoclasts, a double immunofluorescence staining (91) was performed on paraffin sections of tail vertebrae to simultaneously identify osteoclasts and *Brucella*. As osteoclasts express a high level of the enzyme cathepsin K (92), a polyclonal rabbit anti-cathepsin K primary antibody was used to identify osteoclasts along with using polyclonal rabbit antibody against *Brucella* for *Brucella* identification. Using

fluorescently labeled secondary antibodies, we demonstrated that *Brucella* co-localized with osteoclasts (Fig. 2.9 panel A). The colocalization of *Brucella* in different depth of osteoclast was analyzed by using confocal microscopy. Confocal images of Z sectioning demonstrated *Brucella* distribution at various cellular depths inside these cells (Fig. 2.9 panel B). The right panel indicated color intensity plot of *Brucella* distribution throughout the section. Quantitative analysis of the different depth of Z sections revealed a maximum density of *Brucella* in the center of osteoclasts (Fig. 2.9 panel C). When we compared fluorescence intensity, *B. abortus* S19*ΔvjbR* signal was significantly less ($P<0.001$) than *B. abortus* S19 (Fig. 2.9 panel D).

Table 2.1 Clinical manifestation of brucellosis in NSG mice.

	Naive	**S19**	**S19*ΔvjbR***
Body temperature	Normal	Hypothermia	Normal
Body weight	Gain	Loss	Gain
Splenomegaly	No	Yes	No
Bacterial load	No	High	Low
Osteoarticular changes	No	Major	Minor
Splenic changes	No	Major	Minor
Hepatic changes	No	Major	Minor

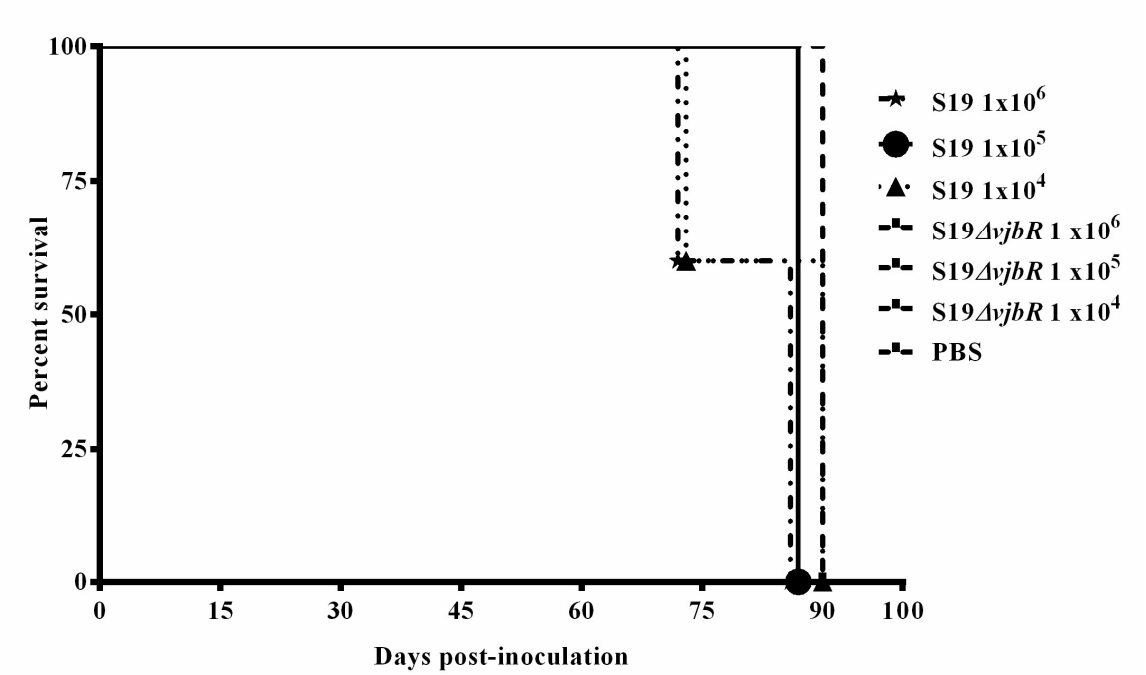

Figure 2.1 Survival profile of NSG mice. Mice were inoculated intraperitoneally with either *B. abortus* S19 or *B. abortus* S19*ΔvjbR* at various doses (1 X 10^4, 1 X 10^5, and 1 X10^6 CFU/mouse) or with PBS. Mice inoculated with PBS or the *B. abortus* S19*ΔvjbR* vaccine candidate survived (100%) longer than mice inoculated with *B. abortus* S19. Reprinted from [138].

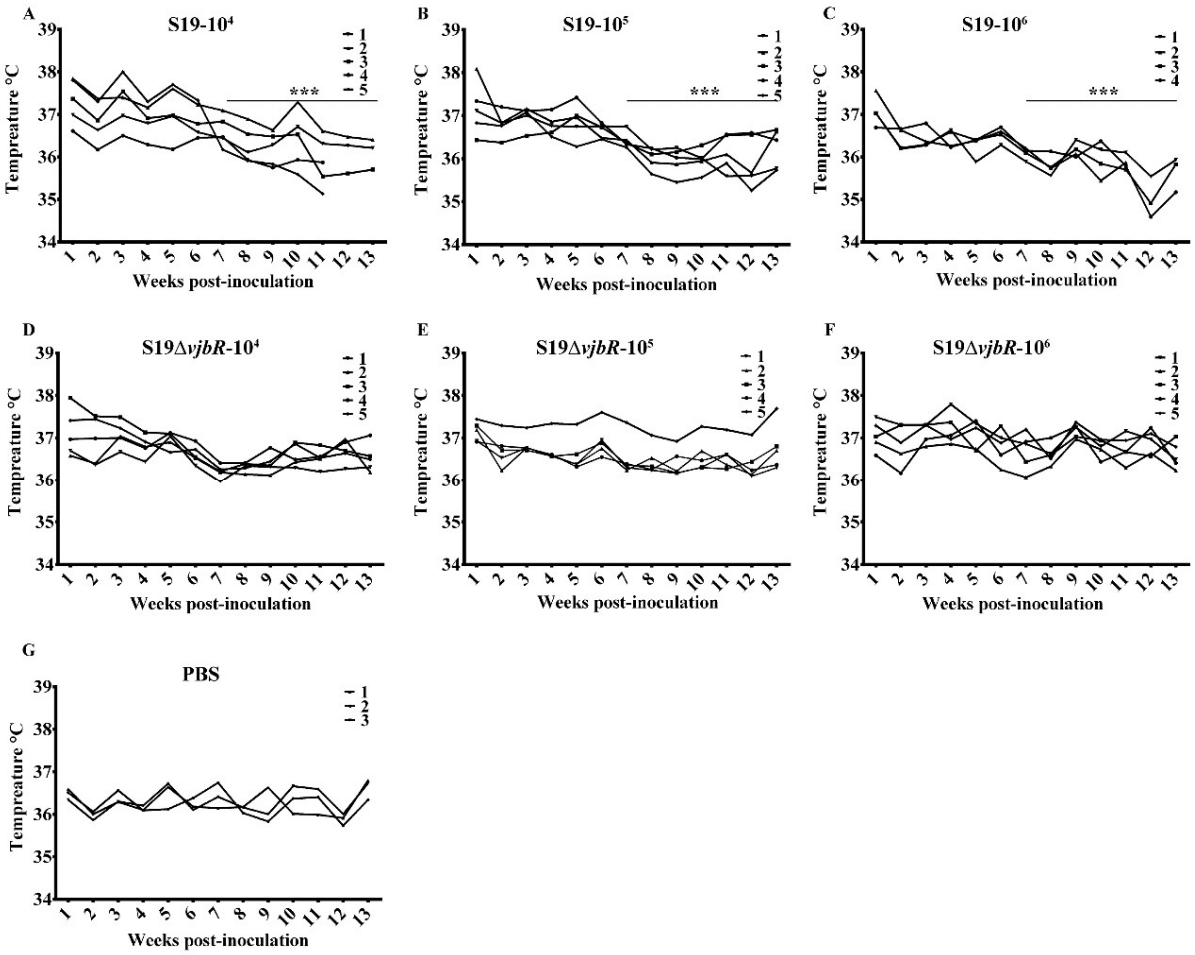

Figure 2.2 Temperature profiles of NSG mice inoculated with *Brucella abortus*. Mice were implanted with transponders, and body temperature was monitored every day over a period of 13 weeks following inoculation (i.p.) with *B. abortus* S19, the *B. abortus* S19*ΔvjbR* vaccine candidate, or PBS, as indicated. No significant changes in body temperature were observed ($P > 0.05$) over time in mice inoculated with *B. abortus* S19*ΔvjbR* or PBS. However, mice inoculated with different doses of *B. abortus* S19 demonstrated a gradual reduction in body temperature (hypothermia) that reached a significant level from week 7 onwards (***, $P < 0.001$). Doses are indicated such that S19-104, for example, indicates 1 X 10^4 CFU/mouse of *B. abortus* S19. Reprinted from [138].

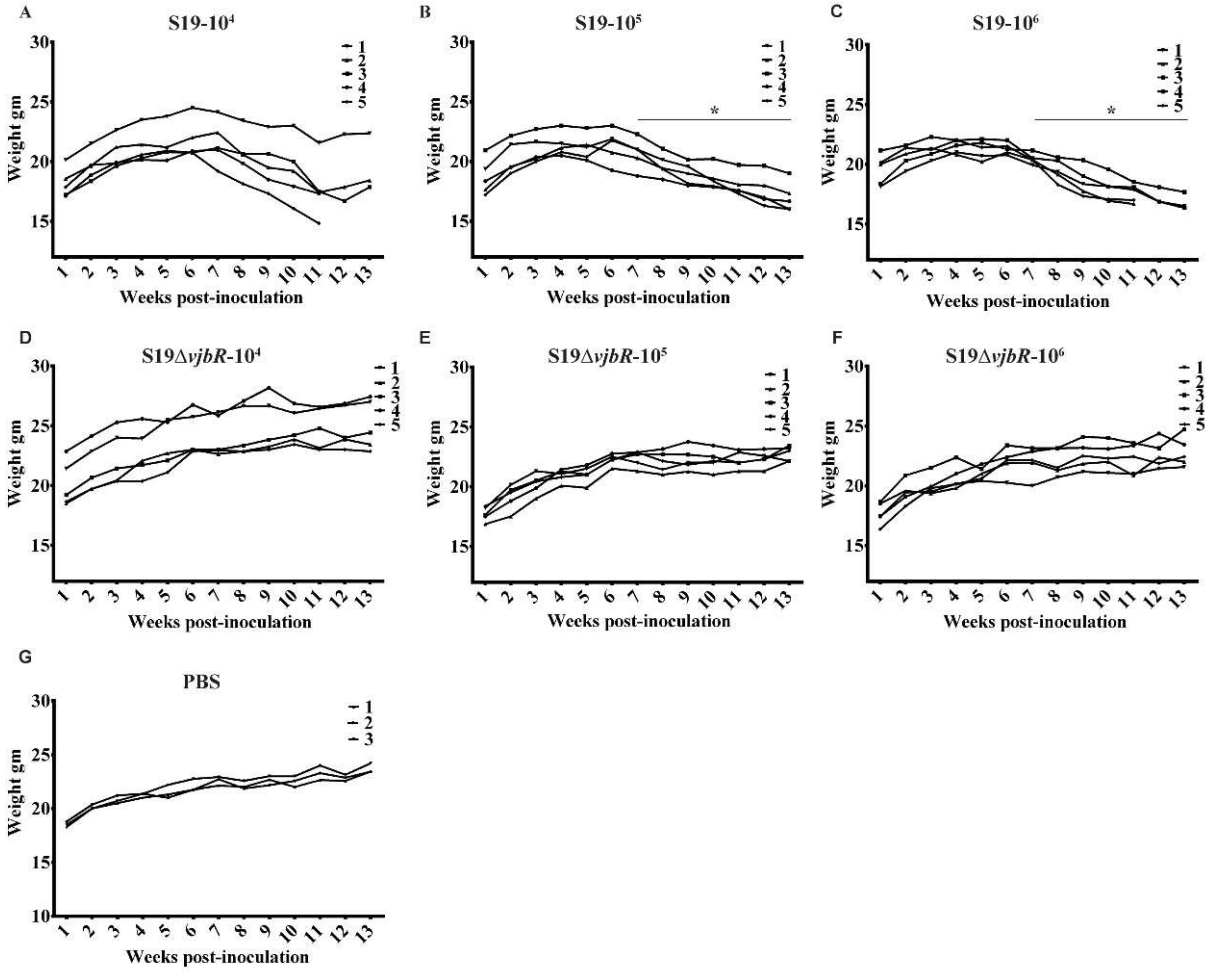

Figure 2.3 Body weight profiles of NSG mice inoculated with attenuated *Brucella abortus*. Body weight was monitored over a period of 13 weeks post-inoculation with 1 X 10^4, 1 X 10^5, and 1 X 10^6 CFU/mouse of either *B. abortus* S19 or the *B. abortus* S19*ΔvjbR* vaccine candidate or with PBS, as indicated. Mice inoculated with 1 X 10^5 and 1 X 10^6 CFU/mouse of *B. abortus* S19 demonstrated significant weight loss by 13 weeks. *, $P < 0.05$. Reprinted from [138].

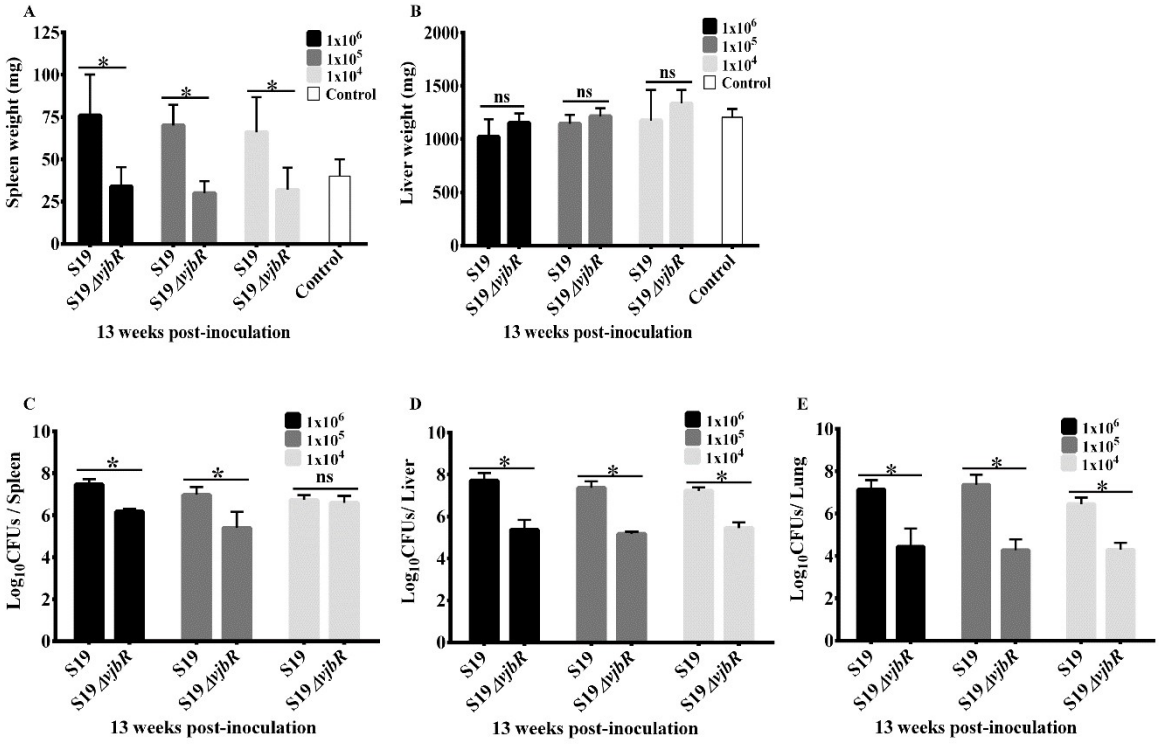

Figure 2.4 Organ weight and bacterial colonization of NSG mice inoculated with *Brucella*. Mice inoculated (i.p.) with *B. abortus* S19 showed a significant increase in spleen weight compared with mice inoculated with the *B. abortus* S19*ΔvjbR* vaccine candidate (A), while there was no significant difference in liver weights in mice inoculated with *Brucella* or PBS (B). Mice inoculated with *B. abortus* S19*ΔvjbR* had significantly reduced bacterial burdens in spleen (C), liver (D), and lung (E) compared to those in the *B. abortus* S19-inoculated group. *, $P < 0.05$; ns, not significant. Reprinted from [138].

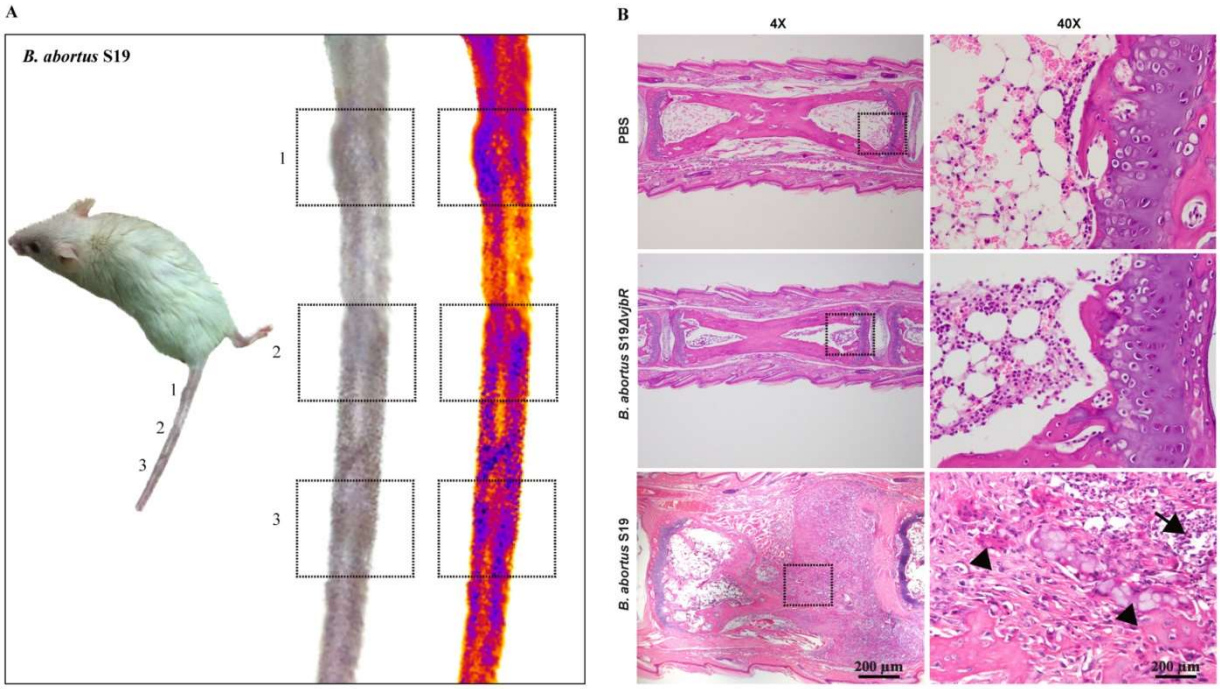

Figure 2.5 Gross image and tail histopathological image from NSG mice inoculated with PBS, *B. abortus* S19*ΔvjbR* (1 X 10^6 CFU/mouse), and *B. abortus* S19 (1 X 10^6 CFU/mouse), as indicated. (A) Representative image of NSG mouse inoculated with *B. abortus* S19 demonstrates inflammation in tail vertebrae. The magnified tail region with or without artificial coloring clearly demonstrates the regions of inflammation or bone damage (boxed selections). (B) Representative images of bone histopathology at low and high magnifications. Magnified images at right correspond with the boxed sections in the left panel. Top and middle panels depict intact bone mass and cartilage with normal appearance. Infection with *B. abortus* S19 induced severe bone resorption and destruction of the intervertebral discs which were replaced by fibrous connective tissue (bottom panel). Magnified images in the bottom right panel show neutrophil and macrophage infiltration (arrows) and activation of osteoclasts (arrowhead). Reprinted from [138].

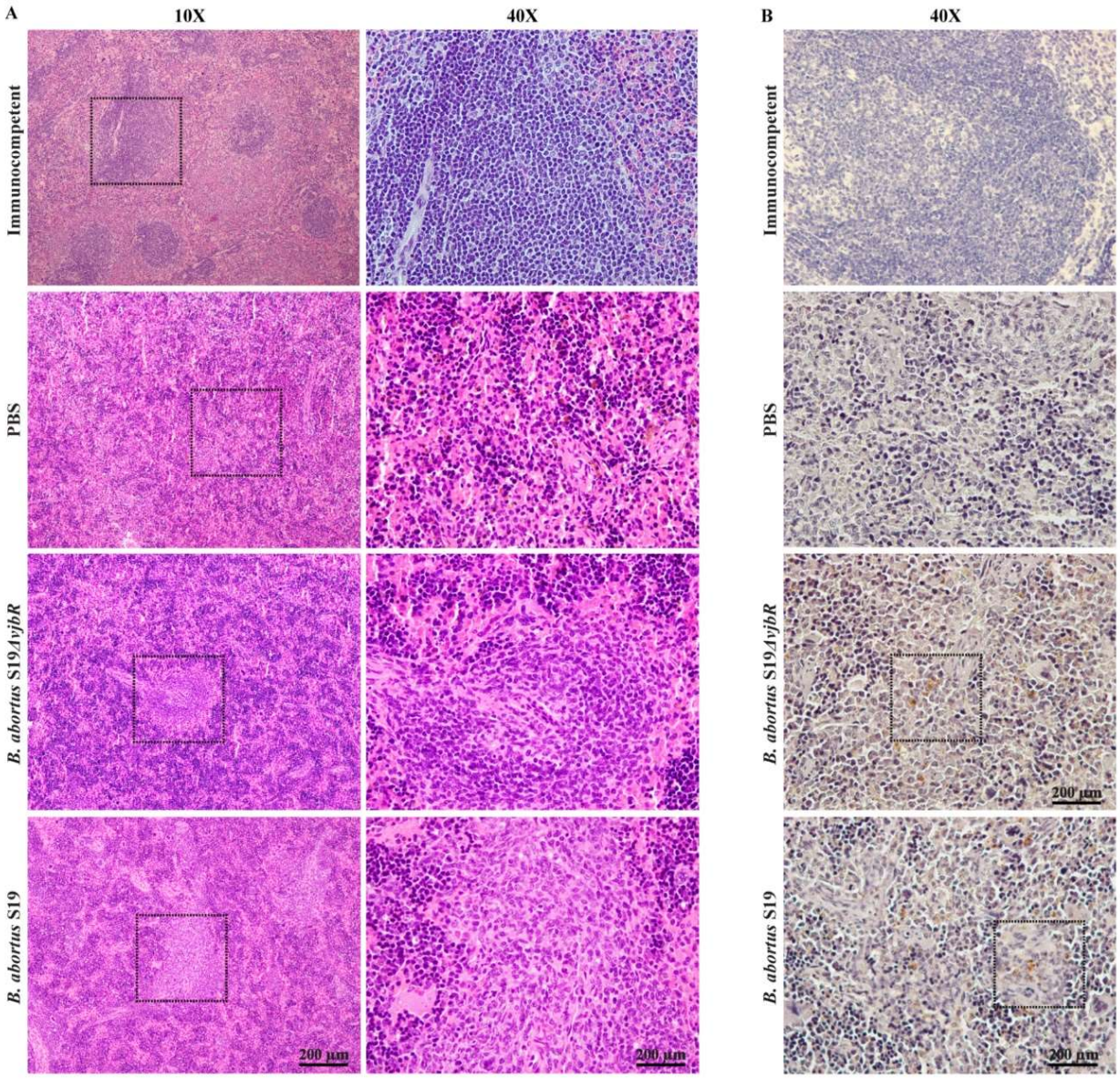

Figure 2.6 Representative images of histopathology of spleen. (A) Representative bright-field image of spleen from immunocompetent mice (top) and from NSG mice inoculated with PBS, *B. abortus* S19*ΔvjbR* (1 X 10^6 CFU/mouse), and *B. abortus* S19 (1 X 10^6 CFU/mouse), as indicated. Images at right are magnifications of the boxed sections in the left panels. Mice infected with *B. abortus* S19 exhibited multifocal neutrophilic and histiocytic splenitis in contrast to mild neutrophilic and histiocytic splenitis in *B. abortus* S19*ΔvjbR*-inoculated mice. (B) Immunohistochemical localization of *Brucella* in mouse spleen (boxed). Reprinted from [138].

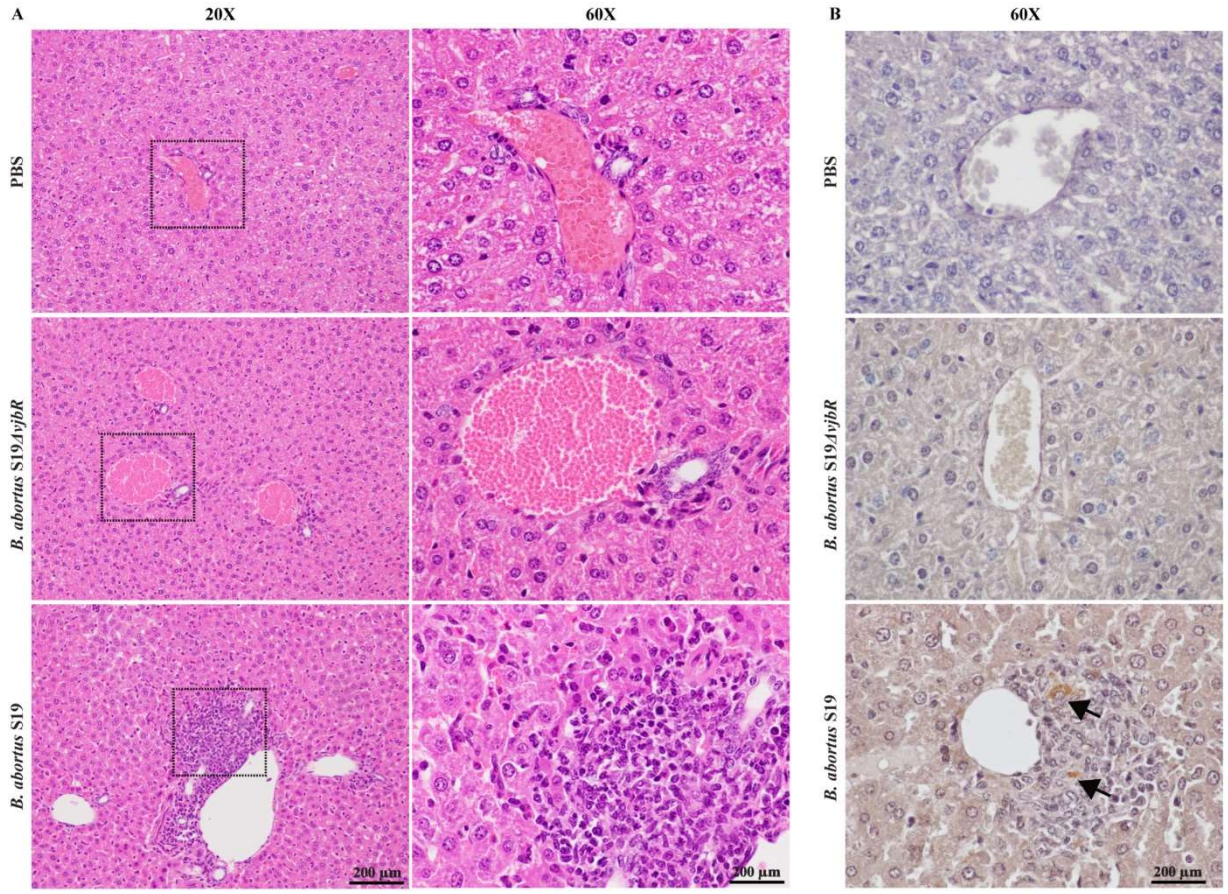

Figure 2.7 Representative images of histopathology of liver. (A) Representative bright-field image of liver from NSG mice inoculated with PBS, *B. abortus* S19*ΔvjbR* (1 X 10^6 CFU/mouse), and *B. abortus* S19 (1 X 10^6 CFU/mouse), as indicated. Images at right are magnifications of the boxed sections in the left panel. Animals infected with *B. abortus* S19 exhibited neutrophilic and histiocytic infiltration. None of the NSG mice inoculated with *B. abortus* S19*ΔvjbR* or PBS showed remarkable lesions. (B) Immunohistochemical localization of *Brucella* in mouse liver (arrows). Reprinted from [138].

Figure 2.8 Immunohistochemical, immunofluorescence, and fluorescence *in situ* hybridization (FISH) analysis of *Brucella* in paraffin sections of tail vertebrae. (A) Representative immunohistochemical images of tail vertebrae of NSG mice inoculated with PBS, *B. abortus* S19*ΔvjbR* (1 X 10^6 CFU/mouse) and *B. abortus* S19 (1 X 10^6 CFU/mouse). *B. abortus* S19-inoculated mice exhibited widely distributed *Brucella* antigens (brown) in the osteoarticular lesions, with the highest concentration in the osteoclasts (arrowhead). Only one mouse inoculated with 1 X 10^6 CFU/mouse of *B. abortus* S19*ΔvjbR* exhibited positive staining for *Brucella* (arrows). (B) Representative immunofluorescence images of tail vertebrae of NSG mice inoculated with PBS, *B. abortus* S19*ΔvjbR* (1 X 10^6 CFU/mouse), and *B. abortus* S19 (1 X 10^6 CFU/mouse). *B. abortus* S19-inoculated mice exhibited strong positive signal for *Brucella* antigens (green) that widely spread in the area of inflammation and osteoclasts (arrowheads), whereas NSG mice inoculated with *B. abortus* S19*ΔvjbR* exhibited a faint signal of *Brucella* antigens in few places (arrows). (C) Representative FISH image reveals hybridization of *Brucella*-specific Bru-996 Alexa Fluor-labeled DNA probe of the 16S rRNA gene with *B. abortus* S19 (red) in tail vertebral sections. Images at right are magnifications of the boxed sections in the left panel. Reprinted from [138].

Figure 2.8 Continued

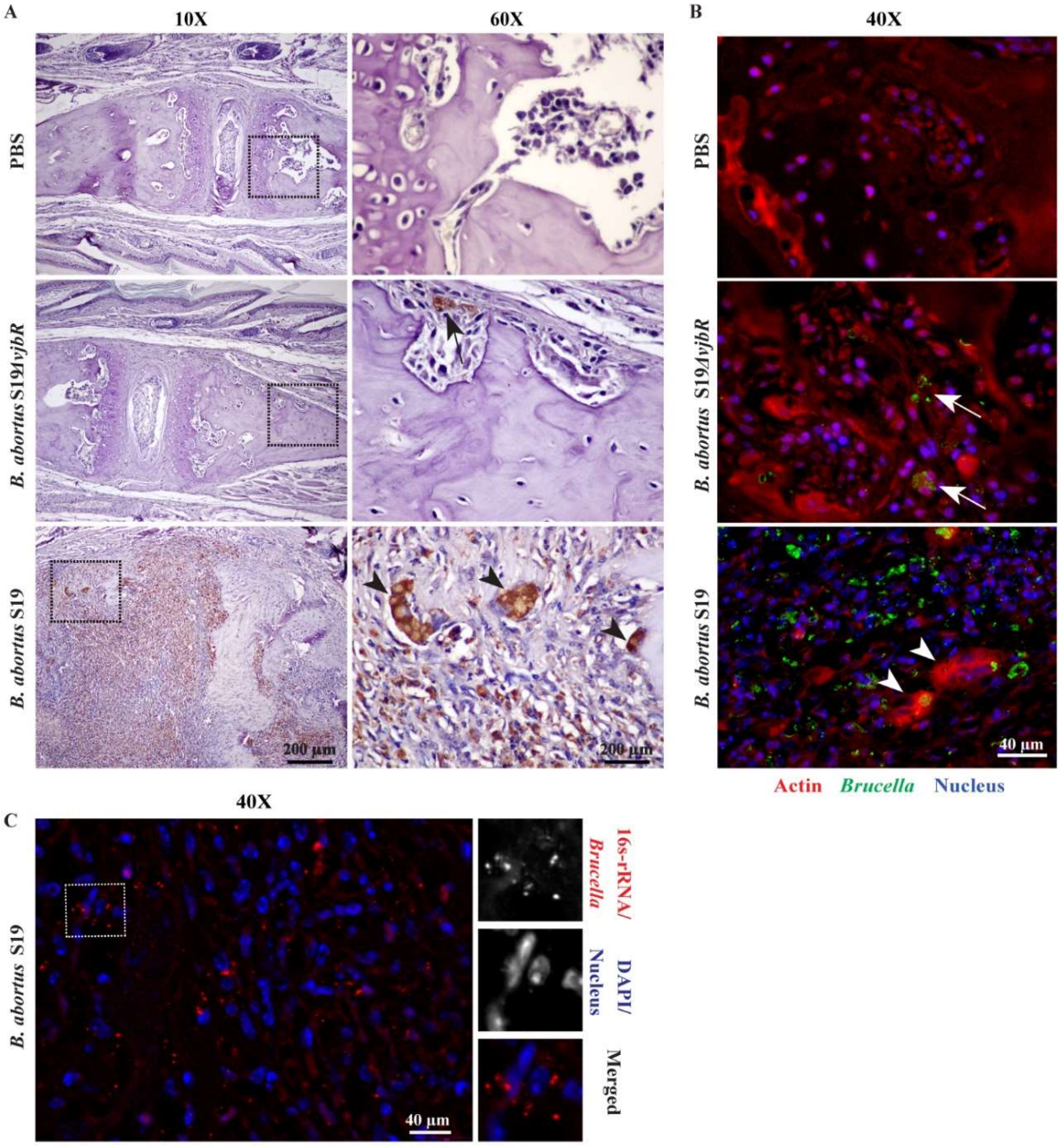

Figure 2.9 *Brucella* colonization in osteoclasts. (A) Representative immunofluorescence image of tail vertebrae of *B. abortus* S19-inoculated mice (1 X 10^6 CFU/mouse) demonstrated colocalization (yellow) of *Brucella* antigen (green) with the osteoclast marker cathepsin (red signal). Images at right are magnifications of the boxed section in the left panel. (B) Representative confocal immunofluorescence images showing a large number of *B. abortus* S19 bacteria (green) inside osteoclasts. The fluorescence intensity plot profile in the right panel corresponds with the images in the left panel. (C) Z sectioning shows *Brucella* localization in different depths of the osteoclast. AU, arbitrary units. (D) Quantitative image analysis shows a significant decrease (***, $P < 0.001$) in *Brucella* colonization in the *B. abortus* S19*ΔvjbR*-inoculated group compared with that in the *B. abortus* S19-inoculated group, as reflected in total pixel intensity. Reprinted from [138].

Figure 2.9 Continued

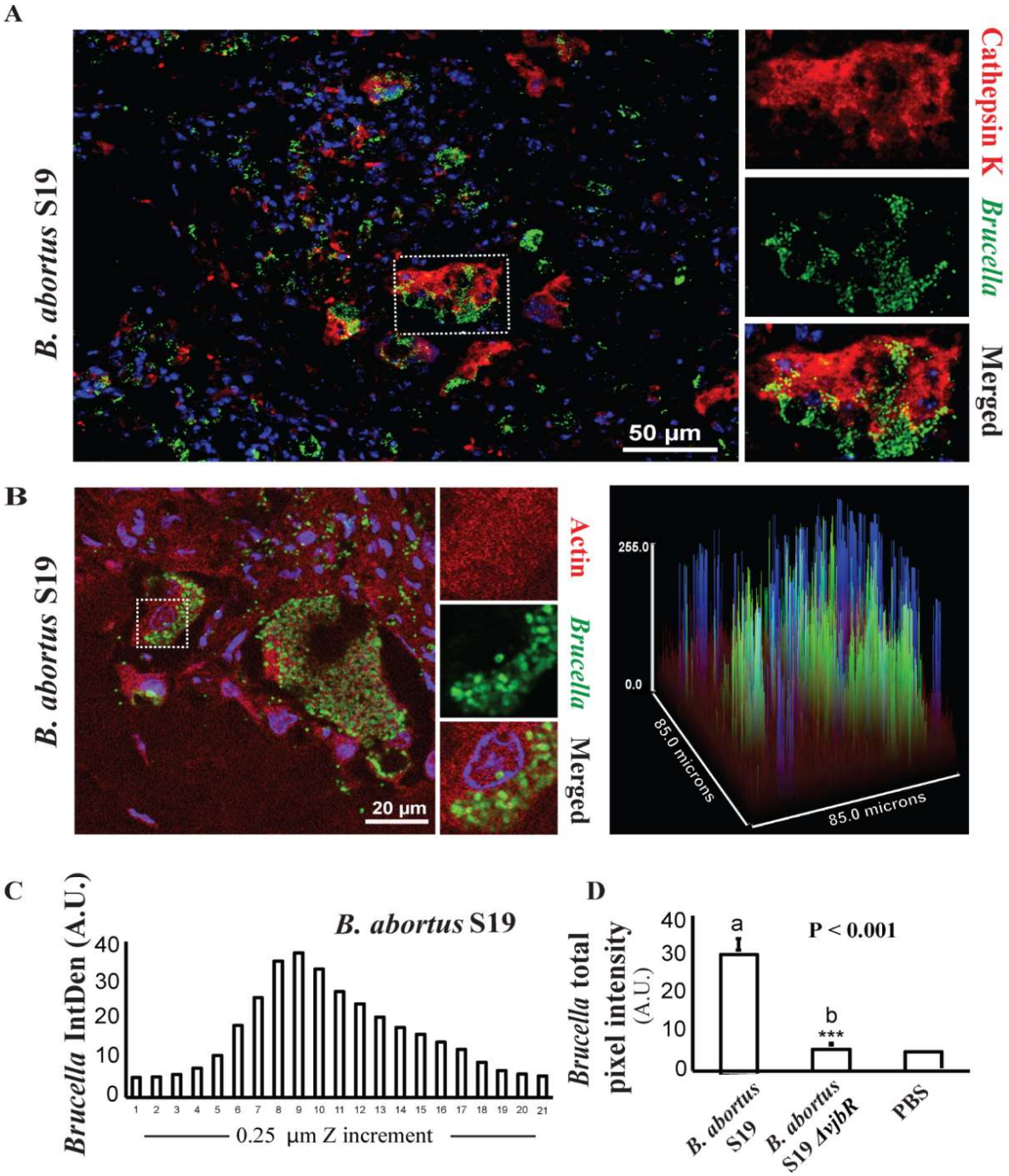

2.4 Discussion

Brucellosis is one of the most common worldwide bacterial zoonotic diseases where osteoarticular complications may rise up to 80% in human cases (37, 38). The study of *Brucella*-induced osteoarthritis has been challenging due to the lack of suitable laboratory animal model as well as the impracticality of using natural hosts. Although few mice models (IFN-$\gamma^{-/-}$, CXCR2$^{-/-}$, IL-1R$^{-/-}$) have been used to understand the mechanism of osteoarticular brucellosis, they required either virulent BSL3 *Brucella* strain to induce detectable bone damage or injection directly into the joints (57-59). The development and characterization of NSG immunocompromised mouse bearing a mutated IL-2 receptor gamma chain (IL2ry^{null}) have facilitated its use as humanized mouse model to study human hemopoietic stem cells engraftment and infectious diseases caused by Epstein Barr virus, Dengue virus, *Salmonella typhi*, and *Plasmodium falciparum* (85, 93-98).

In the present study, we sought to investigate the potential of using NSG mouse model as a means to study the side effects (if any) associated with vaccination and its use to study osteoarticular brucellosis. The currently available *B. abortus* S19 vaccine, which is essential for the control of bovine brucellosis, is a live attenuated vaccine that is not suitable for use in humans (99) due to its known side effects. Very recently Xie et. al., in their meta-analysis have clearly shown various adverse effect associated with the existing licensed *Brucella* vaccines including *Brucella abortus* S19, *Brucella melitensis* Rev1, and *Brucella abortus* RB51. Some of these adverse effects associated with *Brucella abortus* S19 vaccination include arthropathy, arthralgia and myalgia (100). As a

control, we utilized *B. abortus* S19 vaccine to compare with our vaccine candidate *B. abortus* S19*ΔvjbR*. The present study demonstrated that within 13 weeks of *B. abortus* S19 vaccine strain inoculation, NSG immunocompromised mice had to be euthanized due to overwhelming infection. Mice developed gross and histopathological changes and osteoarticular lesions resembling chronic human brucellosis, making it a suitable model not only to study vaccine safety but also osteoarticular brucellosis. NSG mice inoculated with *B. abortus* S19 displayed signs of illness, low survival rate, splenomegaly and high bacterial loads in the spleen, liver, and lung. It is well known that *Brucella* has a tropism to reticuloendothelial tissues such as spleen and liver (101). The high bacterial colonization was associated with marked histiocytic and neutrophilic inflammation which are typically observed in patients with brucellosis (23, 102-106). In contrast, NSG mice inoculated with the vaccine candidate *B. abortus* S19*ΔvjbR* exhibited milder clinical and pathological changes associated with *Brucella* infection, indicating that the *B. abortus* S19*ΔvjbR* vaccine seems to be a safer choice. These support our previous findings that demonstrated the safety of *ΔvjbR* mutant in wild type and IRF-1-/- mice (61, 87, 89).

The previous study showed that NSG mice are not capable of inducing an inflammatory immune reaction against infectious agents (107). Interestingly, in spite of having decreased immunity, NSG mice were capable of mounting inflammation against *Brucella* infection in this study. This may attribute to the presence of neutrophils, monocytes, macrophages, and dendritic cells in NSG mice (84). Taken together, this suggests that the NSG mouse model might be a more sensitive predictor of vaccine

safety for brucellosis, especially in immunodeficient individuals. The most frequent clinical sign associated with brucellosis in humans is undulant fever and weight loss (24, 62). Fever or hyperthermia is a physiological response to an inflammatory process and infection which aims to enhance host survival (108). In this study, NSG mice inoculated with *B. abortus* S19 showed a decrease in body temperature or hypothermia, which is considered as a sign of septicemia and poor health condition (109-111). In mice, interestingly, the vaccine strain *B. abortus* S19*ΔvjbR* did not induce hypothermia in NSG mice which is similar to what we have been previously reported (89). While normal weight gain is considered as a sign of the healthy animal, weight loss is considered as a sign of disease (9, 62). In this study, weight loss was recorded in the *B. abortus* S19-infected NSG mice in a dose-dependent manner, however, this was not the case in NSG mice infected with *B. abortus* S19*ΔvjbR* vaccine candidate. This corroborates that *B. abortus* S19*ΔvjbR* vaccine seems to be safer than *B. abortus* S19.

Once the clinical signs of brucellosis were characterized we focused our attention to the bone lesions as well as immunolocalization of bacterial antigen in the affected areas (112). Although a recent report demonstrated that NSG mice have a mild reduction in trabecular bone mass, they do not display any apparent abnormalities in bone development or bone homeostasis (113). Grossly and histologically we found that the bones in NSG mice are normal despite their immune status. In the present study, NSG mice infected with *B. abortus* S19 developed severe diskospondylitis which is a common finding in the chronic-form of *Brucella*-infected patients (112). Importantly, when animals inoculated with vaccine candidate *B. abortus* S19*ΔvjbR*, no arthritic lesions

were observed. Importantly, *Brucella* antigen distribution as demonstrated by immunohistochemistry, immunofluorescence and FISH techniques revealed a direct relationship of bacterial virulence with pathological changes in the affected tissues. This suggests that the severity of bone damage is not only dependent on inflammatory cell response but also the concentration of *Brucella* antigen. Indeed, *B. abortus* S19 infected NSG mice showed a dose dependent increase in antigen accumulations and damage in the tail.

Brucella as an intracellular pathogen resides insides phagocytic and nonphagocytic cells (114). Confocal microscopy revealed that although *B. abortus* S19 was located both extracellularly and intracellularly, large numbers of bacteria were observed inside mature osteoclasts at different cellular depths. Osteoclasts are multinucleated bone-resorbing cells that differentiate from monocyte/macrophage lineage under the effect of two osteoclastogenic cytokines that are required for their survival and differentiation; receptor activator of nuclear factor kB (NF-kB) ligand (RANKL) and macrophage colony-stimulating factor (MCSF) (115-118). Osteoclasts degrade bone matrix through secretion of several osteolytic enzymes and acids that solubilize bone components (119, 120), and previous studies have reported that activated osteoclasts play a pivotal role in bone destruction, such as an inflammatory bone loss and rheumatoid arthritis (121). In light of the significant bone destruction observed in NSG mice, it is possible that *Brucella* may use these cells as a replicative niche to spread or sustain the infection. Therefore, future studies are required to investigate whether

mature osteoclasts are involved in *Brucella* infection and therefore the progression of *Brucella*-induced bone destruction.

Collectively our results revealed that NSG mice can be used as a more sensitive tool to study potential side effects associated with vaccination of live attenuated vaccine candidates. Interestingly, we observed that it could not only be used to study a potential side effect of vaccination including osteoarticular disease but most importantly as a tool to understand host-antigen interaction that can cause bone damage. While mice inoculated with *B. abortus* S19 developed symptoms of brucellosis, S19*ΔvjbR* did not show significant clinical changes supporting the safety of the S19*ΔvjbR* vaccine candidate.

2.5. Material and Methods

2.5.1. Bacterial strains

Strains used in this experiment included *B. abortus* S19 (NVSL, Ames, IA) and *B. abortus* S19*ΔvjbR* (engineered for a previous study) (61). Tryptic soy agar (TSA; Difco, Becton Dickinson) was used to grow the bacteria at 37 °C with 5% (vol/vol) CO_2 for 3 days. Bacteria were harvested from the plates using phosphate-buffered saline (PBS), pH 7.2 (Gibco), and adjusted to a final concentration of either $1x10^4$, $1x10^5$, or $1x10^6$ CFU/0.1 ml/mouse (i.p.) based on Klett colorimeter meter reading against a standard curve. Viable counts were retrospectively confirmed by serial dilution of *Brucella* and plating onto TSA media.

2.5.2. Animal resource, housing, and care

Six to eight-week-old female NOD.Cg-*Prkdc*^{scid}*Il2rγ*^{tm1Wjl}*/SzJ* (NOD-*scid IL2rγ*^{null}, NSG) mice were obtained from The Jackson Laboratory (Bar Harbor, ME). Mice were housed under specific pathogen-free conditions and acclimated for 2 weeks prior to bacterial inoculation. All experimental procedures and animal care were performed in compliance with the institutional animal care guidelines.

2.5.3. Measurement of body temperature and body weight

Body temperature was measured as described previously (89). Briefly, implantable temperature transponders (IPTT-300) and a handheld reader (DAS-7007; Bio Medic Data Systems, DE) were used according to the manufacturer's instructions. Before bacterial inoculation, the transponders were placed subcutaneously on the left lateral side of the flank using the insertion device. The handheld reader was used to measure the body temperature by putting the detector 5 to 10 cm from the implanted chip site. The basal body temperature and body weight were recorded for each mouse for 3 days prior to inoculation and daily for the duration of the experiment.

2.5.4. Evaluation of virulence of *B. abortus* S19 and *B. abortus* S19*ΔvjbR* in NSG mice

Six groups of mice (n=5) were inoculated intraperitoneally (i.p.) with either 1) *B. abortus* S19, 2) *B. abortus* S19*ΔvjbR* or 3) PBS alone. Each group was given one of three different doses: $1x10^4$, $1x10^5$, and $1x10^6$. Mice were monitored daily for any

clinical signs associated with inoculation. Animals showing abnormal posture, reduced mobility, ruffled coat, or a body temperature below 32°C were immediately euthanized via carbon dioxide asphyxiation. At 13 weeks post-inoculation, all animals that survived were euthanized to determine bacterial burden and associated gross and histopathological findings. Spleens, livers, and lungs were collected, weighed, and mechanically homogenized in 1ml of PBS to determine colony-forming unit (CFU)/organ. 100 µl of serial dilutions of tissue homogenate were plated in duplicate on TSA medium and incubated at 37 °C for 3 days to quantify bacterial CFU.

2.5.5. Evaluation of histopathological changes in NSG mice inoculated with *B. abortus* S19 and *B. abortus* S19*ΔvjbR*

Multiple tissues were evaluated to determine histopathological changes. Spleen, liver, and bone tissues were collected and fixed in 10% neutral-buffered formalin for 5 days and then stored into 70% ethanol. Bone specimens were decalcified in 15% formic acid for approximately 3 days. Tissues were rinsed in tap water, gradually dehydrated in alcohol, cleared in xylene and embedded in paraffin. 5 µm paraffin sections were stained with hematoxylin and eosin (H&E). Histopathological changes between groups were evaluated by a board-certified veterinary pathologist.

2.5.6. Immunohistochemical detection of *B. abortus* in tissue sections

Immunohistochemistry (IHC) was performed on 5 µm thickness formalin-fixed paraffin-embedded (FFPE) tissue sections from different experimental groups. Following

deparaffinization in xylene, sections were rehydrated in multiple serial dilutions of ethanol (100-50%) and washed in distilled water. Antigen recovery was performed using sodium citrate (pH 6) at 80 °C in a water bath for 10 minutes for bone sections and for 20 minutes for the spleen and liver. Endogenous peroxidase removal was performed using BLOXALL (SP-6000, Vector Laboratories, USA) for 10 minutes followed by blocking of nonspecific binding using normal goat serum for 20 minutes at room temperature. Blocked sections were incubated with polyclonal rabbit anti-*Brucella abortus* primary antibody (1:4000) (bs-2229R, Bioss Antibodies, USA) diluted in PBS (pH 7.4) for 60 minutes at room temperature. Following 5 minutes washing in PBS-Tween-20 (PBST) (pH 7.4, 0.05% Tween-20 in 10 mM PBS), biotinylated goat anti-rabbit secondary antibody was added to the sections and incubated for 30 minutes at room temperature. Sections were then rinsed in PBST (pH 7.4) twice for 5 minutes each, followed by incubation with avidin-biotin complex for 30 minutes at room temperature (Vectastain ABC kit instructions, Vector Laboratories, USA). The color was developed using DAB substrate (BDB2004, Biocare Medical, USA) at room temperature for 3 minutes, rinsed with distilled water and counterstained with hematoxylin (Sigma-Aldrich) for 1 minute. Stained tissue sections were mounted with aqueous mounting medium and imaged using brightfield microscope.

2.5.7. Immunofluorescence and confocal microscopic analysis of *B. abortus* in tissue sections

Formalin-fixed paraffin-embedded tissue sections (5µm) of mice from different treatment groups were processed as described above. Following one-hour incubation with

polyclonal rabbit anti-*Brucella abortus* primary antibody (1:1000) (bs-2229R, Bioss Antibodies, USA) at room temperature, fluorescent-tagged goat anti-rabbit IgG H&L Alexa Flour®488 (ab150077, abcam, USA) secondary antibody (1:2000) was added to stain *Brucella*. At the same time Texas Red®-X Phalloidin (T7471, Thermo Fisher Scientific, USA) was added (1:300) to stain F-actin and incubated overnight at 4°C. Mounting media with DAPI (4′,6′-diamidino-2-phenylindole) was added for nuclear staining, and the slides were analyzed by Olympus microscope DP73 and Zeiss LSM 780 confocal microscope. Confocal Z images were collected 0.25 µm gap on a Zeiss LSM 780 confocal microscope equipped with a Plan-Apo 40×/1.40 NA oil objective. Image processing and quantitative data analysis was performed using Fiji.

Double immunofluorescence staining was also performed using polyclonal rabbit anti-cathepsin K antibody as a marker to identify osteoclasts in the tail vertebral tissue sections of mice inoculated with *B. abortus* S19. Formalin-fixed paraffin-embedded sections were deparaffinized in xylene, rehydrated with a serial dilution of ethanol alcohol (100-50%), and washed with distilled water. Antigen retrieval was achieved for 10 minutes using sodium citrate (pH 6) at 80 °C in a water bath. Tissue sections were then rinsed with PBS-Tween-20 (PBST) (pH 7.4, 0.05% Tween-20) twice for 5 minutes between each step. Normal goat serum was added for 20 minutes to block nonspecific binding. Polyclonal rabbit anti-mouse cathepsin K antibody (ab 19027 IgG, Abcam, USA) (1:200) diluted in PBS (pH 7.4) was applied overnight at 4°C. After the slides were washed with PBST twice for 5 minutes. Tissue sections then incubated with goat anti-rabbit IgG H&L Alexa Flour®555 (ab150078, Abcam, USA) fluorescent secondary

antibody (1:2000) diluted in PBS (pH 7.4) for 30 minutes at room temperature. To stain *B. abortus* antigen on the same sections using polyclonal rabbit anti-*Brucella abortus* antibody, the nonspecific binding step was repeated by adding normal goat serum and incubated for 30 minutes at room temperature, then similar IF steps that described above to identify *B. abortus antigen* were exactly followed, and the slides were analyzed by Olympus microscope DP73 using DAPI, FITIC, and TRITC filters, and Fiji software.

2.5.8. Fluorescent in situ Hybridization (FISH) to detect *B. abortus* S19 and *B. abortus* S19*ΔvjbR*

FISH was performed on 4 µM thick paraffin-embedded sections of tail vertebral tissue collected from mice inoculated with *Brucella abortus* S19 and *Brucella abortus* S19*ΔvjbR* as described previously (122). Tissue sections were deparaffinized in xylene, rehydrated in serial dilution of ethanol alcohol (100-70%), and washed in distilled water. Once the tissue sections were air-dried, DNA Bru-996-Alexa 555probe (5′ CCACTAACCGCGACCGGGATG) was added to hybridize with the bacterial 16S rRNA gene (123) at concentration 5ng/µl with hybridization buffer. For nonspecific hybridization, Non338-Alexa 555 probe (5′-CGACGGAGGGCATCCTCA) was used at the same condition (124). Hybridization was carried out in a chamber overnight at 46°C for 14 hours in hybridization buffer (20 mM Tris, 0.9 M NaCl, 0.1% SDS, and 40% formamide) pH 7.2. Then the slides were washed with washing buffer (20 mM Tris, 0.9 M NaCl) pH 7.2 at 48 °C for 20 minutes, rinsed in distilled water, and allowed to air-dry.

Anti-fade mounting media with DAPI was added (125), and the slides were analyzed with an Olympus microscope DP73 using DAPI and TRITC filters and Fiji software.

2.5.9. Statistical analysis

All data analyses were performed using the GraphPad Prisim6.0 (San Diego, CA, USA). The non-parametric two-way analysis of variance (ANOVA) test was used to compare body weight and temperature of different groups. Tukey's multiple comparisons was used to generate *P* value. Mantel-Cox test was used using GraphPad Prism 6.07 (San Diego, CA, USA) to determine significant differences of the survival curve. P values of <0.05 were considered significant.

3. INTERACTION OF *BRUCELLA ABORTUS* WITH OSTEOCLASTS: A STEP TOWARDS UNDERSTANDING OSTEOARTICULAR BRUCELLOSIS AND VACCINE SAFETY

3.1. Summary

Osteoarticular disease is a frequent complication of human brucellosis. Vaccination remains a critical component of brucellosis control but there are currently no vaccines for use in humans and no *in vitro* models for assessing safety of candidate vaccines in reference to development of bone lesions currently exist. While the effect of *Brucella* infection on osteoblasts has been extensively evaluated, little is known about the consequences of osteoclast infection. Murine bone marrow-derived macrophages were derived into mature osteoclasts and infected with *B. abortus* 2308, the vaccine strain S19, and attenuated mutants S19*ΔvjbR* and *B. abortus ΔvirB2*. While *B. abortus* 2308 and S19 replicated inside mature osteoclasts, the attenuated mutants were progressively killed, behavior that mimics infection kinetics in macrophages. Interestingly, *B. abortus* 2308 impaired the growth of osteoclasts without reducing resorptive activity while osteoclasts infected with *B. abortus* S19 and S19*ΔvjbR* were significantly larger and exhibited enhanced resorption. None of the *Brucella* strains induced apoptosis or stimulated nitric oxide or lactose dehydrogenase production in mature osteoclasts. Finally, infection of macrophages or osteoclast precursors with *B. abortus* 2308 resulted in generation of smaller osteoclasts with decreased resorptive activity. Overall, *Brucella* exhibits similar growth characteristics in mature osteoclasts

compared to the primary target cell, the macrophage, but is able to impair the maturation and alter the resorptive capacity of these cells. These results suggest that osteoclasts play an important role in osteoarticular brucellosis and could serve as a useful *in vitro* model for both analyzing host-pathogen interactions and assessing vaccine safety.

3.2. Introduction

Brucellosis is a zoonotic disease caused by a Gram-negative intracellular bacterium of the genus *Brucella*. *B. abortus*, *B. melitensis*, *and B. suis* are the most pathogenic species to humans with more than 500,000 new cases reported annually (126). Unfortunately, there is no available vaccine for use in humans owing in large part to the safety concerns associated with potential residual virulence of live attenuated vaccines (LAVs). In order for safe vaccines to be designed, a thorough understanding of the host-pathogen interactions resulting in the most common complications in humans infection is required (32, 127, 128). Human brucellosis is frequently associated with the development of osteoarticular disease with an incidence ranging from 40-80% (37, 38, 81). Humans, regardless of age or sex, are susceptible to infection and the disease can manifest in both acute and chronic forms as peripheral arthritis, sacroiliitis, or spondylitis (38, 48). Importantly, osteoarticular lesions are also reported in natural hosts as infected dogs commonly develop diskospondylitis while cattle can exhibit arthritis and hygromas (54, 129-132).

Bone is a dynamic tissue that constantly undergoes remodeling coordinated by the synchronized activity of three cell types: osteoblasts (bone-forming), osteocytes, and

osteoclasts (bone-resorbing) (133, 134). Although previous studies have demonstrated the ability of *B. abortus* to invade and replicate within osteoblasts and osteocytes (72, 73, 135, 136), the role of osteoclasts in *Brucella* induced bone loss has not been explored. Mature osteoclasts are highly specialized bone-resorbing, multinucleated cells of hematopoietic origin. In addition to their resorptive activity, osteoclasts regulate osteoblast precursor differentiation and activity as well as immune cell responses (137). Previous investigations from our laboratory using NOD-SCID *IL2rγ*^{null} (NSG) mice have demonstrated that infection with *B. abortus* S19 but not the S19*ΔvjbR* vaccine candidate induced severe bone resorption with accumulation of myriad bacteria within mature osteoclasts (138). This apparent tropism of *Brucella* for osteoclasts and the significant amount of bone destruction in the mice, a lesion which is mediated by osteoclast resorptive activity, prompted the investigation of the effect of *Brucella* infection on these cells. In the present study, we sought to investigate the role of osteoclasts in osteoarticular brucellosis and vaccine safety using an *in vitro* model.

3.3. Results

3.3.1. Characterization of mature osteoclasts derived from murine bone marrow-derived macrophages

An *in vitro* model of osteoclast differentiation from primary cell culture was used to understand the role of osteoclasts in osteoarticular disease (139-141). Mature osteoclasts are multinucleated bone-resorbing cells derived from the monocyte/macrophage lineage under the control of two main cytokines: Macrophage Colony-Stimulating Factor (M-CSF) and Receptor Activator of Nuclear Factor-$_k$B

Ligand (RANKL) (66, 67). In this study, freshly collected mouse bone marrow-derived macrophages (BMDMs) were cultured in αMEM media in the presence of M-CSF and RANKL and monitored for their differentiation and maturation starting from 1-10 days. Cellular characterization following tartrate-resistant acid phosphatase (TRAP) staining demonstrated that the majority of the cells at day 2 were TRAP+ cells with one or two nuclei and were considered osteoclast precursors (pOCs), while the majority of the cells at day 3 were TRAP+ cells with three or more nuclei and were considered multinucleated mature osteoclasts (mOCs) (Fig. 3.1 panel A and B). Cellular fusion and a gradual increase in the size of osteoclasts were observed from day 2 to day 6 of maturation (Fig. 3.1 panel A and C). Although no significant changes in the size of osteoclasts were observed beyond day 6, nuclei disappeared gradually beginning at day 8, followed completely dissolution of a portion of the cells (Fig. 3.1 panel A). Cellular apoptosis was evident with nuclear condensation starting at day 6 followed by nuclear fragmentation on days 7 and 8, leaving an empty space in the wake of dead cells by day 10 (A1, Appendix A). The characterization of the kinetics of osteoclast growth and differentiation using this *in vitro* cellular model permitted us to classify cells at day 2 of macrophage differentiation in the presence of M-CSF and RANKL as osteoclast precursors with cells at day 3 were classified as mature osteoclasts for further infection studies.

3.3.2. *Brucella* invades and replicates inside mature osteoclasts

The kinetics of infection and mechanism behind *Brucella* replication and survival in macrophages has been extensively studied (142, 143). Here we wanted to determine

if mature osteoclasts were also permissive to infection and replication of different *Brucella* strains known to have different levels of virulence including **1**) wild type *B. abortus* 2308, **2**) *B. abortus* 2308*ΔvirB2*, an attenuated mutant incapable of survival in macrophages, **3**) *B. abortus* S19, a commercially available vaccine for use in cattle, and **4**) *B. abortus* S19*ΔvjbR*, a vaccine candidate. Following a pilot study of *Brucella* infection of mature osteoclasts (A2, Appendix A) at different multiplicity of infections (MOI of 50, 100 and 500/cell), downstream experiments were carried out at MOI of 100. When mOCs at day 3 of maturation were infected with the different *Brucella* strains, no significant differences in bacterial invasion was observed at 3h post-infection. In contrast, *B. abortus* 2308 and *B. abortus* S19 were the only strains able to persist and replicate inside the cells while the attenuated mutants were progressively killed (Fig. 3.2 panel A, C, and D). A similar phenotype of bacterial survival and replication was observed in BMDMs (Fig. 3.2 panel B), demonstrating that *B. abortus* is not only capable of infecting mature osteoclasts but also the kinetics of bacterial survival and replication in mature osteoclasts mirrors that seen in the primary target cell, the macrophage (142, 143). Z-sectioning of confocal microscopic images corroborated the bacterial distribution inside different depths of osteoclast cytoplasm. Comparison of the behavior of the virulent strain *B. abortus* 2308 and the vaccine strain *B. abortus* S19, known to be capable of inducing pathology in humans and osteoarthritis in cattle (55, 80) with that of the vaccine candidate S19*ΔvjbR* also provides evidence that osteoclasts have the potential to serve as an *in vitro* model for assessing vaccine safety.

3.3.3. *B. abortus* 2308 impairs the growth of mature osteoclasts

Osteoclast maturation involves the fusion of several mononucleated osteoclast precursors to form multinucleated giant cells. These cells can, in turn, fuse with additional mononucleated or multinucleated precursors in a near continuous fashion until a size of 100 or more nuclei may be attained (144-146). To determine the effect of *Brucella* infection on the maturation and growth of mature osteoclasts, these cells were infected with the different bacterial strains at day 3 of maturation and were stained for TRAP. Interestingly, there was no significant difference in the number of TRAP+mOCs derived following infection with any of the *Brucella* strains compared to uninfected control cells. However, the size of TRAP+mOCs infected with wild type *B. abortus* 2308 was significantly smaller ($p<0.01$) than the size of the uninfected cells or cells infected with different mutant or vaccine strains at 24h and 48h post-infection (Fig. 3.3 panels A-C), suggesting that *B. abortus* 2308 impairs the fusion and growth of mature osteoclasts.

3.3.4. Active infection of mature osteoclasts does not induce significant cell death either by apoptosis or necrosis

To assess the effect of *Brucella* infection on mature osteoclast survival, the level of lactate dehydrogenase (LDH), nitric oxide (NO), and cellular apoptosis were analyzed. Measurement of LDH in the culture supernatant is a useful method for detection of necrotic cell death (147, 148). NO plays an essential role in killing intracellular microbes, regulates osteoclastogenesis (149, 150), and can activate

apoptotic cell death when produced at high levels (151). Regardless of the bacterial strain, no significant changes in the levels of LDH (0.5-4%) or NO production (1.5-3.5 μm) by mOCs, as well as by BMDMs, were observed (Fig. 3.4 panels A-D). Further, terminal deoxynucleotidyl transferase (TdT) dUTP nick-end labeling (TUNEL) of fragmented DNA (152) revealed no significant changes in cellular apoptosis over 48h of infection of mOCs or BMDMs cultured in 96 well plates (Fig. 3.4 panel E and F), indicating that active *Brucella* infection of mature osteoclasts, regardless of virulence, does not induce cell death.

3.3.5. *Brucella abortus* 2308 infected mature osteoclasts resorb calcium matrix at the same level as uninfected cells

Osteoclasts are the only known primary cells of the bone that are able to resorb bone matrix (63, 153). One of most common methods to assess the matrix degradation property of osteoclasts is the resorption-pit assay which evaluates the ability of cultured osteoclasts to degrade a synthetic calcium phosphate coating (140) (A3, Appendix A). To assess the functional activity of *Brucella*-infected mature osteoclasts, BMDMs were cultured in calcium phosphate-coated plates (Corning, MA) in the presence of M-CSF and RANKL. Mature osteoclasts were then infected with the different *B. abortus* strains at day 3 of maturation and incubated for 48h to assess the ability of the cells to resorb calcium matrix. There were no significant differences in calcium matrix resorption by cells infected with *B. abortus* 2308 and *B. abortus* 2308*ΔvirB2* compared to uninfected cells. In contrast, the calcium resorption activity of cells infected with *B. abortus* S19

and its mutant S19*ΔvjbR* was significantly higher ($p<0.001$). Interestingly, TRAP staining showed no significant differences in the total number of TRAP+mOCs between *Brucella*-infected and uninfected cells (Fig. 3.5 panel C). However, cells infected with *B. abortus* S19 and *B. abortus* S19*ΔvjbR* demonstrated more cellular fusion with formation of larger giant cells containing a significantly higher number of nuclei when compared with wild type *B. abortus* 2308*, B. abortus* 2308*ΔvirB2*, or control cells ($p<0.001$) (Fig. 3.5 panel A, B, D, and E). Overall, while highly virulent *B. abortus* 2308 is able to impair the fusion and growth of mature osteoclasts, it does not impact the ability of these cells to resorb bone matrix. Additionally, the increased resorptive activity of osteoclasts infected with *B. abortus* S19 and *B. abortus* S19*ΔvjbR* appears to be the result of larger cell size as previous reports demonstrate (154-156).

3.3.6. Wild type *B. abortus* 2308 infection of BMDMs and osteoclast precursors impairs osteoclastogenesis and calcium matrix resorption

After determining that direct infection of mature osteoclasts by virulent *B. abortus* 2308 did not impact their resorptive capacity, BMDMs and pOCs were infected to determine if infection at an earlier time point could impact osteoclastogenesis and thereby calcium resorption. As previously mentioned, multinucleated mature osteoclasts are generated from the fusion of precursors belonging to the monocyte/macrophage lineage under the influence of M-CSF and RANKL cytokines with maturation progressing from macrophages to osteoclast precursors to mature osteoclasts. BMDMs (Fig. 3.6) or pOCs (Fig. 3.7) plated onto calcium phosphate-coated plates were infected

with the different *B*. *abortus* strains and incubated in the presence of M-CSF and RANKL for 5 days (120h). In contrast to what was observed in *Brucella*-infected mature osteoclasts (A4, Appendix A), TRAP staining of *B. abortus* 2308-infected cells demonstrated significant reduction ($p<0.01$) in the growth of mature osteoclasts derived from infected BMDMs (Fig. 3.6 panel A, B, D, and E) or pOCs (Fig. 3.7 panel A, B, D, and E) as well as significant reduction ($p<0.01$) in calcium matrix resorption compared with uninfected controls (A4, Appendix A). These results indicate an unexpected, direct and negative impact on osteoclast growth and functional activity when infection occurs at the precursor stage. The enhanced bone resorption observed in cases of osteoarticular brucellosis does not, therefore, appear to be due to direct infection of either mature osteoclasts or their precursors by *Brucella* as enhanced functional activity would be expected to occur in cases of osteoarticular disease.

3.3.7. *Brucella* infected osteoblasts fail to drive osteoclastogenesis

As wild type *B. abortus* 2308 infection of mature osteoclasts or their precursors did not enhance osteoclast maturation or alter the functional activity of mature osteoclasts, the involvement of other cells associated with the bone may be responsible for the enhanced resorptive activity of osteoclasts seen in *Brucella*-induced osteoarthritis. Bone homeostasis depends on the functional balances between bone-forming osteoblasts and bone resorbing osteoclasts. To maintain this homeostasis in the adult skeleton, osteoblasts produce two main cytokines which are necessary to promote osteoclast differentiation and maturation (157). Previous *in vitro* studies have shown that *B. abortus* infected-osteoblasts are capable of inducing RANKL expression and

secretion (72, 158) suggesting that infected osteoblasts have the potential to stimulate increased osteoclastogenesis.

In this study, murine MC3T3, a standard pre-osteoblast cell line, was used for the assessment of the impact of osteoblasts on osteoclastogenesis following *B. abortus* infection. First, MC3T3 pre-osteoblast cells were allowed to differentiate and mature for varying duration (7, 14 and 21 days) and expression of alkaline phosphatase (ALP) and mineralization of bone matrix were used as phenotypic markers to characterize osteoblast maturation (159-162). Alkaline phosphatase activity was first detected at day 7 of osteoblasts differentiation. Subsequently, Alizarin red S staining of calcium deposition was noted in few cells by day 14 (Fig. 3.8 panel A) with staining exhibited by 90-100% of the cells by day 21, indicating differentiation of mature osteoblasts. MC3T3 osteoblasts infected (MOI 100) with different *Brucella* strains at day 21 of maturation demonstrated a similar phenotype of bacterial invasion and replication in BMDMs and mOCs (Fig. 3.8 panel B) for *B. abortus* 2308 and S19, as previously reported (72, 73, 135). Additionally, the attenuated strains *B. abortus ΔvirB2* and the vaccine candidate S19*ΔvjbR* were able to invade osteoblasts but unable to survive or replicate.

To evaluate whether *B. abortus* infection of osteoblasts could enhance osteoclastogenesis, both direct and indirect interaction of infected osteoblasts with osteoclasts was assessed. For direct interaction, BMDMs were co-cultured with *Brucella*-infected osteoblasts, while indirect interaction was performed by exposing BMDMs to the supernatant of *Brucella*-infected osteoblasts. Unfortunately, TRAP staining after 7 days of incubation revealed no influence of MC3T3 mature osteoblast

(with or without infection) on BMDM derived osteoclastogenesis *in vitro* (Fig. 3.9 panel A and B). This indicates that the MC3T3 cell line, while useful in evaluating the interactions of *Brucella* with mature osteoblasts, may not be suitable for investigating the effect of these cells on osteoclastogenesis as even uninfected MC3T3 cells were unable to induce osteoclast maturation *in vitro*.

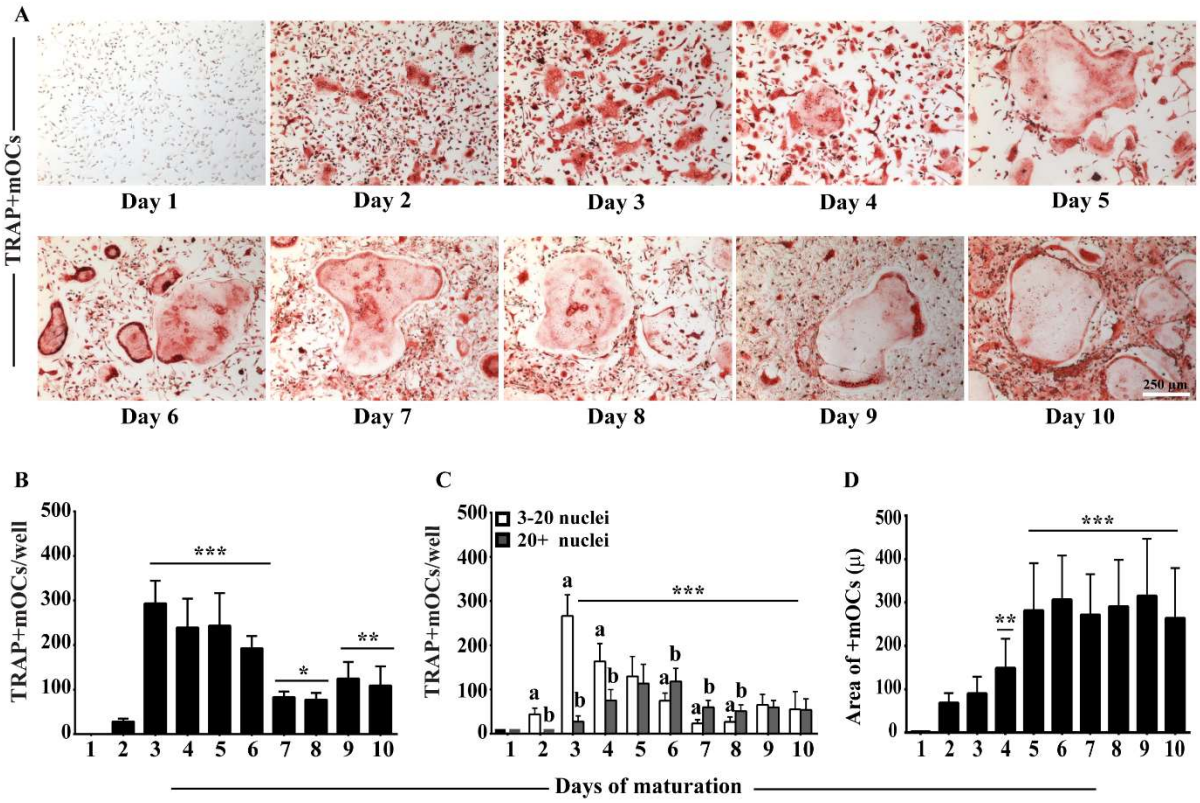

Figure 3.1 Differentiation of bone marrow-derived macrophages into multinucleated mature osteoclasts *in vitro*. Mouse bone marrow-derived macrophages (BMDMs) were cultured in 24 well plates with 20 ng/ml M-CSF and 50 ng/ml RANKL for up to 10 days and mature osteoclasts were characterized based on TRAP staining and nuclei number. TRAP+ cells with ≥ 3 nuclei were considered multinucleated mature osteoclasts (mOCs). (A) Representative brightfield images of TRAP staining during osteoclasts maturation, fusion, and growth. Cellular fusion and size increased gradually over time, reaching a maximum at Day 6. Although there were no changes in the size of mature osteoclasts between day 6 and 10, the number of pyknotic nuclei increased gradually leaving an empty space by day 10 on the dish. (B) Quantitative image analysis revealed that TRAP+ cells began appearing on day 2 and reached a maximum number by day 3. (C) The number of TRAP+ cells with >20 nuclei reached a maximum at day 6. (D) Quantitative analysis of cell size showed a gradual increase with maximum size reached by day 6 of maturation. Bars represent the mean±sd, n=12 wells from three independent experiments. Letters are significantly different from the same group. Asterisks are statistical comparisons performed against Day 2, *P<0.05, ** P<0.01, ***

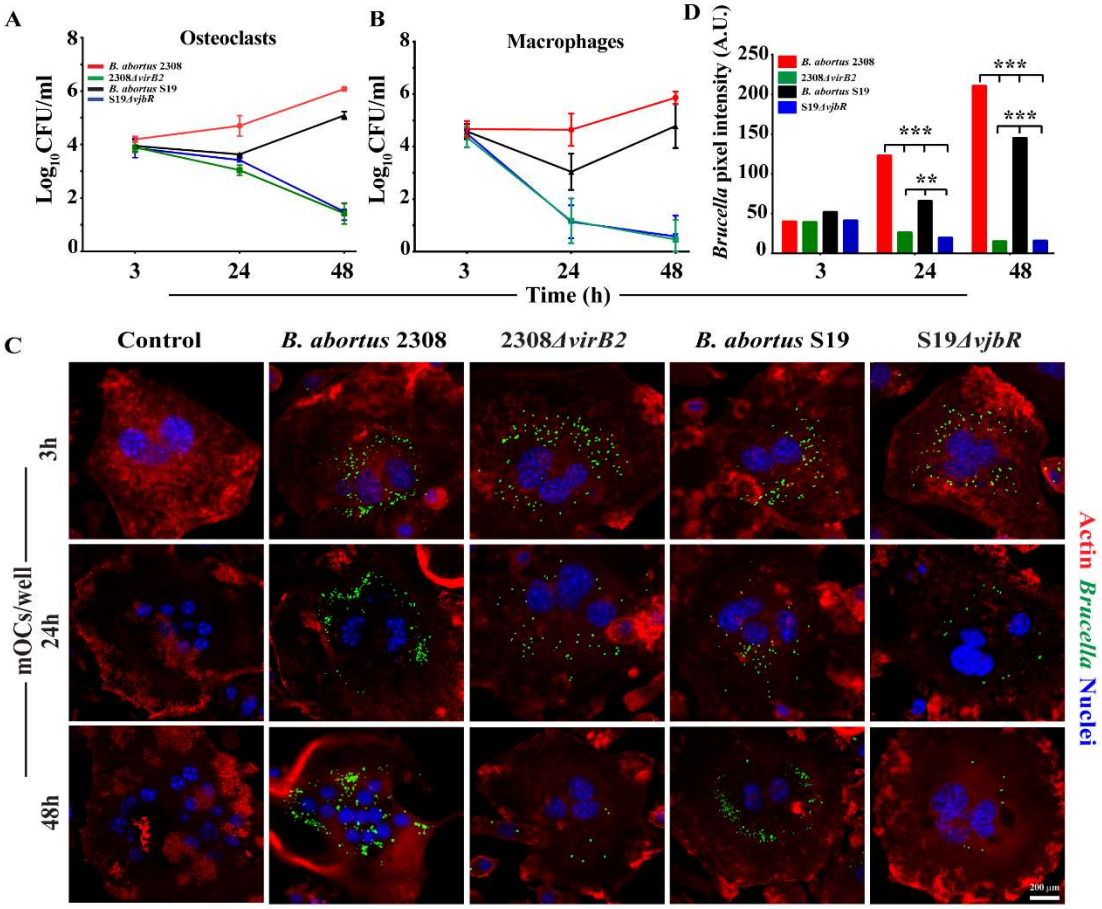

Figure 3.2 *B. abortus* invades and replicates inside mature osteoclasts (mOCs) and bone marrow-derived macrophages (BMDMs). Mouse BMDMs were cultured in 24-well plates with either 20 ng/ml M-CSF + 50 ng/ml RANKL or with 20 ng/ml M-CSF alone. On day 3, BMDMs and TRAP+mOCs were infected with *B. abortus* strains at MOI of 1:100. Following 2h of infection, media was replaced with gentamicin containing media and incubated for different time durations. (A) Invasion and replication of *B. abortus* strains within mOCs. While all strains invaded mOCs at the same level, *B. abortus* 2308 and S19 demonstrated replication by 48hpi, *B. abortus ΔvirB2* and S19*ΔvjbR* were progressively killed. (B) Invasion and replication of *B. abortus* within BMDMs. Identical infection kinetics were observed in BMDMs. (C) Representative confocal immunofluorescence images showing *Brucella* colonization and replication (green) inside osteoclasts. Increased numbers of GFP-*B. abortus* are observed within osteoclasts at 48h with *B. abortus* 2308 and S19, coinciding with replication. (D) Quantitative image analysis shows a significantly (P<0.001) higher level of colonization of *B. abortus* 2308 and *B. abortus* S19 compared with other mutants by 24h and 48h of post-infection. Bars represent the mean±s.d., n=12 wells from four independent experiments, ** P<0.01, *** P<0.001.

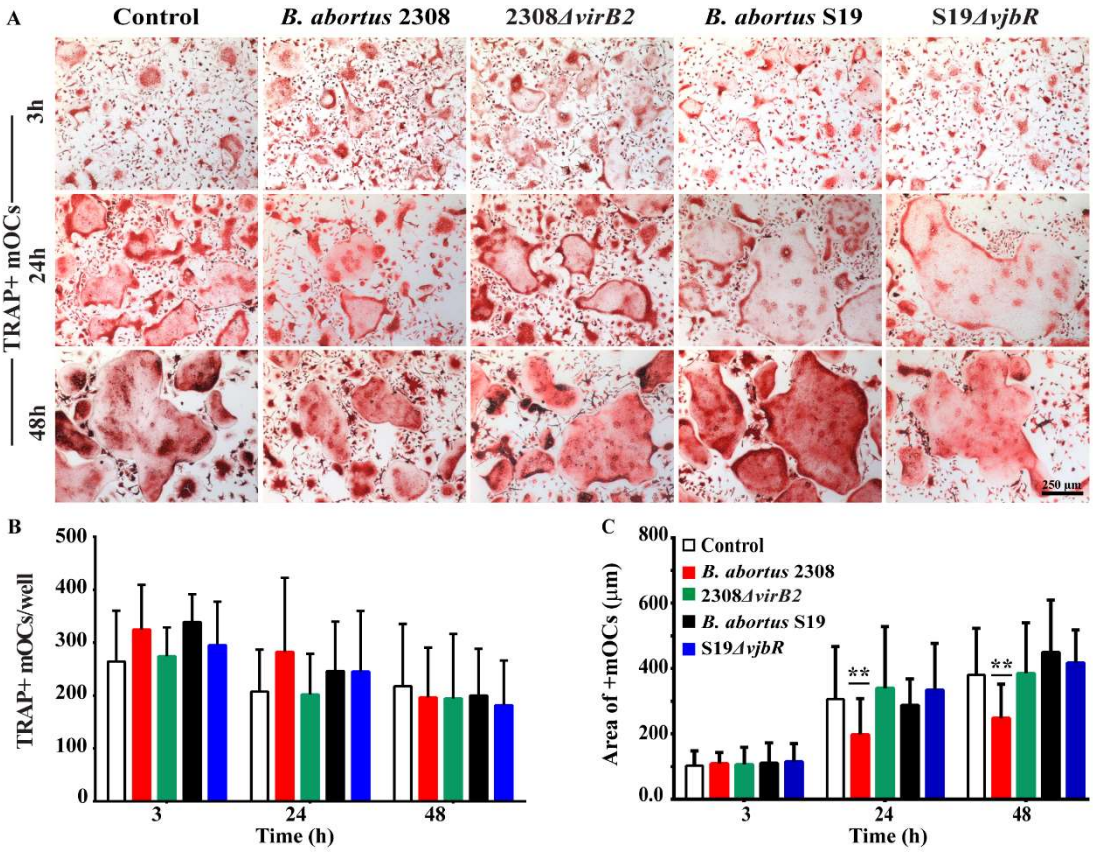

Figure 3.3 Wild type *B. abortus* 2308 impairs fusion and growth of mature osteoclasts. Mouse bone marrow-derived macrophages (BMDMs) were cultured in 24-well plates with 20 ng/ml M-CSF and 50 ng/ml RANKL. On day 3 of maturation, osteoclasts were infected with *B. abortus* strains at MOI of 1:100 and monitored for growth at 3h, 24, and 48h post-infection. (A) Representative brightfield images of TRAP staining showed increased fusion and growth of osteoclasts by 24h and 48h post-infection. Quantitative image analysis revealed no significant changes in the number of TRAP+mOCs following infection, regardless of strain (B), but significant (P<0.01) decrease in the size of mOCs following infection with wild type *B. abortus* 2308 (C). Asterisks are statistical comparisons performed against control or mutant strains. Bars represent the mean±s.d., n=12 wells from four independent experiments, **P<0.01.

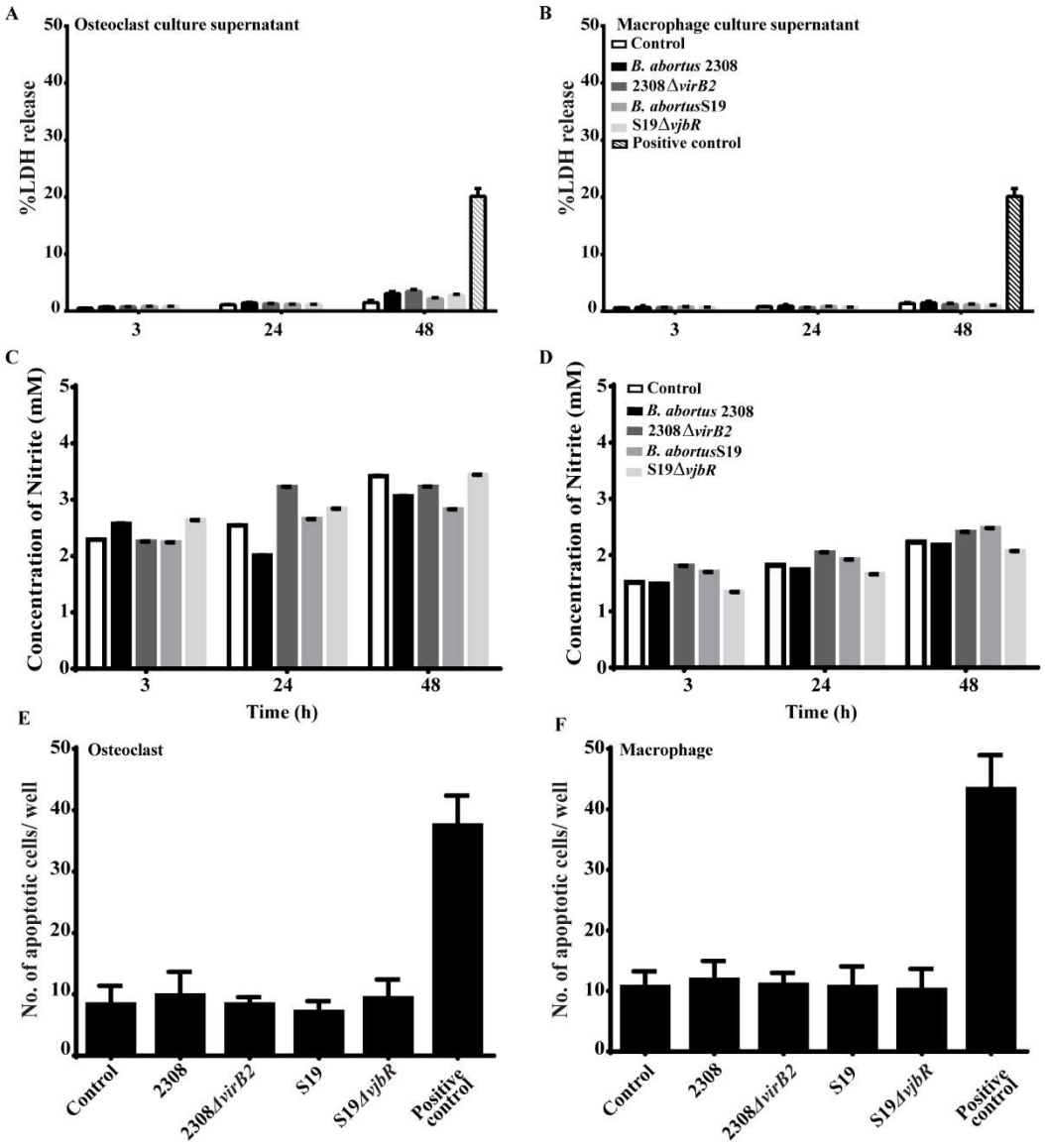

Figure 3.4 *B. abortus* infection does not induce lactic acid dehydrogenase (LDH) and nitric oxide (NO) production or cell death in mature osteoclasts. Mouse BMDMs cultured in the presence of 20 ng/ml M-CSF and 50 ng/ml of RANKL were infected on day 3 of maturation with *B. abortus* strains at MOI of 1:100 to monitor NO production and apoptosis. Cultured supernatants from uninfected and infected cells were collected after 3h, 24h, and 48h post-infection to determine the levels of LDH and NO in the culture supernatant of osteoclasts (A and C) and macrophages (B and D). Quantitative analysis showed no significant difference in cellular apoptosis in mOCs (C) or BMDMs (D). Bars represent the mean±s.d., n=12 wells from four independent experiments, $^{**}P<0.01$, $^{***}P<0.001$.

Figure 3.5 *B. abortus* infected mature osteoclasts can grow and are capable of calcium matrix degradation. Mouse bone marrow-derived macrophages (BMDMs) were cultured on calcium matrix in the presence of 20 ng/ml M-CSF and 50 ng/ml RANKL. On day 3 of maturation, osteoclasts were infected with *B. abortus* strains at MOI of 1:100 and monitored for growth and function 48h post-infection. (A) Representative brightfield images of TRAP stained mOCs demonstrate larger size of mOCs with infection by *B. abortus* S19 and S19*ΔvjbR*. (B) Representative brightfield images showing calcium resorption pits (white) by mOCs following 48h of infection. During infection with *B. abortus* S19 and S19*ΔvjbR*, resorption pits appear larger, coinciding with increased cells size. Resorption pits for mOCs infected with *B. abortus* 2308 and *B. abortus ΔvirB2* appear similar to those of uninfected mOCs. (C) Quantitative image analysis of TRAP staining showing the total number of mOCs and (D) the number of mOCs based on cellular fusion or nuclei. No significant differences in total cell number were observed between groups while mOCs infected with *B. abortus* S19 and S19*ΔvjbR* had a significantly higher number of nuclei. (E) Quantitative analysis of calcium matrix degradation of mOCs infected with *Brucella*. Measurement of the resorbed area was performed using Fiji software. *B. abortus* S19 and S19*ΔvjbR*-infected mOCs resorbed significantly more calcium matrix. Bars represent the mean±s.d., n=12 wells from four independent experiments. Letters are significantly different from the same groups; asterisks are statistical comparisons performed against control or mutant strains, Bars represent the mean±s.d., n=12 wells from four independent experiments, ***$P<0.01$.

Figure 3.5 Continued

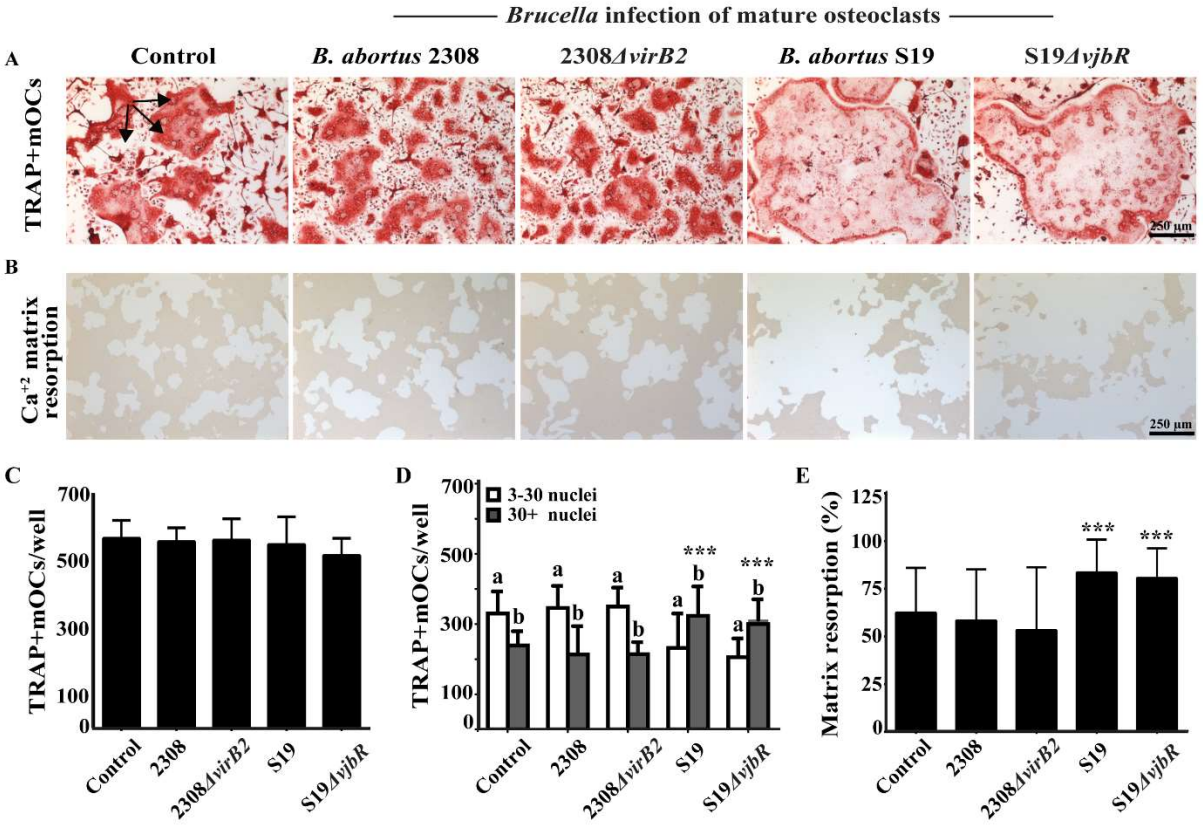

Figure 3.6 Wild type *B. abortus* 2308 infection of BMDMs reduces osteoclastogenesis and matrix degradation activity. Mouse BMDMs cells cultured on calcium matrix with 20 ng/ml M-CSF for 48h were infected with *B. abortus* strains at MOI of 1:100. Infected cells were further incubated with 20 ng/ml of M-CSF and 50 ng/ml of RANKL for 120h to monitor osteoclastogenesis and matrix degradation. (A) Representative brightfield images of TRAP stained uninfected and infected mOCs. The mOCs derived from macrophages infected with *B. abortus* 2308 appear subjectively smaller. (B) Representative brightfield images showing calcium resorption pits (white) by mOCs following 120h of infection. The resorption pits produced by mOCs derived from macrophages infected with *B. abortus* 2308 appear subjectively smaller. (C) Quantitative image analysis of total number of TRAP+ mOCs and (D) the number of mOCs based on cellular fusion or number of nuclei. A significantly lower number of mOCs were derived from macrophages infected by *B. abortus* 2308 and these mOCs also showed significantly fewer nuclei. (E) Quantitative analysis of calcium matrix degradation showed a significant decrease in the amount of calcium matrix degradation by cells infected with wild type *B. abortus* 2308. Measurement of the resorbed area was performed using Fiji software. Bars represent the mean±s.d., n=12 wells from four independent experiments, letters are significantly different from the same group; asterisks are statistical comparisons performed against control or mutant strains, Bars represent the mean±s.d., n=12 wells from four independent experiments, $^{**}P<0.01$.

Figure 3.6 Continued

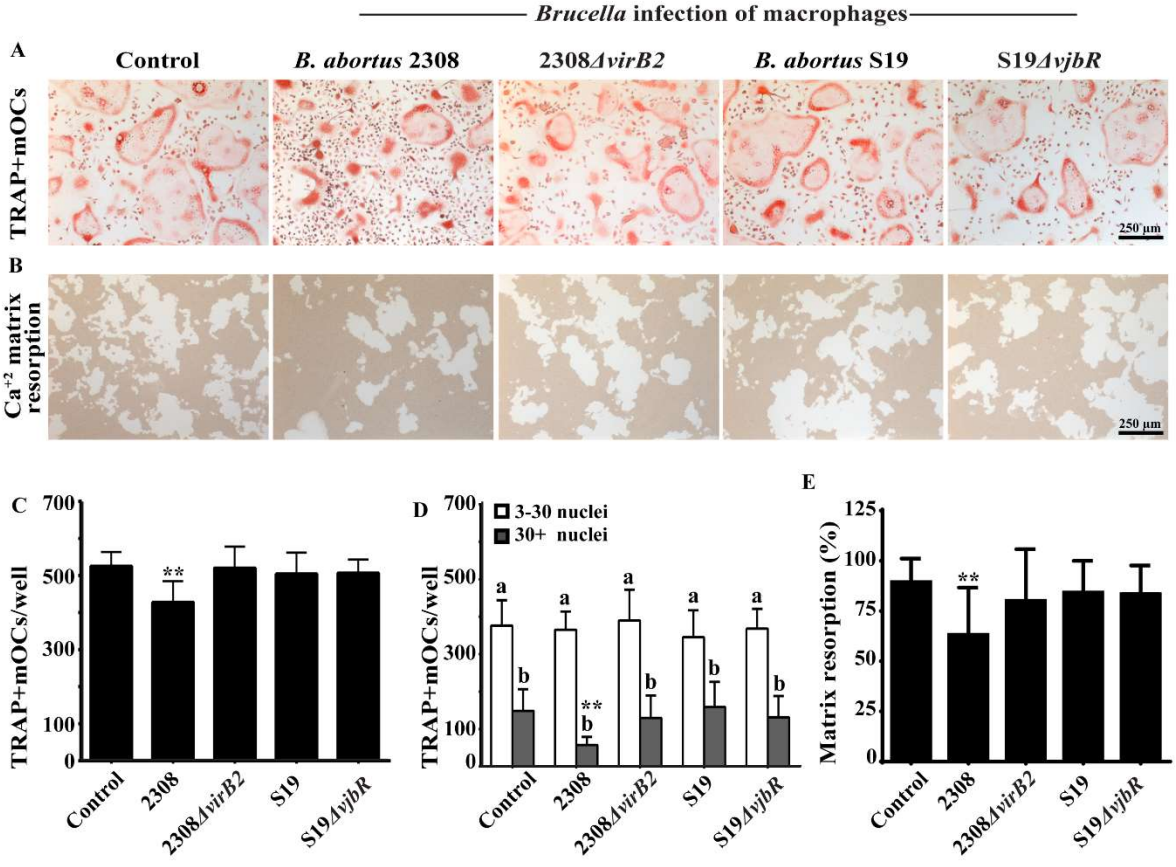

Figure 3.7 Wild type *B. abortus* 2308 infection of osteoclast precursors (pOC) reduces osteoclast growth and matrix degradation activity. Mouse BMDMs cells cultured on calcium matrix in the presence of 20 ng/ml M-CSF and 50 ng/ml of RANKL for 48h (pOC) were infected with *B. abortus* strains at MOI of 1:100 to monitor cell growth and matrix degradation after 120h. (A) Representative brightfield images of TRAP stained uninfected and infected mOCs show no clear differences in cell size or number. (B) Representative brightfield images showing calcium resorption pits (white) by mOCs following 120h of infection. Resorption pits produced by mOCs derived from osteoclast precursors infected with *B. abortus* 2308 appear subjectively smaller. (C) Quantitative image analysis of total number of TRAP+ mOCs and (D) the number of mOCs based on cellular fusion or number of nuclei. While the number of mOCs did not differ significantly between groups, the number of nuclei in mOCs derived from osteoclast precursors infected with *B. abortus* 2308 showed significantly fewer nuclei. (E) Quantitative analysis of calcium matrix degradation showed a significant decrease in the amount of calcium matrix degradation by cells infected with wild type *B. abortus* 2308. Measurement of the resorbed area was performed using Fiji software. Bars represent the mean±s.d., n=12 wells from four independent experiments, letters are significantly different from the same group; asterisks are statistical comparisons performed against control or mutant strains, Bars represent the mean±s.d., n=12 wells from four independent experiments, $**P<0.01$.

Figure 3.7 Continued

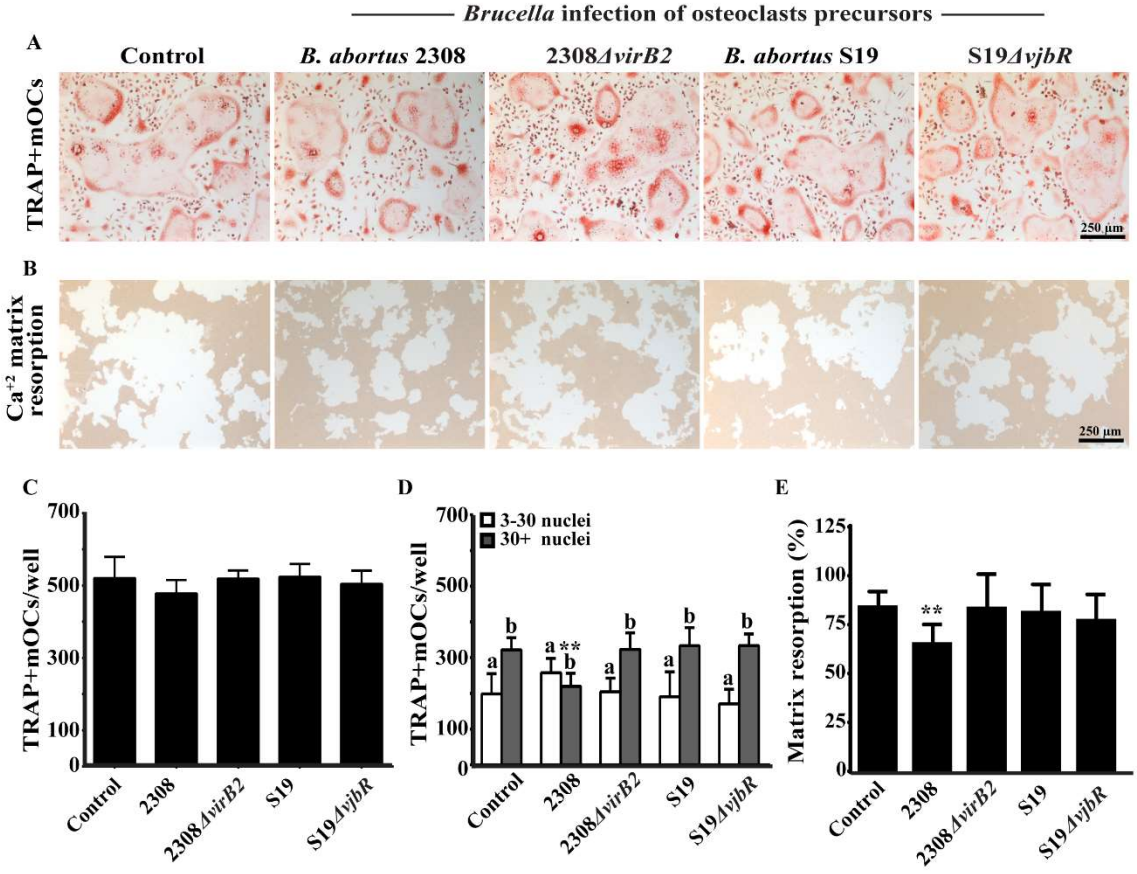

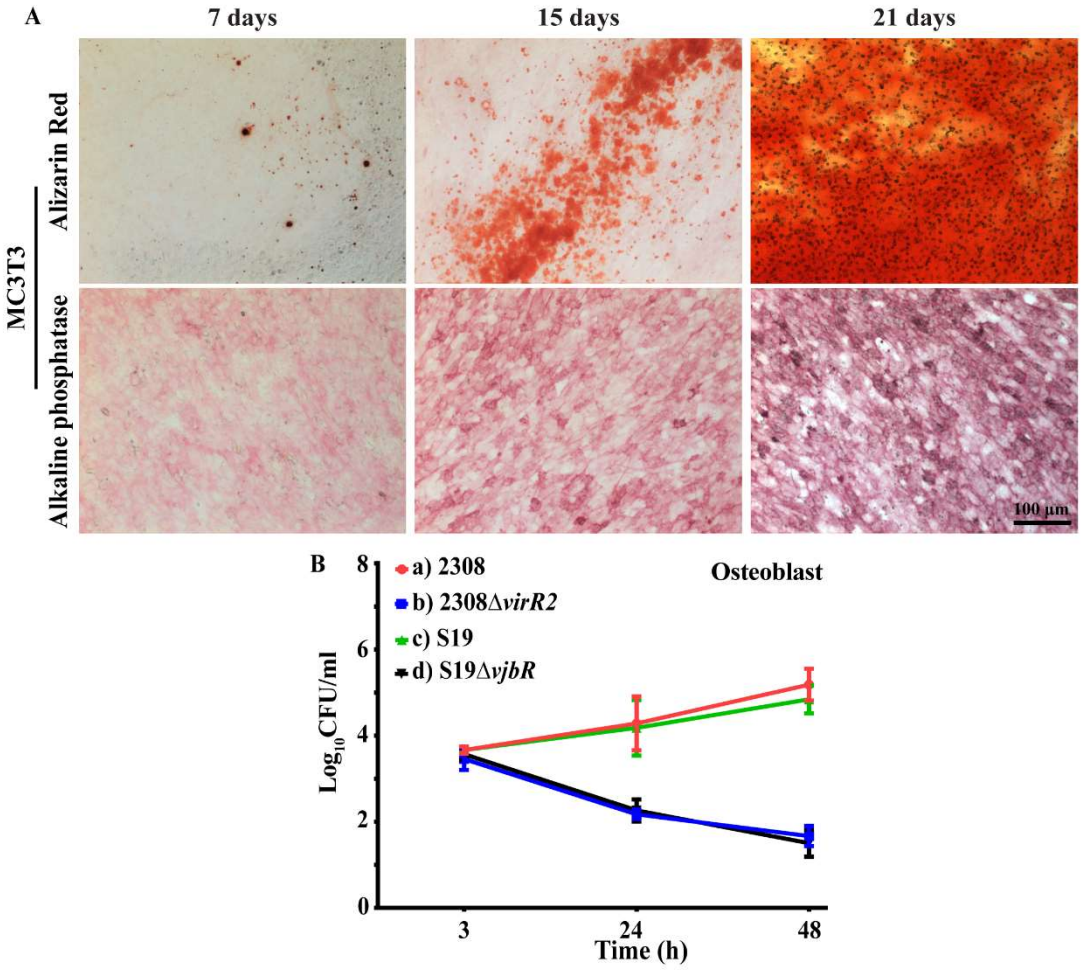

Figure 3.8 *B. abortus* invades and replicates inside differentiated MC3T3 osteoblasts. MC3T3 pre-osteoblast cell line was cultured in osteogenic differentiation media for 21 days to mature. Alizarin red S staining of calcium deposition and alkaline phosphatase activity (A) demonstrate the progressive maturation of MC3T3 cells. (B) Invasion and replication of different *B. abortus* strains within differentiated osteoblast at day 21. As observed with macrophages and mOCs, all strains invade osteoblasts at a similar rate while only *B. abortus* 2308 and S19 demonstrate replication by 48h.

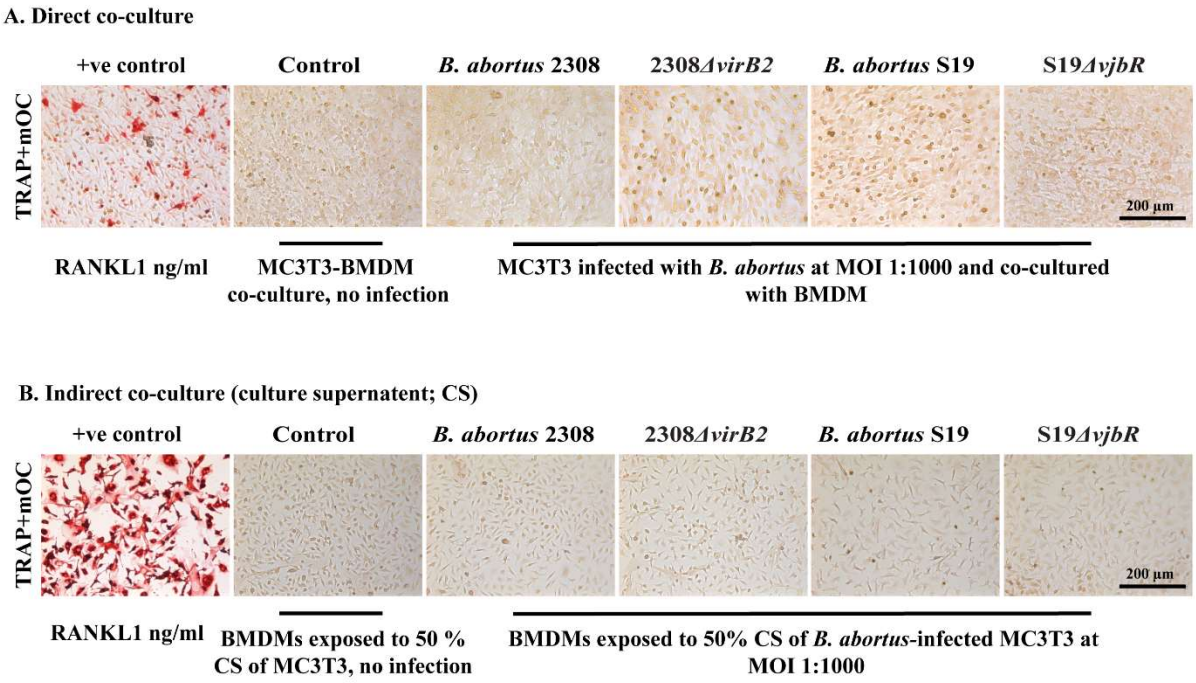

Figure 3.9 *Brucella* infected and uninfected MC3T3 osteoblasts fail to drive osteoclastogenesis *in vitro*. MC3T3 osteoblasts cultured in osteogenic differentiation media for 21 days were infected with different *B. abortus* strains at 1:1000. Cells were incubated for 24h post-infection and (A) directly co-cultured with mouse BMDMs in the presence of osteogenic differentiation media and 20ng/ml M-CSF. (B) Alternatively, mouse BMDMs were cultured with culture supernatants from *Brucella*-infected osteoblasts at different proportion (25% and 50%). After 7 days, cells were stained for TRAP to detect mature osteoclasts. RANKL (1ng/ml) was used as a positive control for osteoclast formation. Neither infected nor uninfected MC3T3 osteoblasts stimulated osteoclastogenesis as evidenced by lack of trap staining at the end of 7 days.

3.4. Discussion

Brucella-induced osteoarticular damage is a commonly described clinical finding associated with human or animal brucellosis (35-37, 81, 163). The development of live attenuated vaccines to protect humans against infection has long been hampered by safety concerns regarding the use of live attenuated vaccines, notably the potential of such vaccines to induce arthritis in livestock (55) and most importantly in humans. Due to the incompletely understood mechanisms of osteoarticular brucellosis, it is challenging to predict the potential side effects that can be associated with the administration of live attenuated vaccines, as some of the most commonly used animal models to study brucellosis do not develop osteoarticular disease in a consistent manner (36, 57, 58). A better understanding of the cellular and molecular events occurring at the joint site during *Brucella* infection through the development of an *in vitro* assay could pave the way for more efficient and inclusive evaluation of safety for new vaccine candidates regarding osteoarticular brucellosis.

In this study, we sought to investigate the role played by osteoclasts during *Brucella* infection using different *B. abortus* strains and vaccine candidates to test whether *Brucella* would be able to invade, replicate, or change the functional activity of osteoclasts. To the best of our knowledge, this study is the first to investigate the direct interaction between different strains of *B. abortus* and osteoclasts. Osteoclastogenesis is a complex process requiring different stimuli and cellular molecules to interact without impairment (117, 164). It is well known that myeloid cells of the monocyte/macrophage

lineage differentiate into osteoclasts precursors in the presence of the cytokines, M-CSF and RANKL (66, 67, 165). Previous studies have demonstrated that multinucleated osteoclasts are formed following mononuclear pre-osteoclasts fusion, during which the nuclei enter into the G0 state which inhibs DNA synthesis and prevents further proliferation of osteoclasts. This allows the osteoclast precursors to gradually grow in size by fusion although early cellular fusion is known to accelerate cell death (63, 166). In this study *ex vivo* differentiation of BMDMs followed a similar pattern of formation of pOCs, mOCs, cellular growth, and apoptotic cell death.

Brucella is known to invade and replicate inside mammalian hosts, and their ability to cause disease relies on their intracellular lifestyle (167). Although *in vitro* infection of osteoclasts with various types of live bacteria known to cause bone destruction, including *S. aureus*, *M. tuberculosis*, and *C. acnes* have been studied (121, 153, 168), the direct interaction of *Brucella* with osteoclasts has never been investigated. A recent study performed by our laboratory has demonstrated severe bone destruction in the tail vertebrae of NSG mice inoculated with *B. abortus* S19 with accumulation of large number of bacteria within mature osteoclasts, an outcome which was not observed during infection with the *Brucella* vaccine candidate S19*ΔvjbR* (138). In this study, we demonstrated that only *B. abortus* 2308 and S19 were able to invade and replicate inside mature osteoclasts. In contrast, *B. abortus* 2308*ΔvirB2* and S19*ΔvjbR* mutants, while able to invade, were not capable of replication or sustained survival. This finding demonstrates that *B. abortus* has a high capacity to invade, survive, and replicate within

a wide variety of phagocytic and nonphagocytic host cells which would allow bacterial cells to escape from host defenses (169).

The ability of *Brucella* to inhibit phagolysosome fusion in macrophages allows these cells to serve as the bacterium's predominant replicative niche (169). Typically, smooth strains of *Brucella* do not induce cell injury and apoptosis in macrophages and instead employ these cells for replication and dissemination (170, 171). We have demonstrated that direct *B. abortus* 2308 infection of mature osteoclasts impairs early fusion of osteoclasts and reduces cellular growth but importantly, does not induce cellular death. As mentioned previously, accelerated growth and fusion of osteoclasts *in vitro* results in premature apoptotic cell death (38, 57). This result therefore suggests that virulent *Brucella* impairs the growth of osteoclasts following invasion in order to prolong the life of the cell, employing the osteoclast in a strategy of intracellular survival and avoidance of immune detection. Prolonged survival of infected osteoclasts might also contribute to the progressive osteoarticular lesions which frequently occur in human cases of brucellosis. In contrast, attenuated *Brucella* strains did not impair cellular growth or induce cell death of mature osteoclasts. This, in turn, suggests that the mature osteoclasts infected with attenuated strains might grow faster and undergo apoptosis earlier than those infected with wild type strains, providing *in vitro* evidence that such strains would be incapable of inducing osteoarticular disease in a vaccinated host and might therefore be safer. While evidence of cell death was not observed using LDH secretion and TUNEL assays in osteoclasts infected with these attenuated strains over

48h, it is possible that increased levels of apoptosis might be observed at later time points.

An imbalance in osteoclast functional activity in bone matrix degradation may lead to bone lysis (121). It has been reported that large osteoclasts are more active, capable of enhanced bone resorption, and are more responsive to environmental stimuli (154-156). Physical characterization of *Brucella* infected osteoclasts in this study revealed phenotypic variation in cell size due to infection with different bacterial strains. This prompted the analysis of functional activity of infected osteoclasts by assessing the amount of calcium phosphate resorption. Previous *in vivo* studies have shown that enhanced osteoclastogenesis during wild type *Brucella* infection was associated with pre-inflammatory and pro-osteoclastogenic mediators (57-59, 153, 172, 173). In the present study, mature osteoclasts infected with wild type *B. abortus* 2308 exhibited calcium matrix resorption activity at a similar level to uninfected controls, indicating that direct infection of mature osteoclasts is not solely responsible for the high levels of bone resorption observed in *Brucella*-induced osteoarthritis. Unexpectedly, infection of mature osteoclasts with *B. abortus* S19 or S19*ΔvjbR* vaccine strains exhibited larger areas of matrix degradation corresponding with a larger cell size. It is important to note that larger cell size can be a double-edge sword regarding functional activity and cellular survival. Although larger cells are capable of absorbing larger areas of matrix (153-156, 174), such cells would be expected to exhibit significantly shorter survival. The larger cell size and enhanced matrix degradation observed with the *B. abortus* S19 or S19*ΔvjbR* vaccine strains might therefore provide additional evidence of safety as

infected osteoclasts would exhibit shortened survival and would be unlikely to contribute to the long-standing and progressive bone loss observed in human *Brucella* infection. Nevertheless, future studies are required to identify the mechanism behind the increased size and resorptive capacity of mature osteoclasts infected with S19 and S19*ΔvjbR* strains.

Several studies have described that bacterial infection has a dual impact on osteoclastogenesis and functional activity of osteoclasts (153, 168). We demonstrated earlier that *B. abortus* 2308 impaired the growth of mature of osteoclasts. As mature osteoclasts are derived from the monocyte/macrophage lineage, we next investigated the effect of *Brucella* infection on osteoclast size and activity at an earlier timepoint, namely macrophages or osteoclast precursors that were then stimulated with RANKL to become osteoclasts. Our results demonstrated that the vaccine strain S19 and the attenuated mutants did not inhibit osteoclastogenesis and the resultant mature osteoclasts were capable of resorbing calcium matrix at a similar level to controls. However, wild type *B. abortus* 2308-infected macrophages or osteoclast precursors exhibited smaller size and smaller areas of calcium resorption. This supports the previous results obtained from infection of mature osteoclasts and provides further evidence that virulent *B. abortus* delays cellular fusion and growth of infected osteoclasts in an effort to prolong the survival of the cell and thereby maximize the utility of the osteoclast as a replicative niche. Additionally, it can be theorized that due to prolonged survival, *Brucella*-infected osteoclasts would be able to continue bone resorption and contribute to progressive bone destruction. This strategy would be in direct contrast to other bacterial pathogens capable

of inducing bone damage, such as wild type *Staphylococcus aureus*, which results in enhanced osteoclast fusion and calcium matrix resorption following infection and inhibits osteoclastogenesis following infection of osteoclast precursors (153). However, it should be noted that bacteria such as *S. aureus* are extracellular pathogens and do not prolong host cell lifespan as a survival strategy.

While the effects of *Brucella* infection on osteoclast growth are intriguing, such cells exist in a complex interaction with numerous other cell types and the interactions of *Brucella* with these cells may also play an important role in the development of osteoarticular disease. For instance, bone resorption by mature osteoclasts coincides with bone formation by osteoblasts in a tightly regulated process to maintain the bone homeostasis (72, 175, 176). Several *in vitro* studies have highlighted the direct impact of *B. abortus* infection on osteoblast function, including increased secretion of RANKL (72, 158), a cytokine that is critical in driving osteoclast formation and bone remodeling. Under pathological circumstances, RANKL triggers osteoclastogenesis and initiates bone destruction, as observed in a variety of bacterial infections (158, 177, 178).

Since invasion of *Brucella* of mature osteoclasts did not enhance osteoclastogenesis, we wanted to see if activation of these cells would occur secondary to invasion of osteoblasts. In order to investigate the additive role of *Brucella* infected osteoblasts on osteoclastogenesis, we first demonstrated *Brucella* replication in differentiated MC3T3 osteoblasts. While wild type *B. abortus* 2308 and *B. abortus* S19 replicated inside osteoblasts, mutant strains, including the vaccine strain candidate S19*ΔvjbR*, failed to replicate. This not only confirms the ability of virulent *Brucella* to

utilize osteoblasts as an additional replicative environment, but also provides further *in vitro* evidence regarding the attenuation and safety of S19*ΔvjbR*. When the ability of the infected osteoblasts to influence osteoclastogenesis was next investigated, *in vitro* direct co-culture of *Brucella* infected MC3T3 cells with BMDMs did not stimulate osteoclastogenesis. Additionally, treatment of BMDMs with culture supernatants from *B. abortus*-infected MC3T3 failed to stimulate osteoclastogenesis, although the addition of 1 ng/ml of RANKL to BMDM culture as a positive control was sufficient to induce TRAP+pOC formation. While it is possible that *Brucella* infection of osteoblasts directly does not drive osteoclastogenesis, it is important to note that uninfected MC3T3 also did not stimulate maturation of osteoclasts. This could indicate that the MC3T3 cell line may not be suitable as an *in vitro* model to assess the interaction of osteoblasts and osteoclasts during *Brucella* infection.

Based on the results obtained in the present study, we hypothesize that intracellular survival and replication of bacteria inside osteoclasts is a critical component in the development of osteoarticular brucellosis. Our results imply that *Brucella* takes advantage of osteoclasts following infection of the mature cells or their precursors and utilizes these cells as an additional environment to replicate by reducing cellular growth and prolonging the life of the cell. By infecting circulating osteoclast precursors, which are abundant in the bloodstream and hematopoietic tissues, *B. abortus* could avoid immune detection and establish a chronic infection in the bones or joints, ultimately resulting in osteoarthritis. Finally, comparison of wild type and vaccine strains of *B. abortus* demonstrates that osteoclasts could serve as a useful *in vitro* model to assess

vaccine safety in terms of potential induction of osteoarticular lesions in the host. Using the *in vitro* cellular model of osteoclast maturation to study host-pathogen interactions and assess the safety of vaccine candidates, we have provided exciting new opportunities to interrogate the effects of *B. abortus* infection on bone and beyond.

3.5. Materials and Methods

3.5.1. Bacterial strains and media

B. abortus 2308, 2308*ΔvirB2*, S19 (NVSL, Ames, IA) and *B. abortus* S19*ΔvjbR* (engineered for a previous study) (61) with or without GFP were used in these experiments. *B. abortus* strains were grown on Tryptic soy agar plates (TSA; Difco, Becton Dickinson) at 37°C with 5% (vol/vol) CO_2 for three days. A single colony was used to inoculate Tryptic soy broth (TSB) and incubated at 37°C overnight. Bacteria were collected by centrifugation and washed twice in phosphate-buffered saline (PBS), pH 7.2 (Gibco). Bacterial density was measured using a Klett colorimeter and compared against a standard curve. Viable counts were measured by plating serial dilutions of inoculum onto TSA plates and quantifying colonies following 3-4 days of incubation at 37°C. All experiments with live bacteria were carried out at biosafety level 3 facilities at the College of Veterinary Medicine and Biomedical Science, Texas A&M University.

3.5.2. Preparation of *Brucella abortus* strains expressing GFP

B. abortus strains expressing the green fluorescent protein (GFP) were made by electroporating the pBBR1-MSC6Y plasmid encoding chloramphenicol resistance into different *Brucella* strains as previously described (179, 180). *B. abortus* 2308,

2308*ΔvirB2*, S19, and *B. abortus* S19*ΔvjbR* were grown in TSB overnight. Bacterial pellets were subsequently washed four times in ice-cold sterile water and resuspended in 0.1 ml of ice-cold sterile water. One µg of pBBR1-MSC6Y plasmid DNA was mixed with bacteria and incubated for 30 min on ice followed by electroporation at Voltage 2500 V, Resistance 200 Ω, and Capacitance 50 µF. Immediately after electroporation, 1 ml of warmed TSB SOC-B media (6% [wt/vol] tryptic soy broth, 10 mM NaCl, 2.5 mM KCl, 10 mM MgCl2, 10 mM MgSO4, and 20 mM glucose) was added and suspensions were incubated at 37°C for 24h. The following day, bacterial suspensions were plated onto TSA with 5 µg/ml chloramphenicol and incubated at 37°C for three days. Single colonies from each bacterial strain were inoculated into 5 ml of TSB with 15 µg/ml chloramphenicol and incubated at 37°C for 24h. Following microscopic confirmation of fluorescence, 25% glycerol stock of positive clones were made and stored at -80ºC for future use.

3.5.3. Cell culture

Murine bone marrow-derived macrophages (BMDMs) were harvested from the femur and tibia and cultured as previously described with some modifications (181-184). Briefly, bone marrow cells collected from the femur and tibia of 4-6-week-old female C57BL/6 mice (5-7 mice per experiment) were cultured at 1 x 10^6 cells/ml in αMEM media (Life Technologies, Beverly, MA) supplemented with 10% FBS and 20 ng/ml of recombinant mouse M-CSF (R&D Systems). Following two days of incubation at 37ºC with 5% CO2, nonadherent cells were discarded and adherent cells were subcultured as BMDMs. For osteoclast differentiation, BMDMs were cultured (2.5 x 10^4 cells/well in

24-well culture plates) in αMEM media supplemented with 10% FBS, 50 ng/ml of recombinant mouse RANK-L (R&D systems), and 20 ng/ml of recombinant mouse M-CSF (184). For osteoclast maturation, cells were cultured for different times (1-10 days), replacing 50% of the media with fresh media every two days. To characterize and identify osteoclasts, cells were fixed in 4% paraformaldehyde and stained for tartrate-resistant acid phosphatase (TRAP). TRAP-positive cells with 1-2 nuclei were classified as osteoclast precursors (pOC), while TRAP-positive cells with ≥ 3 nuclei were classified as multinucleated mature osteoclasts (mOCs) (184). Osteoclast precursor infections were performed at day 2, while infection of mature osteoclasts was conducted at day 3 in the presence of 50 ng/ml of recombinant mouse RANK-L and 20 ng/ml of recombinant mouse M-CSF.

The mouse MC3T3-E1 cell line (ATCC® CRL-2593™) was used for osteoblast studies. MC3T3-E1 cells were seeded in complete growth media at 1 x 10^5/well in 24-well tissue culture plates and incubated at 37°C with 5% CO_2. After 24h, old media was replaced with αMEM differentiation media (0.5 ml) supplemented with 10% FBS, 50μg/ml ascorbic acid, and 4 mM β-glycerol-phosphate. Differentiation media was replaced every other day for 30 days, and osteoblast maturation was confirmed by measuring calcium deposition and alkaline phosphatase activity.

3.5.4. Cellular infection

BMDMs were cultured either in standard tissue culture plates (Genesee Scientific, 25-107) or in calcium phosphate-coated plates (Corning® Osteo Assay Surface, 3987) and differentiated into mature osteoclasts in the presence of 50 ng/ml of

recombinant mouse RANK-L and 20 ng/ml of recombinant mouse M-CSF. Cells were infected with *B. abortus* 2308, 2308*ΔvirB2*, S19, and S19*ΔvjbR* at an MOI of 100. Immediately following infection, plates were centrifuged for 5 minutes at 200g to synchronize infection (185). Following 2h of incubation at 37°C with 5% CO_2 to allow bacterial entry, extracellular bacteria were removed by washing twice and incubating in differentiation media with 50 µg/ml of gentamicin for 1h (153). To evaluate bacterial invasion and replication, cells at different time points (3h, 24h, and 48h) were washed twice in PBS and lysed in 0.5% (vol/vol) H_2O-Tween 20. Immediately following lysis, lysates were serially diluted (1/10) in PBS and plated on TSA plates. After 3-4 days of incubation at 37°C, colonies were enumerated to quantify bacterial CFU. Undifferentiated BMDMs were infected simultaneously to serve as a control.

Infection of the mouse osteoblast MC3T3-E1 cell line was performed at day 21 to assess cellular invasion and survival. Cells were infected with the same *B. abortus* strains at an MOI of 100. Following cellular infection, plates were centrifuged, incubated, and treated with gentamicin followed by lysis of cells, serial dilution, and plating of suspensions onto TSA plates, as described above.

3.5.5. Direct co-culture of *Brucella*-infected MC3T3-E1 osteoblasts and BMDMs

MC3T3 cells, cultured in complete osteoblast differentiation media for 21 days, were infected with *B. abortus* strains for 2h at an MOI 100 or 1000. At 24h post-infection, cells were washed twice with warm media and incubated for 7 days following addition of fresh differentiation media containing $2.5x10^4$ of BMDMS. On day 3, cultured supernatants were replaced with fresh osteogenic differentiation media

supplemented with 20 ng/ml of M-CSF. As positive controls of mOC formation, uninfected MC3T3 cells and BMDMs were co-cultured in the presence of 20 ng/ml of M-CSF and varying concentrations of RANKL (1, 6.25, and 12 ng/ml) to determine the minimum level of RANKL required for mOC formation. To identify mOCs, cells were fixed by 4% paraformaldehyde for 2h and stained for TRAP.

3.5.6. Stimulation with conditioned media

Culture supernatants from *Brucella*-infected mature MC3T3-E1 osteoblasts at MOI of 100:1 and 1000:1 were aspirated at 24h post-infection, passed through a 0.22-μm filter, and used as conditioned media to stimulate uninfected BMDMs for 7 days. Conditioned media was used at either 25% or 50% concentration in the presence of 20 ng/ml of M-CSF, and on day 3, all media was replaced. As positive controls of mOC formation, M-CSF and different concentration of RANKL were used, as previously described. After seven days of incubation, media was aspirated, and cells were fixed in 4% paraformaldehyde for 2h at room temperature and stained for TRAP.

3.5.7. Neutralization experiments

Neutralization experiments were conducted using 500 ng/ml of anti-RANKL neutralizing antibody (AF462, R&D systems) or its isotype control (AB-108-C, R&D systems). Supernatants from *Brucella*-infected osteoblasts were preincubated with the anti-RANKL neutralizing antibody or its isotype control for 1 h at 37°C with 5% CO_2 before being used to stimulate BMDMs.

3.5.8. Determination of nitric oxide concentrations

The level of nitric oxide (NO) was determined by measuring the released NO metabolites (nitrites) using modified Griess reagent (Sigma, G4410) at 3h, 24h, and 48h post-infection. Briefly, 100 µl of Griess reagent was mixed with 100 µl of culture supernatant in a 96-well plate, incubated for 15 minutes, and spectrophotometric measurement was performed at 540 nm. Nitrite concentration was measured against a freshly made NaNO2 standard curve.

3.5.9. Determination of cell death

LDH released into culture supernatants of infected and uninfected cells at 3h, 24h, and 48h post-infection was determined using the CytoTox 96 nonradioactive cytotoxicity assay kit (Promega, G1780) according to the manufacturer's instructions (185). Cell cytotoxicity was expressed as the percentage of LDH release, which was calculated using the following formula: percentage of LDH release =100 X (test LDH release - spontaneous release) / (maximum release - spontaneous release).

3.5.10. Apoptosis assays

BMDMs were cultured at $5x10^3$/well in 96-well tissue culture plates (Genesee Scientific, 25-109) and differentiated into mature osteoclasts in the presence of 50 ng/ml of recombinant mouse RANKL and 20 ng/ml of recombinant mouse M-CSF. Cells were infected with *B. abortus* 2308, 2308*ΔvirB2*, S19, and S19*ΔvjbR* at an MOI of 100. Immediately following infection, plates were centrifuged, incubated, and treated with

gentamicin, as described above. Apoptotic cells were detected using TdT *in situ* apoptosis detection kit-DAB (R&D, 4810-30-K).

3.5.11. Osteoclast resorption assay

BMDMs cultured in calcium phosphate-coated plates (Corning, MA) were differentiated into mature osteoclasts and infected on day 3. Following 48h of infection, culture supernatants were aspirated, and 10% bleach was added for 5 minutes to remove the cells. The wells were washed twice in dH_2O and dried at room temperature. Resorption pits were observed under a brightfield microscope, and images were quantified using Fiji (https://imagej.net/Fiji/Downloads). TRAP staining was simultaneously performed in unbleached cells to characterize mature osteoclasts and correlate with pit formation.

3.5.12. Tartrate-resistant acid phosphatase (TRAP) staining

TRAP staining was performed as following: uninfected and *Brucella*-infected cells were washed three times with PBS, then fixed with 4% paraformaldehyde for 2h at room temperature. Fixative was aspirated and the cells were washed three time with PBS and incubated with TRAP staining solution (0.504 % sodium acetate, 0.232 % glacial acetic acid, 1.412 % potassium sodium tartrate tetrahydrate, 4.16% sodium nitrite, 2 N HCL, 4% pararosaniline solution, and 10% Naphthol AS-BI solution) for 30-45 minutes at 37ºC until desired staining intensity was achieved. Subsequently, the TRAP staining solution was removed, cells were washed three times with distilled water, and the plates were left upside down to dry before counting TRAP+mature osteoclasts having ≥3 nuclei per cell.

3.5.13. Confocal microscopy

BMDMs seeded at a concentration of 2.5 x 10^4 cells/well in 24 well black microplates (Ibidi, 82406) in the presence of 50 ng/ml of recombinant mouse RANKL and 20 ng/ml of recombinant mouse M-CSF were infected with GFP-*B. abortus* strains for 3h, 24h, and 48h and subsequently fixed in 4% paraformaldehyde. Cells were permeabilized in 0.25% Triton X100 in PBS for 5 min, washed twice with PBS, and stained for F-actin using Texas Red®-X Phalloidin (T7471, Thermo Fisher Scientific, USA) at 1:300 for overnight at 4°C. Following washing in PBS, cell nuclei were stained using Hoechst 33342 solution (62249, Thermo Fisher Scientific, USA) for 10 minutes. Washed cells stored in PBS were imaged and analyzed using a Zeiss 780 confocal microscope.

3.5.14. Alizarin red S and Alkaline phosphatase staining

To assess calcium deposition, Alizarin red staining was used. MC3T3-E1 cells were seeded at 1 x 10^5/well onto 24-well tissue culture plates. On days 7, 14, and 21 of differentiation, cells were washed in PBS, fixed in 4% paraformaldehyde, stained in 2% (wt/vol) Alizarin red S, and visualized by light microscopy (72). At the same time points, ALP staining of osteoblasts was performed using ALP kit (86R-1KT, Sigma-Aldrich) according to the manufacturer's instructions.

3.5.15. Statistical analysis

Each experiment was repeated at least three times and statistical analysis was performed using one-way and two-way analysis of variance (ANOVA), followed by

Tukey's range test using GraphPad Prism software, version 4.0. Data are represented as means ± standard deviations (SD). A p-value of <0.05 was considered significant.

4. CONCLUSIONS

This work characterizes an improved laboratory animal model (NSG mice) as well as an in vitro model (osteoclasts) to study the molecular mechanisms and pathological lesions (e.g., osteoarticular disease) associated with live attenuated *Brucella* vaccines. The results obtained under Aim 1 demonstrated that while NSG mice inoculated with S19 developed arthritis, S19*ΔvjbR*-inoculated mice did not show significant clinical changes, supporting the safety of the S19*ΔvjbR* vaccine candidate and validating the superiority of this model in assessing vaccine safety in the context of osteoarticular disease. Under Aim 2, an in vitro model of osteoclast maturation from mouse bone marrow-derived macrophages was standardized and used to study the effects of wild type and attenuated *Brucella* spp. infection on osteoclast maturation and activity. While the calcium matrix resorption assay demonstrated the bone-resorbing capacity of osteoclasts with or without infection, intracellular survival and replication of bacteria reflected as most critical in developing osteoarticular disorder in brucellosis as observed in our in vivo study. These models pave the way for future studies of (i) vaccine safety, (ii) host-pathogen interactions and intracellular trafficking, (ii) cellular and immune mechanisms of osteoarticular brucellosis, (iv) pathogenesis of bone disease in other infections conditions.

5. REFERENCES

1. Banai M. 2002. Control of small ruminant brucellosis by use of Brucella melitensis Rev.1 vaccine: laboratory aspects and field observations. Vet Microbiol 90:497-519.
2. Hensel ME, Arenas-Gamboa AM. 2018. A Neglected Animal Model for a Neglected Disease: Guinea Pigs and the Search for an Improved Animal Model for Human Brucellosis. Front Microbiol 9:2593.
3. Lucero NE, Ayala SM, Escobar GI, Jacob NR. 2008. Brucella isolated in humans and animals in Latin America from 1968 to 2006. Epidemiol Infect 136:496-503.
4. Whatmore AM, Koylass MS, Muchowski J, Edwards-Smallbone J, Gopaul KK, Perrett LL. 2016. Extended Multilocus Sequence Analysis to Describe the Global Population Structure of the Genus Brucella: Phylogeography and Relationship to Biovars. Front Microbiol 7:2049.
5. de Figueiredo P, Ficht TA, Rice-Ficht A, Rossetti CA, Adams LG. 2015. Pathogenesis and immunobiology of brucellosis: review of Brucella-host interactions. Am J Pathol 185:1505-17.
6. Franco MP, Mulder M, Gilman RH, Smits HL. 2007. Human brucellosis. Lancet Infect Dis 7:775-86.
7. Meltzer E, Sidi Y, Smolen G, Banai M, Bardenstein S, Schwartz E. 2010. Sexually transmitted brucellosis in humans. Clin Infect Dis 51:e12-5.

8. Seleem MN, Boyle SM, Sriranganathan N. 2010. Brucellosis: a re-emerging zoonosis. Vet Microbiol 140:392-8.

9. Young EJ. 1983. Human brucellosis. Rev Infect Dis 5:821-42.

10. Pappas G, Papadimitriou P, Akritidis N, Christou L, Tsianos EV. 2006. The new global map of human brucellosis. Lancet Infect Dis 6:91-9.

11. Ariza J, Corredoira J, Pallares R, Viladrich PF, Rufi G, Pujol M, Gudiol F. 1995. Characteristics of and risk factors for relapse of brucellosis in humans. Clin Infect Dis 20:1241-9.

12. Poester FP, Goncalves VS, Paixao TA, Santos RL, Olsen SC, Schurig GG, Lage AP. 2006. Efficacy of strain RB51 vaccine in heifers against experimental brucellosis. Vaccine 24:5327-34.

13. Lilenbaum W, de Souza GN, Ristow P, Moreira MC, Fraguas S, Cardoso Vda S, Oelemann WM. 2007. A serological study on *Brucella abortus*, caprine arthritis-encephalitis virus and Leptospira in dairy goats in Rio de Janeiro, Brazil. Vet J 173:408-12.

14. Fretin D, Whatmore AM, Al Dahouk S, Neubauer H, Garin-Bastuji B, Albert D, Van Hessche M, Menart M, Godfroid J, Walravens K, Wattiau P. 2008. Brucella suis identification and biovar typing by real-time PCR. Vet Microbiol 131:376-85.

15. Verger JM, Grayon M, Zundel E, Lechopier P, Olivier-Bernardin V. 1995. Comparison of the efficacy of Brucella suis strain 2 and Brucella melitensis Rev.

1 live vaccines against a Brucella melitensis experimental infection in pregnant ewes. Vaccine 13:191-6.

16. Glynn MK, Lynn TV. 2008. Brucellosis. J Am Vet Med Assoc 233:900-8.

17. Corbel MJ. 1997. Brucellosis: an overview. Emerg Infect Dis 3:213-21.

18. Meador VP, Deyoe BL. 1989. Intracellular localization of *Brucella abortus* in bovine placenta. Vet Pathol 26:513-5.

19. Xavier MN, Paixao TA, Poester FP, Lage AP, Santos RL. 2009. Pathological, immunohistochemical and bacteriological study of tissues and milk of cows and fetuses experimentally infected with *Brucella abortus*. J Comp Pathol 140:149-57.

20. Joffee B, Diamond MT. 1966. Brucellosis due to self-inoculation. Ann Intern Med 65:564-5.

21. Kim S, Lee DS, Watanabe K, Furuoka H, Suzuki H, Watarai M. 2005. Interferon-gamma promotes abortion due to Brucella infection in pregnant mice. BMC Microbiol 5:22.

22. Hasanjani Roushan MR, Ebrahimpour S. 2015. Human brucellosis: An overview. Caspian J Intern Med 6:46-7.

23. Colmenero Jde D, Queipo-Ortuno MI, Maria Reguera J, Angel Suarez-Munoz M, Martin-Carballino S, Morata P. 2002. Chronic hepatosplenic abscesses in Brucellosis. Clinico-therapeutic features and molecular diagnostic approach. Diagn Microbiol Infect Dis 42:159-67.

24. Castano MJ, Solera J. 2009. Chronic brucellosis and persistence of Brucella melitensis DNA. J Clin Microbiol 47:2084-9.

25. Deveer M, Sozen H, Cullu N, Sivrioglu AK. 2013. Splenic abscess due to acute brucellosis. BMJ Case Rep 2013.

26. Koca YS, Barut I, Koca T, Kaya O, Aktas RA. 2016. Acute Abdomen Caused by Brucellar Hepatic Abscess. Am J Trop Med Hyg 94:73-5.

27. Ruben B, Band JD, Wong P, Colville J. 1991. Person-to-person transmission of Brucella melitensis. Lancet 337:14-5.

28. Tuon FF, Gondolfo RB, Cerchiari N. 2017. Human-to-human transmission of Brucella - a systematic review. Trop Med Int Health 22:539-546.

29. Ebel ED, Williams MS, Tomlinson SM. 2008. Estimating herd prevalence of bovine brucellosis in 46 USA states using slaughter surveillance. Prev Vet Med 85:295-316.

30. Treanor JJ, Johnson JS, Wallen RL, Cilles S, Crowley PH, Cox JJ, Maehr DS, White PJ, Plumb GE. 2010. Vaccination strategies for managing brucellosis in Yellowstone bison. Vaccine 28 Suppl 5:F64-72.

31. Adams LG. 2002. The pathology of brucellosis reflects the outcome of the battle between the host genome and the Brucella genome. Vet Microbiol 90:553-61.

32. Hou H, Liu X, Peng Q. 2019. The advances in brucellosis vaccines. Vaccine 37:3981-3988.

33. Coventry MB, Ivins JC, et al. 1949. Infection of the hip by Brucella suis. J Am Med Assoc 141:320-5.

34. Jaffray D, MacKenzie IG. 1979. *Brucella abortus* arthritis. Arthritis Rheum 22:806.

35. Solera J, Lozano E, Martinez-Alfaro E, Espinosa A, Castillejos ML, Abad L. 1999. Brucellar spondylitis: review of 35 cases and literature survey. Clin Infect Dis 29:1440-9.

36. Giambartolomei GH, Arriola Benitez PC, Delpino MV. 2017. Brucella and Osteoarticular Cell Activation: Partners in Crime. Front Microbiol 8:256.

37. Gotuzzo E, Alarcon GS, Bocanegra TS, Carrillo C, Guerra JC, Rolando I, Espinoza LR. 1982. Articular involvement in human brucellosis: a retrospective analysis of 304 cases. Semin Arthritis Rheum 12:245-55.

38. Rajapakse CN. 1995. Bacterial infections: osteoarticular brucellosis. Baillieres Clin Rheumatol 9:161-77.

39. Pappas G, Akritidis N, Bosilkovski M, Tsianos E. 2005. Brucellosis. N Engl J Med 352:2325-36.

40. Wong TM, Lou N, Jin W, Leung F, To M, Leung F. 2014. Septic arthritis caused by Brucella melitensis in urban Shenzhen, China: a case report. J Med Case Rep 8:367.

41. Miron D, Garty I, Tal I, Horovitz Y, Kedar A. 1987. Sacroiliitis as a sole manifestation of Brucella melitensis infection in a child. Clin Nucl Med 12:466-7.

42. Ozturk M, Yavuz F, Altun D, Ulubay M, Firatligil FB. 2015. Postpartum Bilateral Sacroiliitis caused by Brucella Infection. J Clin Diagn Res 9:QD07-8.

43. Kadanali A, Uslu H, Bayraktar R, Varoglu E. 2012. Detection of orchitis and sacroiliitis due to brucellosis by 99mTc polyclonal human immunoglobulin scintigraphy. Clin Nucl Med 37:671-3.

44. Owlia MB, Danesh-Ardakani M. 2016. Frequency of sacroiliitis among patients with low back pain. Electron Physician 8:2094-100.

45. Cobbaert K, Pieters A, Devinck M, Devos M, Goethals I, Mielants H. 2007. Brucellar spondylodiscitis: case report. Acta Clin Belg 62:304-7.

46. Raptopoulou A, Karantanas AH, Poumboulidis K, Grollios G, Raptopoulou-Gigi M, Garyfallos A. 2006. Brucellar spondylodiscitis: noncontiguous multifocal involvement of the cervical, thoracic, and lumbar spine. Clin Imaging 30:214-7.

47. Aktug-Demir N, Kolgelier S, Ozcimen S, Sumer S, Demir LS, Inkaya AC. 2014. Diagnostic clues for spondylitis in acute brucellosis. Saudi Med J 35:816-20.

48. al-Eissa YA, Kambal AM, Alrabeeah AA, Abdullah AM, al-Jurayyan NA, al-Jishi NM. 1990. Osteoarticular brucellosis in children. Ann Rheum Dis 49:896-900.

49. Kelly PJ, Martin WJ, Schirger A, Weed LA. 1960. Brucellosis of the bones and joints. Experience with thirty-six patients. JAMA 174:347-53.

50. Laajam MA. 1985. Synovial rupture complicating Brucella arthritis. Br J Rheumatol 24:191-3.

51. Wallach JC, Delpino MV, Scian R, Deodato B, Fossati CA, Baldi PC. 2010. Prepatellar bursitis due to *Brucella abortus:* case report and analysis of the local immune response. J Med Microbiol 59:1514-8.

52. Alp E, Doganay M. 2008. Current therapeutic strategy in spinal brucellosis. Int J Infect Dis 12:573-7.

53. Priest JR, Low D, Wang C, Bush T. 2008. Brucellosis and sacroiliitis: a common presentation of an uncommon pathogen. J Am Board Fam Med 21:158-61.

54. Wanke MM. 2004. Canine brucellosis. Anim Reprod Sci 82-83:195-207.

55. Johnson B, Mosier DA, Morton RJ, Confer AW. 1994. Experimental *Brucella abortus* strain 19 arthritis in young cattle. J Vet Diagn Invest 6:56-61.

56. Coid CR, Vaughan LC. 1957. Incidence of carpal hygromas in dairy cattle infected with *Br. abortus* and maintained in an isolation compound. J Comp Pathol 67:53-6.

57. Skyberg JA, Thornburg T, Kochetkova I, Layton W, Callis G, Rollins MF, Riccardi C, Becker T, Golden S, Pascual DW. 2012. IFN-gamma-deficient mice develop IL-1-dependent cutaneous and musculoskeletal inflammation during experimental brucellosis. J Leukoc Biol 92:375-87.

58. Lacey CA, Keleher LL, Mitchell WJ, Brown CR, Skyberg JA. 2016. CXCR2 Mediates Brucella-Induced Arthritis in Interferon gamma-Deficient Mice. J Infect Dis 214:151-60.

59. Magnani DM, Lyons ET, Forde TS, Shekhani MT, Adarichev VA, Splitter GA. 2013. Osteoarticular tissue infection and development of skeletal pathology in murine brucellosis. Dis Model Mech 6:811-8.

60. Grillo MJ, Blasco JM, Gorvel JP, Moriyon I, Moreno E. 2012. What have we learned from brucellosis in the mouse model? Vet Res 43:29.

61. Arenas-Gamboa AM, Ficht TA, Kahl-McDonagh MM, Gomez G, Rice-Ficht AC. 2009. The *Brucella abortus* S19 DeltavjbR live vaccine candidate is safer than S19 and confers protection against wild-type challenge in BALB/c mice when delivered in a sustained-release vehicle. Infect Immun 77:877-84.

62. Silva TM, Costa EA, Paixao TA, Tsolis RM, Santos RL. 2011. Laboratory animal models for brucellosis research. J Biomed Biotechnol 2011:518323.

63. Ikeda K, Takeshita S. 2016. The role of osteoclast differentiation and function in skeletal homeostasis. J Biochem 159:1-8.

64. Bonewald LF. 2011. The amazing osteocyte. J Bone Miner Res 26:229-38.

65. Zhao S, Zhang YK, Harris S, Ahuja SS, Bonewald LF. 2002. MLO-Y4 osteocyte-like cells support osteoclast formation and activation. J Bone Miner Res 17:2068-79.

66. Jacome-Galarza CE, Percin GI, Muller JT, Mass E, Lazarov T, Eitler J, Rauner M, Yadav VK, Crozet L, Bohm M, Loyher PL, Karsenty G, Waskow C, Geissmann F. 2019. Developmental origin, functional maintenance and genetic rescue of osteoclasts. Nature 568:541-545.

67. Rucci N, Teti A. 2016. The "love-hate" relationship between osteoclasts and bone matrix. Matrix Biol 52-54:176-190.

68. Chellaiah MA. 2005. Regulation of actin ring formation by rho GTPases in osteoclasts. J Biol Chem 280:32930-43.

69. Palokangas H, Mulari M, Vaananen HK. 1997. Endocytic pathway from the basal plasma membrane to the ruffled border membrane in bone-resorbing osteoclasts. J Cell Sci 110 (Pt 15):1767-80.

70. Scott CC, Gruenberg J. 2011. Ion flux and the function of endosomes and lysosomes: pH is just the start: the flux of ions across endosomal membranes influences endosome function not only through regulation of the luminal pH. Bioessays 33:103-10.

71. Madel MB, Ibanez L, Wakkach A, de Vries TJ, Teti A, Apparailly F, Blin-Wakkach C. 2019. Immune Function and Diversity of Osteoclasts in Normal and Pathological Conditions. Front Immunol 10:1408.

72. Scian R, Barrionuevo P, Fossati CA, Giambartolomei GH, Delpino MV. 2012. *Brucella abortus* invasion of osteoblasts inhibits bone formation. Infect Immun 80:2333-45.

73. Scian R, Barrionuevo P, Giambartolomei GH, Fossati CA, Baldi PC, Delpino MV. 2011. Granulocyte-macrophage colony-stimulating factor- and tumor necrosis factor alpha-mediated matrix metalloproteinase production by human osteoblasts and monocytes after infection with B*rucella abortus.* Infect Immun 79:192-202.

74. Pesce Viglietti AI, Arriola Benitez PC, Gentilini MV, Velasquez LN, Fossati CA, Giambartolomei GH, Delpino MV. 2015. *Brucella abortus* Invasion of Osteocytes Modulates Connexin 43 and Integrin Expression and Induces

Osteoclastogenesis via Receptor Activator of NF-kappaB Ligand and Tumor Necrosis Factor Alpha Secretion. Infect Immun 84:11-20.

75. Bercovich Z. 2000. The use of skin delayed-type hypersensitivity as an adjunct test to diagnose brucellosis in cattle: a review. Vet Q 22:123-30.

76. Dean AS, Crump L, Greter H, Hattendorf J, Schelling E, Zinsstag J. 2012. Clinical manifestations of human brucellosis: a systematic review and meta-analysis. PLoS Negl Trop Dis 6:e1929.

77. Young EJ, Hasanjani Roushan MR, Shafae S, Genta RM, Taylor SL. 2014. Liver histology of acute brucellosis caused by Brucella melitensis. Hum Pathol 45:2023-8.

78. Bossi P, Tegnell A, Baka A, Van Loock F, Hendriks J, Werner A, Maidhof H, Gouvras G, Task Force on B, Chemical Agent Threats PHDECL. 2004. Bichat guidelines for the clinical management of brucellosis and bioterrorism-related brucellosis. Euro Surveill 9:E15-6.

79. Dorneles EM, Lima GK, Teixeira-Carvalho A, Araujo MS, Martins-Filho OA, Sriranganathan N, Al Qublan H, Heinemann MB, Lage AP. 2015. Immune Response of Calves Vaccinated with *Brucella abortus* S19 or RB51 and Revaccinated with RB51. PLoS One 10:e0136696.

80. Ashford DA, di Pietra J, Lingappa J, Woods C, Noll H, Neville B, Weyant R, Bragg SL, Spiegel RA, Tappero J, Perkins BA. 2004. Adverse events in humans associated with accidental exposure to the livestock brucellosis vaccine RB51. Vaccine 22:3435-9.

81. Adetunji SA, Ramirez G, Foster MJ, Arenas-Gamboa AM. 2019. A systematic review and meta-analysis of the prevalence of osteoarticular brucellosis. PLoS Negl Trop Dis 13:e0007112.

82. Aydin M, Fuat Yapar A, Savas L, Reyhan M, Pourbagher A, Turunc TY, Ziya Demiroglu Y, Yologlu NA, Aktas A. 2005. Scintigraphic findings in osteoarticular brucellosis. Nucl Med Commun 26:639-47.

83. Rajashekara G, Glover DA, Krepps M, Splitter GA. 2005. Temporal analysis of pathogenic events in virulent and avirulent Brucella melitensis infections. Cell Microbiol 7:1459-73.

84. Shultz LD, Lyons BL, Burzenski LM, Gott B, Chen X, Chaleff S, Kotb M, Gillies SD, King M, Mangada J, Greiner DL, Handgretinger R. 2005. Human lymphoid and myeloid cell development in NOD/LtSz-scid IL2R gamma null mice engrafted with mobilized human hemopoietic stem cells. J Immunol 174:6477-89.

85. Kang YK, Ko Y, Choi A, Choi HJ, Seo JH, Lee M, Lee JA. 2016. Humanizing NOD/SCID/IL-2Rgammanull (NSG) mice using busulfan and retro-orbital injection of umbilical cord blood-derived CD34(+) cells. Blood Res 51:31-6.

86. Libby SJ, Brehm MA, Greiner DL, Shultz LD, McClelland M, Smith KD, Cookson BT, Karlinsey JE, Kinkel TL, Porwollik S, Canals R, Cummings LA, Fang FC. 2010. Humanized nonobese diabetic-scid IL2rgammanull mice are susceptible to lethal Salmonella Typhi infection. Proc Natl Acad Sci U S A 107:15589-94.

87. Arenas-Gamboa AM, Ficht TA, Kahl-McDonagh MM, Rice-Ficht AC. 2008. Immunization with a single dose of a microencapsulated Brucella melitensis mutant enhances protection against wild-type challenge. Infect Immun 76:2448-55.

88. Delrue RM, Deschamps C, Leonard S, Nijskens C, Danese I, Schaus JM, Bonnot S, Ferooz J, Tibor A, De Bolle X, Letesson JJ. 2005. A quorum-sensing regulator controls expression of both the type IV secretion system and the flagellar apparatus of Brucella melitensis. Cell Microbiol 7:1151-61.

89. Arenas-Gamboa AM, Rice-Ficht AC, Fan Y, Kahl-McDonagh MM, Ficht TA. 2012. Extended safety and efficacy studies of the attenuated Brucella vaccine candidates 16 M(Delta)vjbR and S19(Delta)vjbR in the immunocompromised IRF-1-/- mouse model. Clin Vaccine Immunol 19:249-60.

90. Warnke R, Pederson M, Williams C, Levy R. 1978. A study of lymphoproliferative diseases comparing immunofluorescence with immunohistochemistry. Am J Clin Pathol 70:67-75.

91. Mason DY, Micklem K, Jones M. 2000. Double immunofluorescence labelling of routinely processed paraffin sections. J Pathol 191:452-61.

92. Duong le T, Leung AT, Langdahl B. 2016. Cathepsin K Inhibition: A New Mechanism for the Treatment of Osteoporosis. Calcif Tissue Int 98:381-97.

93. Brehm MA, Jouvet N, Greiner DL, Shultz LD. 2013. Humanized mice for the study of infectious diseases. Curr Opin Immunol 25:428-35.

94. Racki WJ, Covassin L, Brehm M, Pino S, Ignotz R, Dunn R, Laning J, Graves SK, Rossini AA, Shultz LD, Greiner DL. 2010. NOD-scid IL2rgamma(null) mouse model of human skin transplantation and allograft rejection. Transplantation 89:527-36.

95. Jaiswal S, Pazoles P, Woda M, Shultz LD, Greiner DL, Brehm MA, Mathew A. 2012. Enhanced humoral and HLA-A2-restricted dengue virus-specific T-cell responses in humanized BLT NSG mice. Immunology 136:334-43.

96. Jaiswal S, Pearson T, Friberg H, Shultz LD, Greiner DL, Rothman AL, Mathew A. 2009. Dengue virus infection and virus-specific HLA-A2 restricted immune responses in humanized NOD-scid IL2rgammanull mice. PLoS One 4:e7251.

97. Jimenez-Diaz MB, Mulet T, Viera S, Gomez V, Garuti H, Ibanez J, Alvarez-Doval A, Shultz LD, Martinez A, Gargallo-Viola D, Angulo-Barturen I. 2009. Improved murine model of malaria using Plasmodium falciparum competent strains and non-myelodepleted NOD-scid IL2Rgamma null mice engrafted with human erythrocytes. Antimicrob Agents Chemother 53:4533-6.

98. White RE, Ramer PC, Naresh KN, Meixlsperger S, Pinaud L, Rooney C, Savoldo B, Coutinho R, Bodor C, Gribben J, Ibrahim HA, Bower M, Nourse JP, Gandhi MK, Middeldorp J, Cader FZ, Murray P, Munz C, Allday MJ. 2012. EBNA3B-deficient EBV promotes B cell lymphomagenesis in humanized mice and is found in human tumors. J Clin Invest 122:1487-502.

99. Osman AE, Hassan AN, Ali AE, Abdoel TH, Smits HL. 2015. Brucella melitensis Biovar 1 and *Brucella abortus* S19 Vaccine Strain Infections in

Milkers Working at Cattle Farms in the Khartoum Area, Sudan. PLoS One 10:e0123374.

100. Xie J, Wang J, Li Z, Wang W, Pang Y, He Y. 2018. Ontology-Based Meta-Analysis of Animal and Human Adverse Events Associated With Licensed Brucellosis Vaccines. Front Pharmacol 9:503.

101. Greenfield RA, Drevets DA, Machado LJ, Voskuhl GW, Cornea P, Bronze MS. 2002. Bacterial pathogens as biological weapons and agents of bioterrorism. Am J Med Sci 323:299-315.

102. Baldwin CL, Parent M. 2002. Fundamentals of host immune response against *Brucella abortus*: what the mouse model has revealed about control of infection. Vet Microbiol 90:367-82.

103. Kahl-McDonagh MM, Arenas-Gamboa AM, Ficht TA. 2007. Aerosol infection of BALB/c mice with Brucella melitensis and *Brucella abortus* and protective efficacy against aerosol challenge. Infect Immun 75:4923-32.

104. Stevens MG, Olsen SC, Pugh GW, Jr., Palmer MV. 1994. Immune and pathologic responses in mice infected with *Brucella abortus* 19, RB51, or 2308. Infect Immun 62:3206-12.

105. Tobias L, Cordes DO, Schurig GG. 1993. Placental pathology of the pregnant mouse inoculated with *Brucella abortus* strain 2308. Vet Pathol 30:119-29.

106. Akritidis N, Tzivras M, Delladetsima I, Stefanaki S, Moutsopoulos HM, Pappas G. 2007. The liver in brucellosis. Clin Gastroenterol Hepatol 5:1109-12.

107. Foreman O, Kavirayani AM, Griffey SM, Reader R, Shultz LD. 2011. Opportunistic bacterial infections in breeding colonies of the NSG mouse strain. Vet Pathol 48:495-9.

108. Kluger MJ. 1991. Fever: role of pyrogens and cryogens. Physiol Rev 71:93-127.

109. Clemmer TP, Fisher CJ, Jr., Bone RC, Slotman GJ, Metz CA, Thomas FO. 1992. Hypothermia in the sepsis syndrome and clinical outcome. The Methylprednisolone Severe Sepsis Study Group. Crit Care Med 20:1395-401.

110. Kushimoto S, Gando S, Saitoh D, Mayumi T, Ogura H, Fujishima S, Araki T, Ikeda H, Kotani J, Miki Y, Shiraishi S, Suzuki K, Suzuki Y, Takeyama N, Takuma K, Tsuruta R, Yamaguchi Y, Yamashita N, Aikawa N, Group JSRS. 2013. The impact of body temperature abnormalities on the disease severity and outcome in patients with severe sepsis: an analysis from a multicenter, prospective survey of severe sepsis. Crit Care 17:R271.

111. Marik PE, Zaloga GP. 2000. Hypothermia and cytokines in septic shock. Norasept II Study Investigators. North American study of the safety and efficacy of murine monoclonal antibody to tumor necrosis factor for the treatment of septic shock. Intensive Care Med 26:716-21.

112. Dayan L, Deyev S, Palma L, Rozen N. 2009. Long-standing, neglected sacroiliitis with remarked sacro-iliac degenerative changes as a result of Brucella spp. infection. Spine J 9:e1-4.

113. Rapp AE, Bindl R, Recknagel S, Erbacher A, Muller I, Schrezenmeier H, Ehrnthaller C, Gebhard F, Ignatius A. 2016. Fracture Healing Is Delayed in Immunodeficient NOD/scidIL2Rgammacnull Mice. PLoS One 11:e0147465.

114. Sola-Landa A, Pizarro-Cerda J, Grillo MJ, Moreno E, Moriyon I, Blasco JM, Gorvel JP, Lopez-Goni I. 1998. A two-component regulatory system playing a critical role in plant pathogens and endosymbionts is present in *Brucella abortus* and controls cell invasion and virulence. Mol Microbiol 29:125-38.

115. Feng X, Teitelbaum SL. 2013. Osteoclasts: New Insights. Bone Res 1:11-26.

116. Teitelbaum SL. 1993. Bone remodeling and the osteoclast. J Bone Miner Res 8 Suppl 2:S523-5.

117. Teitelbaum SL, Ross FP. 2003. Genetic regulation of osteoclast development and function. Nat Rev Genet 4:638-49.

118. Kaneko K, Miyamoto Y, Tsukuura R, Sasa K, Akaike T, Fujii S, Yoshimura K, Nagayama K, Hoshino M, Inoue S, Maki K, Baba K, Chikazu D, Kamijo R. 2018. 8-Nitro-cGMP is a promoter of osteoclast differentiation induced by RANKL. Nitric Oxide 72:46-51.

119. Boyce BF. 2013. Advances in the regulation of osteoclasts and osteoclast functions. J Dent Res 92:860-7.

120. Boyle WJ, Simonet WS, Lacey DL. 2003. Osteoclast differentiation and activation. Nature 423:337-42.

121. Hoshino A, Hanada S, Yamada H, Mii S, Takahashi M, Mitarai S, Yamamoto K, Manome Y. 2014. Mycobacterium tuberculosis escapes from the phagosomes of

infected human osteoclasts reprograms osteoclast development via dysregulation of cytokines and chemokines. Pathog Dis 70:28-39.

122. Janeczko S, Atwater D, Bogel E, Greiter-Wilke A, Gerold A, Baumgart M, Bender H, McDonough PL, McDonough SP, Goldstein RE, Simpson KW. 2008. The relationship of mucosal bacteria to duodenal histopathology, cytokine mRNA, and clinical disease activity in cats with inflammatory bowel disease. Vet Microbiol 128:178-93.

123. Wellinghausen N, Nockler K, Sigge A, Bartel M, Essig A, Poppert S. 2006. Rapid detection of Brucella spp. in blood cultures by fluorescence in situ hybridization. J Clin Microbiol 44:1828-30.

124. Amann RI, Binder BJ, Olson RJ, Chisholm SW, Devereux R, Stahl DA. 1990. Combination of 16S rRNA-targeted oligonucleotide probes with flow cytometry for analyzing mixed microbial populations. Appl Environ Microbiol 56:1919-25.

125. Chan V, Crocetti G, Grehan M, Zhang L, Danon S, Lee A, Mitchell H. 2005. Visualization of Helicobacter species within the murine cecal mucosa using specific fluorescence in situ hybridization. Helicobacter 10:114-24.

126. Atluri VL, Xavier MN, de Jong MF, den Hartigh AB, Tsolis RM. 2011. Interactions of the human pathogenic Brucella species with their hosts. Annu Rev Microbiol 65:523-41.

127. Schurig GG, Sriranganathan N, Corbel MJ. 2002. Brucellosis vaccines: past, present and future. Vet Microbiol 90:479-96.

128. Dorneles EM, Sriranganathan N, Lage AP. 2015. Recent advances in *Brucella abortus* vaccines. Vet Res 46:76.

129. Anderson GI, Binnington AG. 1983. Discospondylitis and orchitis associated with high Brucella titre in a dog. Can Vet J 24:249-52.

130. Johnson CA, Carter TD, Dunn JR, Baer SR, Schalow MM, Bellay YM, Guerra MA, Frank NA. 2018. Investigation and characterization of Brucella canis infections in pet-quality dogs and associated human exposures during a 2007-2016 outbreak in Michigan. J Am Vet Med Assoc 253:322-336.

131. Thomas WB. 2000. Diskospondylitis and other vertebral infections. Vet Clin North Am Small Anim Pract 30:169-82, vii.

132. Corbel MJ. 2006. Brucellosis in humans and animals. World Health Organization W.H.O., Food and Agriculture Organization

of the United Nations F.A.O., and World Organisation for Animal Health O.I.E., Geneva.

133. Florencio-Silva R, Sasso GR, Sasso-Cerri E, Simoes MJ, Cerri PS. 2015. Biology of Bone Tissue: Structure, Function, and Factors That Influence Bone Cells. Biomed Res Int 2015:421746.

134. Nollet M, Santucci-Darmanin S, Breuil V, Al-Sahlanee R, Cros C, Topi M, Momier D, Samson M, Pagnotta S, Cailleteau L, Battaglia S, Farlay D, Dacquin R, Barois N, Jurdic P, Boivin G, Heymann D, Lafont F, Lu SS, Dempster DW, Carle GF, Pierrefite-Carle V. 2014. Autophagy in osteoblasts is involved in mineralization and bone homeostasis. Autophagy 10:1965-77.

135. Delpino MV, Fossati CA, Baldi PC. 2009. Proinflammatory response of human osteoblastic cell lines and osteoblast-monocyte interaction upon infection with Brucella spp. Infect Immun 77:984-95.

136. Scian R, Barrionuevo P, Rodriguez AM, Arriola Benitez PC, Garcia Samartino C, Fossati CA, Giambartolomei GH, Delpino MV. 2013. Bru*cella* abortus invasion of synoviocytes inhibits apoptosis and induces bone resorption through RANKL expression. Infect Immun 81:1940-51.

137. Boyce BF, Yao Z, Xing L. 2009. Osteoclasts have multiple roles in bone in addition to bone resorption. Crit Rev Eukaryot Gene Expr 19:171-80.

138. Khalaf OH, Chaki SP, Garcia-Gonzalez DG, Ficht TA, Arenas-Gamboa AM. 2019. NOD-scid IL2rgamma(null) Mouse Model is suitable to Study Osteoarticular Brucellosis and Vaccine Safety. Infect Immun doi:10.1128/IAI.00901-18.

139. Tevlin R, McArdle A, Chan CK, Pluvinage J, Walmsley GG, Wearda T, Marecic O, Hu MS, Paik KJ, Senarath-Yapa K, Atashroo DA, Zielins ER, Wan DC, Weissman IL, Longaker MT. 2014. Osteoclast derivation from mouse bone marrow. J Vis Exp doi:10.3791/52056:e52056.

140. Marino S, Logan JG, Mellis D, Capulli M. 2014. Generation and culture of osteoclasts. Bonekey Rep 3:570.

141. Lacey DL, Boyle WJ, Simonet WS, Kostenuik PJ, Dougall WC, Sullivan JK, San Martin J, Dansey R. 2012. Bench to bedside: elucidation of the OPG-RANK-

RANKL pathway and the development of denosumab. Nat Rev Drug Discov 11:401-19.

142. Celli J. 2006. Surviving inside a macrophage: the many ways of Brucella. Res Microbiol 157:93-8.

143. Roop RM, 2nd, Bellaire BH, Valderas MW, Cardelli JA. 2004. Adaptation of the Brucellae to their intracellular niche. Mol Microbiol 52:621-30.

144. Akchurin T, Aissiou T, Kemeny N, Prosk E, Nigam N, Komarova SV. 2008. Complex dynamics of osteoclast formation and death in long-term cultures. PLoS One 3:e2104.

145. Gardner CR. 2007. Morphological analysis of osteoclastogenesis induced by RANKL in mouse bone marrow cell cultures. Cell Biol Int 31:672-82.

146. Kopesky P, Tiedemann K, Alkekhia D, Zechner C, Millard B, Schoeberl B, Komarova SV. 2014. Autocrine signaling is a key regulatory element during osteoclastogenesis. Biol Open 3:767-76.

147. Decker T, Lohmann-Matthes ML. 1988. A quick and simple method for the quantitation of lactate dehydrogenase release in measurements of cellular cytotoxicity and tumor necrosis factor (TNF) activity. J Immunol Methods 115:61-9.

148. Phan TT, See P, Lee ST, Chan SY. 2001. Protective effects of curcumin against oxidative damage on skin cells in vitro: its implication for wound healing. J Trauma 51:927-31.

149. Chan ED, Chan J, Schluger NW. 2001. What is the role of nitric oxide in murine and human host defense against tuberculosis?Current knowledge. Am J Respir Cell Mol Biol 25:606-12.

150. Nilforoushan D, Gramoun A, Glogauer M, Manolson MF. 2009. Nitric oxide enhances osteoclastogenesis possibly by mediating cell fusion. Nitric Oxide 21:27-36.

151. van't Hof RJ, Ralston SH. 1997. Cytokine-induced nitric oxide inhibits bone resorption by inducing apoptosis of osteoclast progenitors and suppressing osteoclast activity. J Bone Miner Res 12:1797-804.

152. Byndloss MX, Tsai AY, Walker GT, Miller CN, Young BM, English BC, Seyffert N, Kerrinnes T, de Jong MF, Atluri VL, Winter MG, Celli J, Tsolis RM. 2019. *Brucella abortus* Infection of Placental Trophoblasts Triggers Endoplasmic Reticulum Stress-Mediated Cell Death and Fetal Loss via Type IV Secretion System-Dependent Activation of CHOP. MBio 10.

153. Trouillet-Assant S, Gallet M, Nauroy P, Rasigade JP, Flammier S, Parroche P, Marvel J, Ferry T, Vandenesch F, Jurdic P, Laurent F. 2015. Dual impact of live *Staphylococcus aureus* on the osteoclast lineage, leading to increased bone resorption. J Infect Dis 211:571-81.

154. Trebec DP, Chandra D, Gramoun A, Li K, Heersche JN, Manolson MF. 2007. Increased expression of activating factors in large osteoclasts could explain their excessive activity in osteolytic diseases. J Cell Biochem 101:205-20.

155. Lees RL, Sabharwal VK, Heersche JN. 2001. Resorptive state and cell size influence intracellular pH regulation in rabbit osteoclasts cultured on collagen-hydroxyapatite films. Bone 28:187-94.

156. Piper K, Boyde A, Jones SJ. 1992. The relationship between the number of nuclei of an osteoclast and its resorptive capability in vitro. Anat Embryol (Berl) 186:291-9.

157. Xiong J, Onal M, Jilka RL, Weinstein RS, Manolagas SC, O'Brien CA. 2011. Matrix-embedded cells control osteoclast formation. Nat Med 17:1235-41.

158. Pesce Viglietti AI, Gentilini MV, Arriola Benitez PC, Giambartolomei GH, Delpino MV. 2018. *B. Abortus* Modulates Osteoblast Function Through the Induction of Autophagy. Front Cell Infect Microbiol 8:425.

159. Bellows CG, Aubin JE, Heersche JN. 1991. Initiation and progression of mineralization of bone nodules formed in vitro: the role of alkaline phosphatase and organic phosphate. Bone Miner 14:27-40.

160. Buckwalter JA, Cooper RR. 1987. Bone structure and function. Instr Course Lect 36:27-48.

161. Kim CH, Kang BS, Lee TK, Park WH, Kim JK, Park YG, Kim HM, Lee YC. 2002. IL-1beta regulates cellular proliferation, prostaglandin E2 synthesis, plasminogen activator activity, osteocalcin production, and bone resorptive activity of the mouse calvarial bone cells. Immunopharmacol Immunotoxicol 24:395-407.

162. Lee CW, Lin CC, Lin WN, Liang KC, Luo SF, Wu CB, Wang SW, Yang CM. 2007. TNF-alpha induces MMP-9 expression via activation of Src/EGFR, PDGFR/PI3K/Akt cascade and promotion of NF-kappaB/p300 binding in human tracheal smooth muscle cells. Am J Physiol Lung Cell Mol Physiol 292:L799-812.

163. Khateeb MI, Araj GF, Majeed SA, Lulu AR. 1990. Brucella arthritis: a study of 96 cases in Kuwait. Ann Rheum Dis 49:994-8.

164. Teitelbaum SL. 2007. Osteoclasts: what do they do and how do they do it? Am J Pathol 170:427-35.

165. Cappariello A, Maurizi A, Veeriah V, Teti A. 2014. The Great Beauty of the osteoclast. Arch Biochem Biophys 558:70-8.

166. Tanaka S, Takahashi N, Udagawa N, Tamura T, Akatsu T, Stanley ER, Kurokawa T, Suda T. 1993. Macrophage colony-stimulating factor is indispensable for both proliferation and differentiation of osteoclast progenitors. J Clin Invest 91:257-63.

167. Celli J. 2019. The Intracellular Life Cycle of Brucella spp. Microbiol Spectr 7.

168. Aubin GG, Baud'huin M, Lavigne JP, Brion R, Gouin F, Lepelletier D, Jacqueline C, Heymann D, Asehnoune K, Corvec S. 2017. Interaction of Cutibacterium (formerly Propionibacterium) acnes with bone cells: a step toward understanding bone and joint infection development. Sci Rep 7:42918.

169. Celli J, de Chastellier C, Franchini DM, Pizarro-Cerda J, Moreno E, Gorvel JP. 2003. Brucella evades macrophage killing via VirB-dependent sustained interactions with the endoplasmic reticulum. J Exp Med 198:545-56.

170. Pei J, Wu Q, Kahl-McDonagh M, Ficht TA. 2008. Cytotoxicity in macrophages infected with rough Brucella mutants is type IV secretion system dependent. Infect Immun 76:30-7.

171. Wang M, Qureshi N, Soeurt N, Splitter G. 2001. High levels of nitric oxide production decrease early but increase late survival of *Brucella abortus* in macrophages. Microb Pathog 31:221-30.

172. Delpino MV, Barrionuevo P, Macedo GC, Oliveira SC, Genaro SD, Scian R, Miraglia MC, Fossati CA, Baldi PC, Giambartolomei GH. 2012. Macrophage-elicited osteoclastogenesis in response to *Brucella abortus* infection requires TLR2/MyD88-dependent TNF-alpha production. J Leukoc Biol 91:285-98.

173. Lacey CA, Mitchell WJ, Brown CR, Skyberg JA. 2017. Temporal Role for MyD88 in a Model of Brucella-Induced Arthritis and Musculoskeletal Inflammation. Infect Immun 85.

174. Boissy P, Saltel F, Bouniol C, Jurdic P, Machuca-Gayet I. 2002. Transcriptional activity of nuclei in multinucleated osteoclasts and its modulation by calcitonin. Endocrinology 143:1913-21.

175. Adamopoulos IE. 2018. Inflammation in bone physiology and pathology. Curr Opin Rheumatol 30:59-64.

176. Hill PA. 1998. Bone remodelling. Br J Orthod 25:101-7.

177. Claro T, Widaa A, O'Seaghdha M, Miajlovic H, Foster TJ, O'Brien FJ, Kerrigan SW. 2011. *Staphylococcus aureus* protein A binds to osteoblasts and triggers signals that weaken bone in osteomyelitis. PLoS One 6:e18748.

178. Takayanagi H. 2010. The unexpected link between osteoclasts and the immune system. Adv Exp Med Biol 658:61-8.

179. Kahl-McDonagh MM, Ficht TA. 2006. Evaluation of protection afforded by *Brucella abortus* and *Brucella melitensis* unmarked deletion mutants exhibiting different rates of clearance in BALB/c mice. Infect Immun 74:4048-57.

180. Lai F, Schurig GG, Boyle SM. 1990. Electroporation of a suicide plasmid bearing a transposon into *Brucella abortus*. Microb Pathog 9:363-8.

181. Fowler TW, Kamalakar A, Akel NS, Kurten RC, Suva LJ, Gaddy D. 2015. Activin A inhibits RANKL-mediated osteoclast formation, movement and function in murine bone marrow macrophage cultures. J Cell Sci 128:683-94.

182. Franco GC, Kajiya M, Nakanishi T, Ohta K, Rosalen PL, Groppo FC, Ernst CW, Boyesen JL, Bartlett JD, Stashenko P, Taubman MA, Kawai T. 2011. Inhibition of matrix metalloproteinase-9 activity by doxycycline ameliorates RANK ligand-induced osteoclast differentiation in vitro and in vivo. Exp Cell Res 317:1454-64.

183. Lee NK, Choi YG, Baik JY, Han SY, Jeong DW, Bae YS, Kim N, Lee SY. 2005. A crucial role for reactive oxygen species in RANKL-induced osteoclast differentiation. Blood 106:852-9.

184. Nishimura K, Shindo S, Movila A, Kayal R, Abdullah A, Savitri IJ, Ikeda A, Yamaguchi T, Howait M, Al-Dharrab A, Mira A, Han X, Kawai T. 2016. TRAP-

positive osteoclast precursors mediate ROS/NO-dependent bactericidal activity via TLR4. Free Radic Biol Med 97:330-341.

185. Pei J, Ficht TA. 2004. *Brucella abortus* rough mutants are cytopathic for macrophages in culture. Infect Immun 72:440-50.

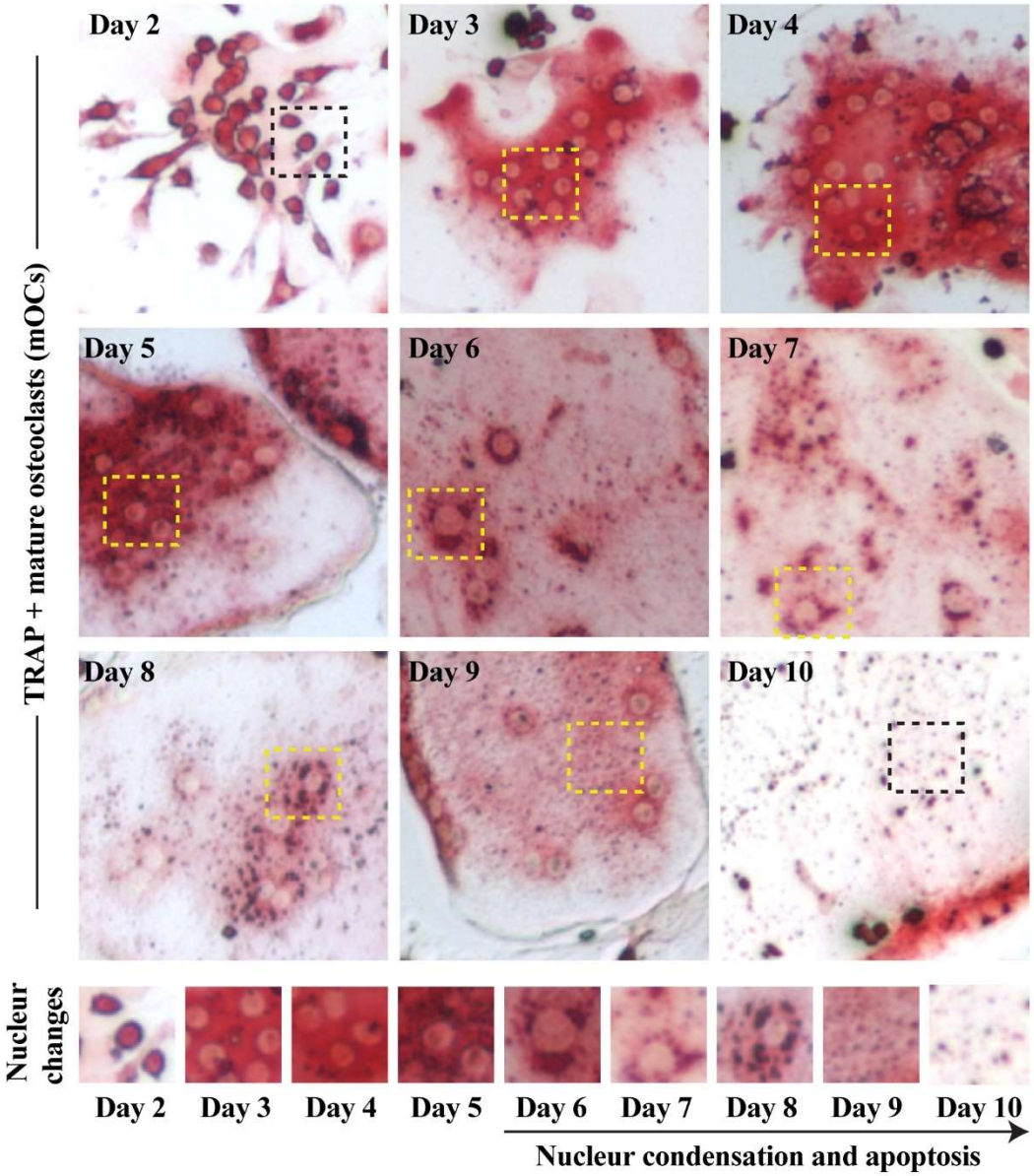

A-1 Nuclear changes and apoptosis during osteoclasts maturation and growth. Murine bone marrow-derived macrophages (BMDMs) were cultured in 24 well plates with 20 ng/ml M-CSF and 50 ng/ml RANKL up to 10 days to monitor apoptosis in multinucleated osteoclasts. Brightfield images represent apoptotic events in osteoclasts with appearance of nuclear condensation at day 6 of maturation, followed by nuclear fragmentation by day 7 and day 8 leading to cell death by day 10 of maturations. Bottom panel corresponds with the square selection in the top panel.

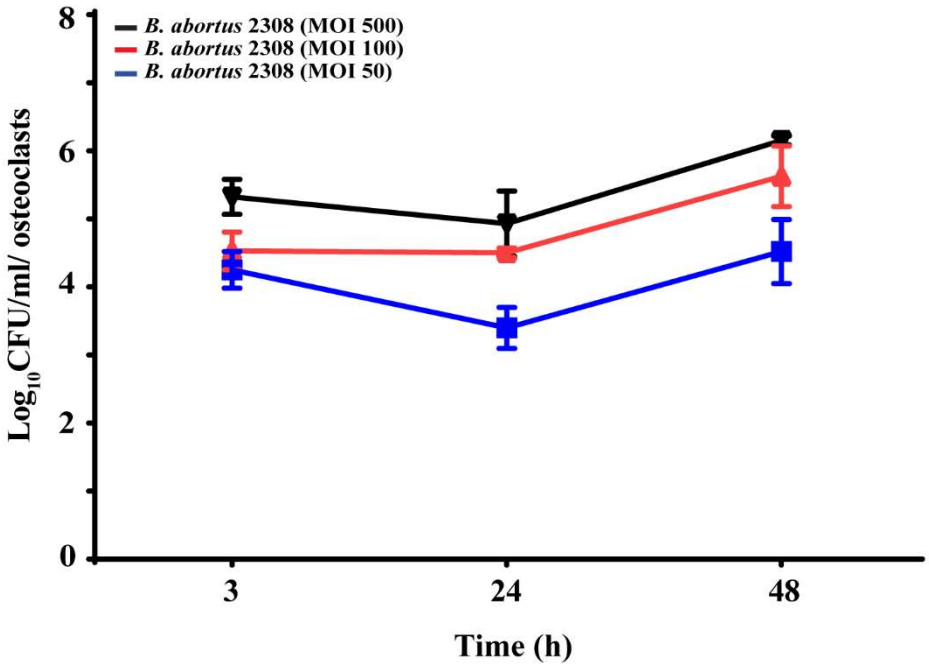

A-2 *B. abortus* invades and replicates inside mature osteoclasts (mOCs) in a dose-dependent manner. Mouse BMDMs were cultured in 24 well plates with 20 ng/ml M-CSF + 50 ng/ml RANKL. On day 3, TRAP+mOCs were infected with *B. abortus* strains at MOI of 1:50, 1:100. 1:500. Following 2h of infection, media was replaced with gentamicin containing media and incubated for different time durations. Results demonstrated that *B. abortus* 2308 invades and replicates mOCs in a dose-dependent manner. MOI 1:100 was used in different experiments.

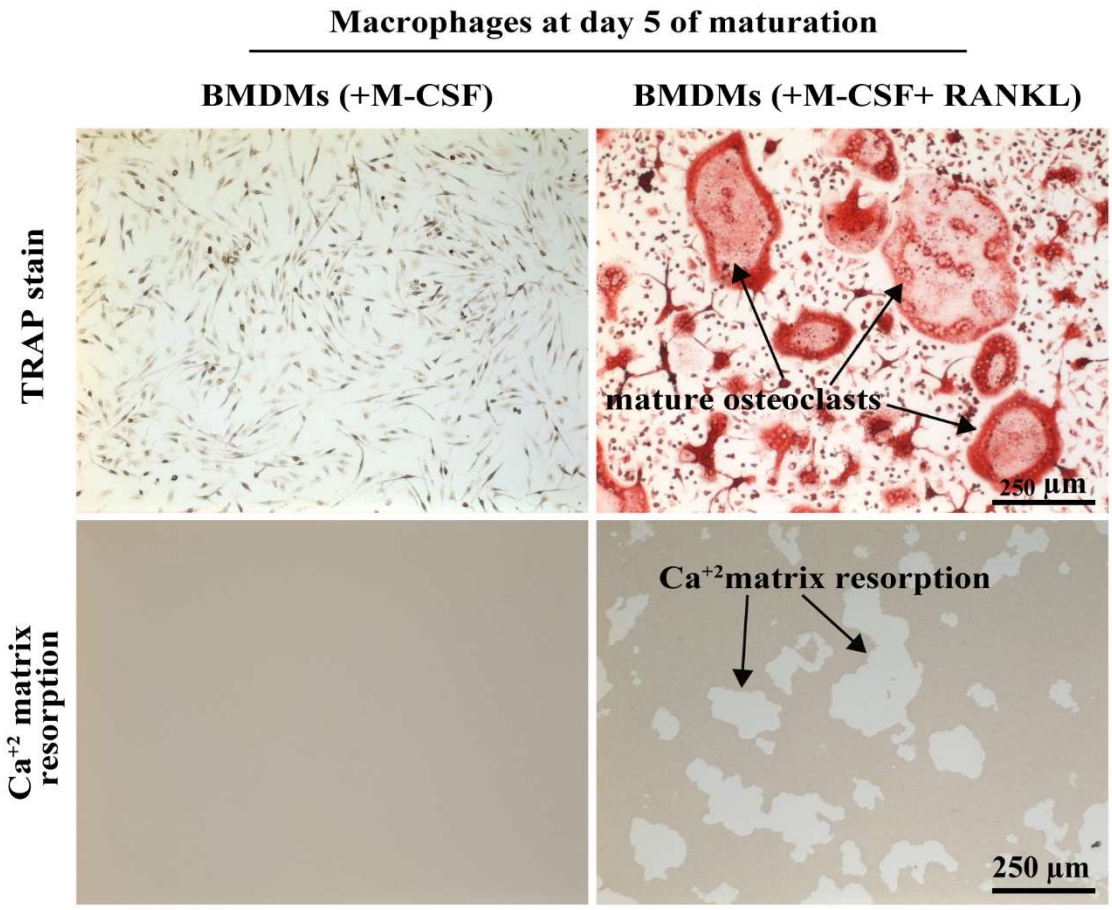

A-3 Mature osteoclasts but not macrophages are capable of degrading calcium matrix. Mouse bone marrow-derived macrophages (BMDMs) were cultured in 24 well calcium matrix-coated plated in the presence of either 20 ng/ml M-CSF or both 20 ng/ml M-CSF and 50 ng/ml RANKL for 5 days. One group of cells were washed, fixed, and stained for TRAP positivity (top panel) and another group were processed for matrix degradation (bottom panel). Representative brightfield images show TRAP-negative macrophages and TRAP+ osteoclasts (red cell, arrow). The bottom left panel shows lack of calcium matrix degradation by macrophages, while the bottom right panel shows calcium matrix degradation by mature osteoclasts (white degraded areas are identified using arrow), as expected.

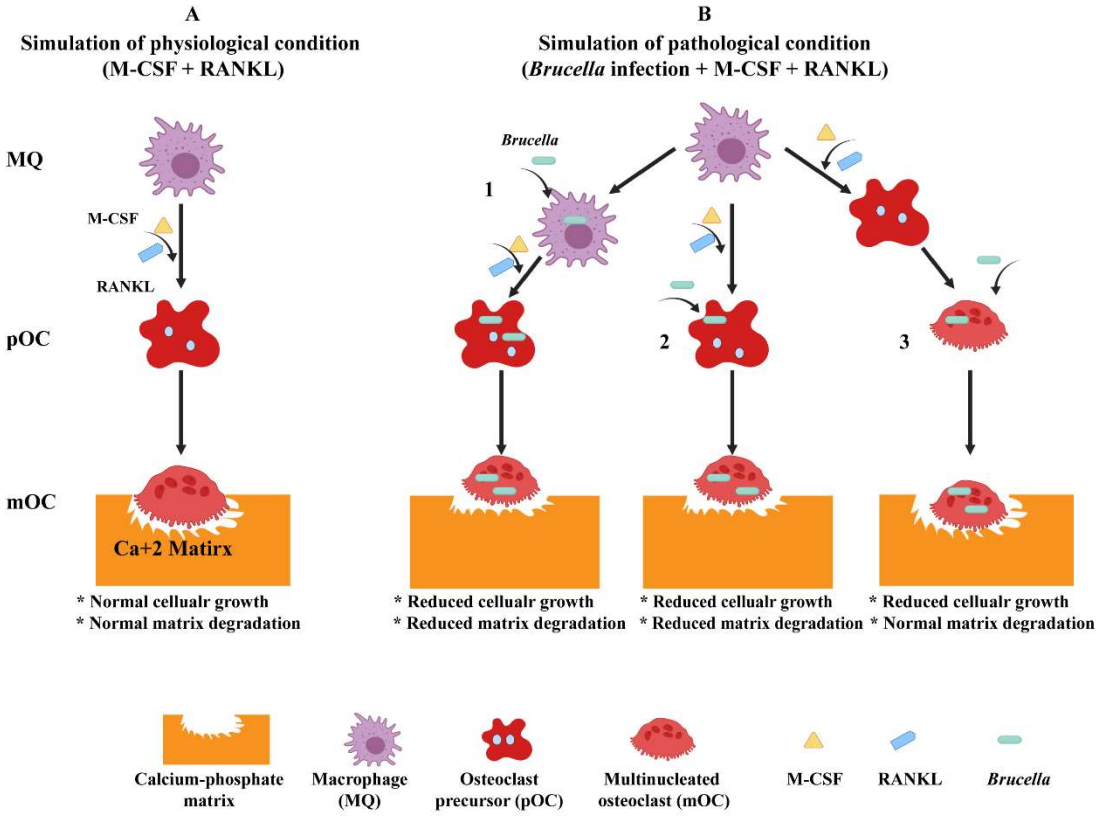

A-4 Schematic representation of the effect of wild type *Brucella* infection on calcium matrix degradation. (A) Diagram showing simulation of physiological condition where BMDMs, in the presence of M-CSF and RANKL, differentiate into osteoclast precursors followed by mature osteoclasts capable of calcium matrix degradation. (B) Diagram showing that simulation of pathological conditions during *B. abortus* 2308 infection of BMDMs (1) or osteoclast precursors (2) had a negative impact on cellular development and matrix degradation (lower level), while infection of mature osteoclasts (3) impaired cellular growth without changing the resorption activity compared to uninfected mature osteoclasts (A).